TRABAJO ESPECIAL DE GRADO

SEISMIC RESPONSE OF DEEP TUNNELS.

CONTINUUM AND DISCONTINUUM NUMERICAL ANALYSIS

Presentado ante la Ilustre
Universidad Central de Venezuela
Por el Br. Franco Rattia
Victor Hugo
Para optar al Título
de Ingeniero Geofísico

Caracas, 2008

TRABAJO ESPECIAL DE GRADO

SEISMIC RESPONSE OF DEEP TUNNELS.

CONTINUUM AND DISCONTINUUM NUMERICAL ANALYSIS

TUTOR ACADÉMICO: Prof. Inírida Rodríguez Millán.

Presentado ante la Ilustre
Universidad Central de Venezuela
Por el Br. Franco Rattia
Victor Hugo
Para optar al Título
de Ingeniero Geofísico

Caracas, 2008

Caracas, Diciembre de 2008

Los abajos firmantes, miembros del Jurado designado por el Consejo de la Escuela de Ingeniería Geológica, Minas y Geofísica, para evaluar el Trabajo Especial de Grado presentado por el Bachiller Victor Hugo Franco Rattia, titulado:

“Seismic response of deep tunnels.
Continuum and discontinuum numerical analysis”

Consideran que el mismo cumple con los requisistos exigidos por el plan de studios conducente al Título de Ingeniero Geofísico, y sin que ello signifique que se hacen solidarios con las ideas expuestas por el autor, lo declaran APROBADO.

Prof. José Cavada
Jurado

Prof. Jesús Gonzales
Jurado

Prof. Inírida Rodríguez Millán
Tutor Academico

A Rosa, Nancy
y Vicfrancy

AGRADECIMIENTOS

A la ilustre Universidad Central de Venezuela por haberme acogido en su calurosa casa de forma abierta, hogareña y maternal sin ninguna condición y mucho menos pidiendo algo a cambio; dandome así, la posibilidad de descubrir otro mundo, otras personas y escuchar otras ideas que sin duda alguna han cambiando mi manera de ver las cosas, actuar y permitiendome soñar en los pocos años en que los fui su hospite. Sin que me quede nada por dentro eres la mejor casa de estudio que este país puede ofrecer.

A mi madre Nancy por haber siempre estado conmigo apoyadandome en cada una de las deciciones que me toco asumir ante la vida y mi carrera universitaria; y vaya que he tomado deciciones erroneas, pero siempre allí motivandome a vivir y buscar la felicidad.

A mi abuela Rosa que sin saberlo se convirtio en la particpe escondida que me empujo hacia el camino de la Ingeniería, enseñandome el valor de los primeros numeros: suma, resta, multiplicación y división.

A mi hermana Vicfrancy por haberme siempre dado animo a salir a delante en esos momentos grises y por ,también, haberse sacrificado junto con mi madre y abuela para que yo pudiera percibir un futuro muy distinto a lo que mi realidad me ofrecía.

Por ultimo, quisiera agredecer al resto de mi familia, amigos, compañeros y profesores que de forma directa o inderecta han contribuido en la creación de un ingeniero y en el convertimiento de un niño en una persona, hombre y finalmente en un ser humano.

Gracias

Franco R., Victor H.

SEISMIC RESPONSE OF DEEP TUNNELS. CONTINUUM AND DISCONTINUUM NUMERICAL ANALYSIS

Tutor Académico: Prof. Inírida Rodríguez Millán.

Tesis. Caracas, U.C.V. Facultad de Ingeniería. Escuela de Geología, Minas y Geofísica. Departamento de Geofísica. Año 2008, 154 p.

Palabras Claves: Italia, Túnel, Análisis Numérico, Análisis Sísmico, Terremoto.

Resumen. La cresciente necesidad de nuevas líneas de transporte y red de servicios han generado un incremento de demanda por un ampliado y elaborado uso del espacio subterráneo en áreas urbanas. Algunos de estos proyectos reguardan la construcción de nuevas líneas de metro, redes de agua, gas, telecominicaciones y conexiones electricas; así como estacionamentos subterráneos. Otras aplicaciones para la construcción de obras subterráneas comprenden el cruce de barreras naturales como ríos y montañas, para su uso tanto de autopistas como de ferrovías. Estas estructuras son proyectadas siguiendo el método estático, donde el estado tensional calculado depende de la geometría de escavación y de las propiedades del macizo rocoso.

Actualmente, se debe tener en cuenta las fuerzas debido a terremotos. La ocurrencia de eventos sísmicos no solo representa un factor potencial en la perdida de vidas humanas ; sino también, daños en las infraestructuras , que pueden seriamente influir en la funcionalidad de servicios de una región, durante y después de un sismo.

El objetivo de esta tesis consiste en el desarrollo de una razional y consistente metodología de análisis sísmico de túneles en rocas. Serán mostrados diferentes métodos de diversos autores sobre este tema prestando mayor atención al análisis de la estructura. Esta tesis parte con el estudio de diversos túneles que han sufrido daños sísmicos entre los cuales: el terremoto de 1995 Kobe (Japón), el terremoto de 1999 Chi-Chi (Taiwan) y el terremoto de 1989 Loma Prieta (USA).

En general, el análisis debido a fuerzas sísmicas viene efectuada en términos de deformación y esfuerzos impuestos sobre la estructura del terreno circondante, normalmente a causa de la interación entre ambos.

Los métodos aplicados comprenden el análisis de túneles en condición estática y condición dinámica, considerando dos medios, uno continuo y el otro discontinuo. El modelo continuo considera el macizo rocoso representado por uníco cuerpo homogeneo, en vez, en el modelo discontinuo el macizo rocoso es subdividido por uno ó más sistema de discontinuidades.

Las principales fases de análisis comprenden: (a) caracterización del macizo rocoso para el análisis en condición estática, (b) análisis estática, (c) defenición del input sísmico, (d) análisis dinámica, (e) sobraposición de los efectos estáticos y dinámicos tanto para los modelos en continuo como en discontinuo.

La respuesta del túnel será examinada en dirección transversal. Sobre esta dirección tanto la respuesta estática como aquella dinámica, al continuo y discontinuo, serán estudiadas siguiendo un análisis numérico mediante la aplicación del Método a los Elementos Distintos. Este método permite representar el macizo rocoso como un conjunto de bloques que pueden ser considerados como “deformables” o “no deformables”. Los juntos y las discontinuidades son considerados como interfaces entre cuerpos distintos.

El software empleado en este trabajo, que toma in consideración el método anteriormente descrito, se llama UDEC, del inglés Universal Distinct Element Code. Este progama permite análizar el túnel en condición estática y dinámica previo al inserimento del input sísmico, tanto para medios discontinuos como continuos.

Los resultados obtenidos con el análisis numérico fuerón confrontados con aquellos obtenido mediante metodos análiticos, con el objetivo de comprovar la eficiencia del programa. El método propuesto fué aplicado a un túnel situado en la Italia meridional. El túnel forma parte de la línea ferroviaria que conecta los puebos de Caserta y Foggia, que sen encuentran situadas en la parte norte de la cadena montañosa de los Appennini Meridionali, una de las zonas sísmicamente más activas en Italia.

INDEX

INDEX OF FIGURES

INDEX OF TABLES

CHAPTER I

INTRODUCTION

Growing needs for modern transportation and utility networks have given rise to an increased demand for a more extensive and elaborate use of underground space. Some of these projects are related to urban development, which requires the construction of more metro system, underground water mains, gas pipes, telecommunication and electric power networks, as well as underground parking facilities. Other applications of underground construction include the crossing of natural barriers such a river and mountains that are found across the alignment of major road, motorway or railway link projects.

As it is well know, underground structures are basically designed with regards to static stress. Theses stresses are among other things depending on the geometry of the rock excavation and the surrounding and on the properties of the rock material. Changes in these stresses can be due to changes in the geometry, e.g. from enlarging of the excavations. Also stresses might be changed because the exterior stresses on the rock are varied.

Such variations can be induced by different kinds of dynamic effects. Major influences on the design of underground facilities in certain areas are given by seismic effects. These effects can be characterized by the acceleration (velocity or displacement) as a function of time.

Therefore, one can no longer be certain that seismic effects will be negligible. In fact, in recent large earthquakes in several countries, large numbers of underground “lifelines” (communications, gas liner, water pipe lines, sewer pipe lines ,etc) vital to

the recovery of a city following an earthquake have been severely damaged by ground motions and displacements of faults.

1.1. General effects of earthquakes

There are two broad categories of earthquake effects in tunnels: ground shaking and ground failure. When seismic waves propagate through the earth's crust, the resulting ground motion, are considered as ground shaking. The area experiencing this shaking may cover hundreds of square miles in the vicinity of the fault rupture. The intensity of the shaking attenuates with distance from the fault rupture.

There are two basic categories of ground shaking (see Figure 1.1). Body waves travel within the earth's inner layers. These waves can be either longitudinal P or transverse shear S waves.

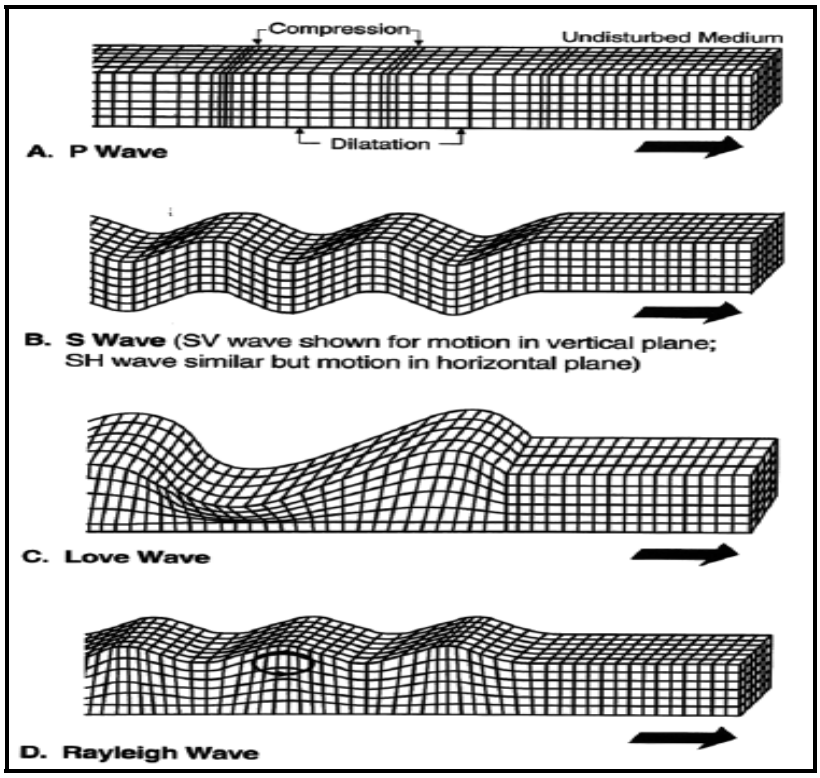

Figure 1.1. Ground response to seismic waves (St. John and Zahrah, 1987).

P waves move in a compressional motion similar to the motion of a slinky, while the S wave move in a shear motion perpendicular to the direction of the wave trend. These waves propagate in any direction underground. Surface waves travel along the earth's surface in the same matter a ripple would travel through water. These waves can either be Rayleigh or Love waves.

Love waves shake the surface side-to-side. Rayleigh waves move the surface of the earth around in a circle, forward and down then back and up. This is the same as the motion in an ocean wave (Merritt, et al. 1985). Any tunnel structure will be deformed as the ground is deformed by the traveling waves.

Ground failure can include different types of ground instability. These can include faulting, liquefaction, and tectonic uplift and subsidence. Faulting occurs when an increase in stress causes rocks to break. Liquefaction is a phenomenon in which the strength and stiffness of a soil is reduced by earthquake shaking or other rapid loading. Tectonic uplift and subsidence is the upward and downward movement of the ground due to plate movement. These phenomena have been responsible for tremendous amounts of damage in historical earthquakes around the world. Each of these hazards could possibly be detrimental to tunnel structures (Merritt, et al. 1985).

1.2. Response of underground structures to earthquakes

Studies realized in the past have shown that underground structures are less vulnerable to earthquakes respect to structures built at surface, but the associated risk may be high, since even a low level of damage could affect the serviceability of a wide network. However underground structures cannot be considered completely exempt to the effects of ground shaking, as it is going to be described in the next chapter.

A careful review of the seismic damages suffered by underground facilities shows that most tunnels were located in the vicinity of causative faults. The characteristics

of ground motion in the vicinity of the source can be different from that of the far-field. The ground motion is characterized by strong, coherent (narrow band) long period pulses and is severely affected by the rupture mechanism, the direction of rupture propagation relative to the site, and possible permanent ground displacements resulting from fault slip.

The seismic analysis of underground structures is a complex process because involves the interaction between several disciplines as soil, rock and structural dynamics, structural geology, seismotectonics and engineering seismology.

The difference between underground structures and surface facilities from the seismic effects point of view are due, since the overall mass of the structure is usually small compared with the mass of the surrounding soil and the overall confinement provides high level of radiation damping. The response of an underground structure to a seismic event is basically governed by the behavior of the surrounding ground and not by the inertia characteristics of the structure itself, as the response to such event is substantially depending on the induce ground deformation.

1.3. Purpose

The purpose of this thesis is to develop a rational and consistent seismic design methodology for lined tunnels that would also be applicable to other underground lined structures with similar characteristics. The results presented provide data for simple and practical application of this methodology.

While the general public is often skeptical about the performance of underground structures, tunnel designers know that underground structures are among the safest shelters during earthquakes, based primarily on damage data reported in the past. Yet one certainly would not want to run away from a well designed building into a buried tunnel when seismic events occur if that tunnel had been built with no seismic considerations.

In recent years, however, the enhanced awareness of seismic hazards for underground structures has prompted an increased understanding of factors influencing the seismic behavior of underground structures.

Despite this understanding, significant disparity exists among engineers in design philosophy, loading criteria, and methods of analysis.

This thesis, also, shows a simplified approach for studying the seismic response of deep tunnels, which takes into account the interaction of the underground structure, the surrounding ground and the presence of near-fault ground motion. This response is studied through a simplified approach in order to estimate the stresses increment in the lined tunnel due to earthquake that allow to establish the general approaches for seismic design.

Also, the analysis of the transversal response, which consist in estimating the lining internal forces due to ovaling deformation, is performed in this work by considering a lined tunnel in plane strain conditions, because is one of the phenomenon that could represent a significant damage at the moment in which the seismic criteria is taking into account for the tunnel design.

Therefore, this study has the following goals:

- To maintain a consistent seismic design philosophy and a consistent design criteria both for underground structures and other civil engineering facilities.
- To use simple yet rational methods of analysis of evaluating earthquake effects on underground structures. The methodology should be consistent for structures with different section geometries.

1.4. Scope of this study

The work performed to achieve these goals consisted of:

- A summary of observed earthquake effects on underground structures.
- A quantitative description of ground behavior during traveling seismic waves. Various modes of ground deformation, rock mass alteration and their engineering implications for tunnel design are discussed.
- A review of current seismic design methodology for circular mined tunnels for the transversal and longitudinal response deformation.
- The development of a refined (yet simple) method for evaluating the earthquake ovalling effects on circular linings in a rock mass which is represented as a discotinuum. These methods consider the soil-structure interaction effects and is built from a theory that is similar to most mining/underground engineers.
- The application of the approaches described above to a deep lined tunnel in Southern Italy. The infrastructure is part of the railway switch line connecting Caserta-Foggia, located in the northern sector of the Southern Apennines, one of the most active seismic regions in Italy. The response of a transverse cross-section of the tunnel will be calculated by analytical solution for both static and dynamic analysis in a continuum and a discontinuum medium. For the dynamic analysis, the analytical solutions are going to be compared to the numerical solutions.

CHAPTER II

GENERAL ASPECTS OF UNDERGROUND STRUCTURES IN SEISMIC CONDITIONS

2.1. Introduction

It is known that underground structures will become in the future a useful source that provides multiple opportunities: transport infrastructure, energy and materials storage, residuals cemeteries, transportation facilities, defense installations, etc. Here it's about subsurface structures with a variety of shapes and sizes, in different ground properties, different geological environments and different security levels. It is not possible to neglect the seismic effects. In fact, in recent large earthquakes several underground structures have suffered severe damages. The effects of earthquake damage to underground structures may be attributed to three factors: (a) fault slip; (b) ground failure; and (c) shaking.

Damages due to fault slip have been reported in tunnels where the opening passes through a fault zone. Since nothing can be done to avoid such ground motions, anticipation measures aim to accommodate ground motions without undue damage. Ground failure, such as rock slides, landslides squeezing, soil liquefaction, and soil subsidence, have damage portals and shallow excavations. This is an indirect consequence of seismic loading.

Damage due to shaking for lined tunnels may include cracking, spalling and failure of the additional seismic loading. For unlined tunnels in rock, the damage may be rock fall, spalling and local opening of joints and block motion. Such phenomena have been documented for excavations subjected to seismic loading due to earthquakes and underground explosions. Therefore, the design of underground structures to withstand

seismic loading, has aspects that are very different from the seismic design of surface structures.

Some of these structures, commonly used in urban areas, are large diameter tunnels, cut and cover structures and portal structures (Figure 2.1). Large diameter tunnels are linear underground structures in which the length is much larger than the cross sectional dimension. These structures can be grouped into three broad categories, each having distinct design features and construction methods: (a) bored or mined tunnels; (b) cut and cover tunnels; and (c) immersed tube tunnels (Power et al., 1996).

Bored or mined tunnels are unique because they are constructed without significantly affecting the soil or rock above the excavation. Cut and cover structures are those in which an open excavation is made, the structure is constructed, and fill is placed over the finished structure. Immersed tube tunnels are sometimes employed to traverse a body of water.

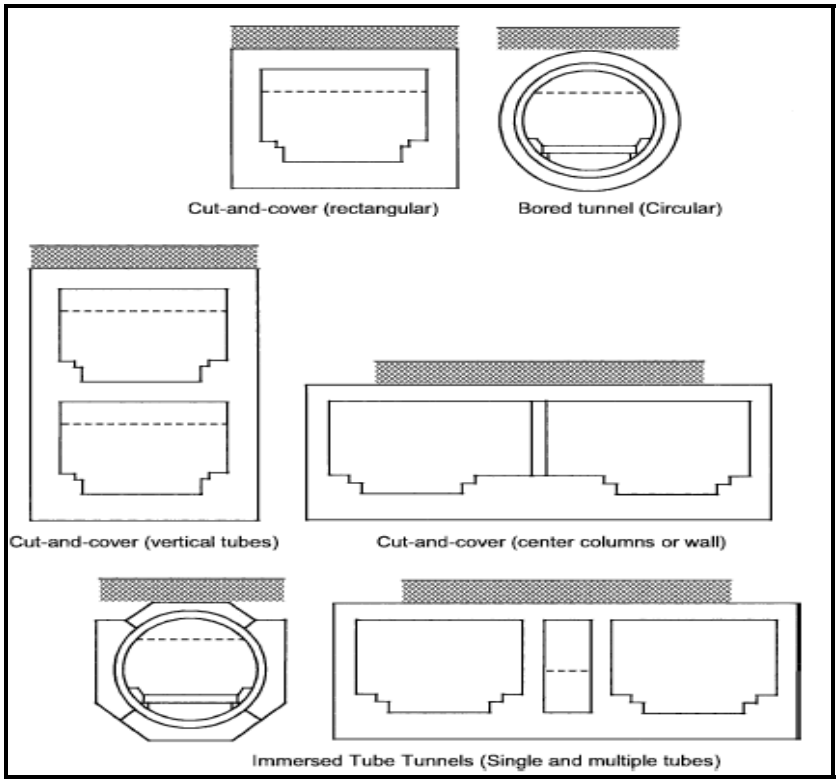

Figure 2.1. Cross section of tunnels (after Power et al., 1996).

Taking in to account this brief information the scope of this chapter is to show a synthesis of the current state of knowledge in the area of seismic design and analysis of underground structures. It will be shown some methods of analysis of underground structures subjected to seismic motion due to earthquake activity, and examples of performance and damage to underground structures of major earthquake around the world.

As a next step, it will be presented a proposed classification system for rock masses, an inventory of the leading additional geotechnical properties of the rock mass to be acquired when the structure lies in a seismic context, and means of obtaining these dynamic properties.

Then, it will be described the seismic action at and below the ground surface on vibratory motion, the different seismic hazard analysis to characterize the potential for strong motions, the potential fault motion and the frequency in which the faults release stored energy. Finally, some design recommendations for underground structures will be described.

2.2. Earthquake Damage on Underground Structures

A lot of studies were made in order to register earthquake damage to underground facilities; since the KANTO earthquake in 1923, the first disaster recorded, to the present day. As an example ASCE (1974) describes the damage in the Los Angeles area as a result of the 1971 San Fernando Earthquake.

JSCE (1988) describes the performance of several underground structures, including an immersed tube tunnel during shaking in Japan. Sharma and Judd (1991) created an extensive database of seismic damage to underground structures using 192 case histories. General observations can be made relating the seismic performance of underground structures:

1. Underground facilities suffer considerably less damage than surface structures.

2. Reported damage decreases with increasing overburden depth. Deep tunnels seem to be safer and less vulnerable to earthquake shaking respect to shallow tunnels.

3. Underground facilities constructed in soils could suffer more damage than openings constructed in competent rock.

4. Lined and grouted tunnels are safer than unlined tunnels in rock. Shaking damage can be reduced by stabilizing the ground around the tunnel and by improving the contact between the lining and the surrounding ground through grouting.

5. Tunnels are more stable under a symmetric load, which improves ground-lining interaction. Improving the tunnel lining by placing thicker and stiffer sections without stabilizing surrounding poor ground may result in excess seismic forces in the lining. Backfilling with non-cyclically mobile material and rock-stabilizing measures may improve the safety and stability of shallow tunnels.

6. Damage may be related to peak ground acceleration and velocity based on the magnitude and epicentral distance of the affected earthquake.

7. Duration of strong-motion shaking during earthquakes is of utmost importance because it may cause fatigue failure and therefore, large deformations.

8. High frequency motions may explain the local spalling of rock or concrete along planes of weakness. These frequencies, which rapidly attenuate with distance, may be expected mainly at small distances from the causative fault.

9. Ground motion may be amplified upon incidence with a tunnel if wavelengths are between one and four times the tunnel diameter.

10. Damage at near tunnel portals may be significant due to slope instability.

The following are some cases of seismic performance of underground structures:

2.2.1. Bay Area Rapid Transit (BART) system, San Francisco, CA, USA

The BART system is one of the first underground structures made considering the seismic loading (Kuesel, 1969). On the San Francisco site, the system consists of underground stations and tunnels in fill and soft Bay Mud deposits, and it is connected to Oakland via the transbay-immersed tube tunnel.

During the 1989 Loma Prieta Earthquake, the BART facilities sustained no damage and operated on a 24-h basis after the earthquake. This is primarily because the system was designed under stringent seismic design considerations. Special seismic joints (Bickel and Tanner, 1982) were designed to accommodate differential movements at ventilation buildings. The system has been designed to support earth and water loads while maintaining watertight connections and not exceeding allowable differential movements. No damage was observed at these flexible joints, though it is not exactly known how far the joints moved during the earthquake (PB, 1991).

2.2.2. Alameda Tubes, Oakland, CA, USA

The Alameda Tubes are a pair of immersed-tube tunnels connected from Alameda Island to Oakland in the San Francisco Bay Area. These are some of the first tube tunnels built in 1927 and 1963 without seismic design considerations. During the

Loma Prieta Earthquake, the ventilation buildings suffered some structural cracking. Limited water leakage into the tunnels was also observed, as was liquefaction of loose deposits above the tube at the Alameda portal. Peak horizontal ground accelerations measured in the area ranged between 0.1 to 0.25 g (EERI, 1990).

2.2.3. Earthquake Damage in Japan

According to the Yoshikawa and Fukuchi (1984) recompilation of "Earthquake Damage to Railway Tunnels in Japan", there have been five important earthquakes that produced many tunnel damages. Table 2.1 shows the above mentioned five earthquakes with a description of the state of damage.

The table shows a tendency of the number of damage depending on the magnitude of the earthquake with one exception, that is the Near-OSHIMA earthquake (M=7,0). This is because a significant earthquake fault traversing the railway line.

Table 2.1. Five important earthquake and number of damaged portions

(Yoshikawa and Fukuchi, 1984).

	Earthquake	KANTO (1923) *M*=7.9	KITAIZU (1930) *M*=7.0	FUKUI (1948) *M*=7.2	NIIGATA (1964) *M*=7.5	N-OSHIMA (1978) *M*=7.0
Portal	lining cracked	55		1	5	5
	lining cracked and unlevelled	14		1		2
	lining concrete fallen	8				2
	deformed	1		1		
	collapsed	15				2
Interior	lining cracked	89	1	2	16	9
	lining cracked and unlevelled	15			44	1
	lining concrete fallen	17	1	1	6	4
	deformed	15	1	1	4	3
	collapsed	18	1			1
Category of damage	L (light)	56			12	3
	M (medium)	12		1	7	4
	H (heavy)	25	1	1		2

There were only two cases where the earthquake fault traversing the tunnel was put in motion, in both cases the damage became disastrous. One is the dislocation and partial collapse of the TANNA tunnel during construction caused by the KITA-IZU earthquake in 1930, the other was the dislocation and deformation of the INATORI tunnel caused by the Near-OSHIMA earthquake in 1978.

Figure 2.2 shows the earthquake fault traversing the TANNA tunnel. At 335-395 m back to the western portal, the timber structure was destroyed causing the upper grounds of about 1200 m^3 to fall down.

Figure 2.3 shows the scheme of deformation and dislocation of the INATORI tunnel by an earthquake fault in motion due to the Near-OSHIMA earthquake. The fault intersects the tunnel in the middle part. This point was designed with an almost circular cross-section and thick lining with invert concrete to overcome a poor fractured and solfataric-clay geology.

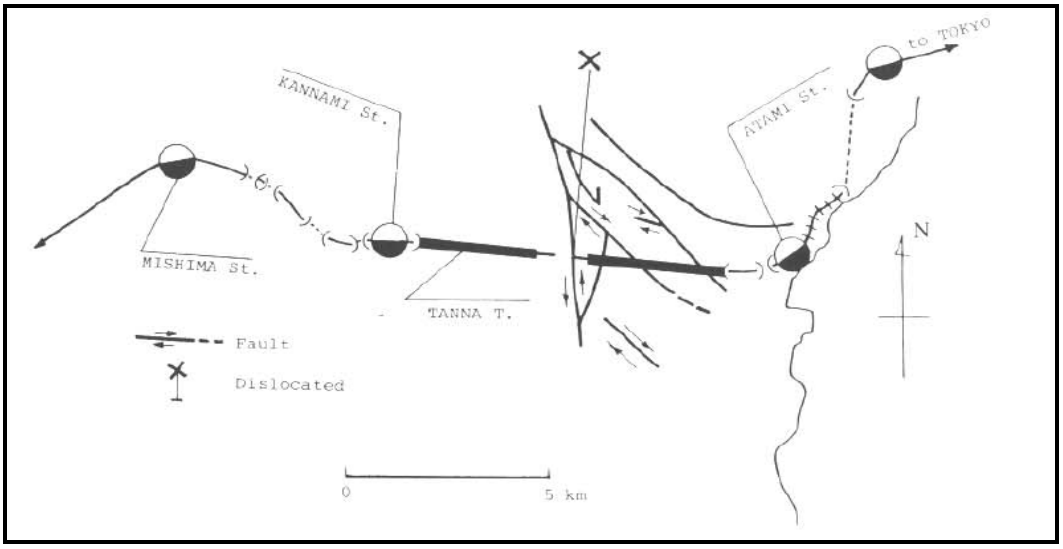

Figure 2.2. Earthquake faults across the TANNA tunnel (Yoshikawa and Fukuchi, 1984).

Nevertheless, bending and distortion of the cross section took place due to the fault in motion. As a result, large cracks in axial direction at the arch spring line and at the

crown, fall of arch concrete linings, and heaving of railway track caused by a collapse of invert concrete, took place. The deformation of the cross-section at the middle part is shown in Fig. 2.4. For the restoration of this tunnel, backfill grouting was carried out, and especially for severely deformed section, linings were chipped and then reinforced far stronger than before by reinforcing bars and steel fibre concrete.

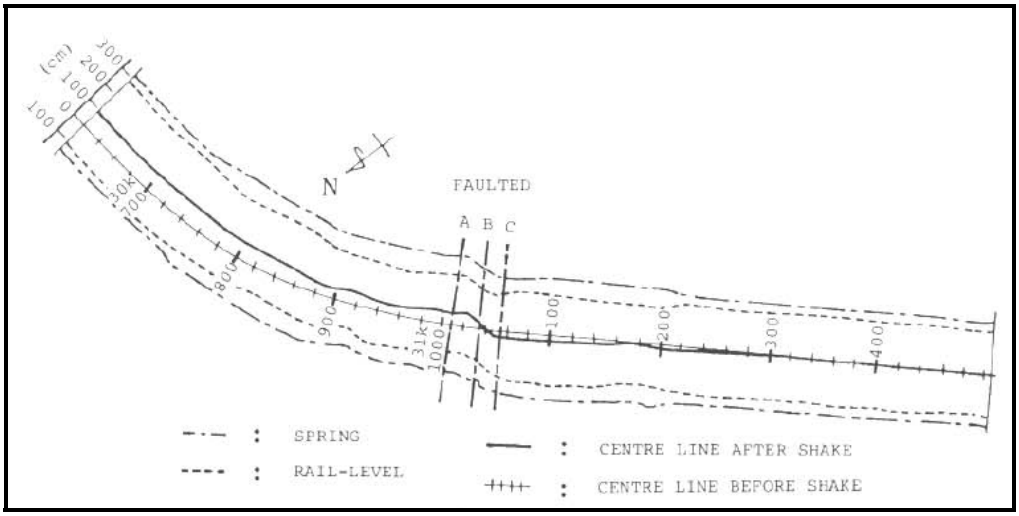

Figure 2.3. Dislocation and deformation, INATORI tunnel (Yoshikawa and Fukuchi, 1984).

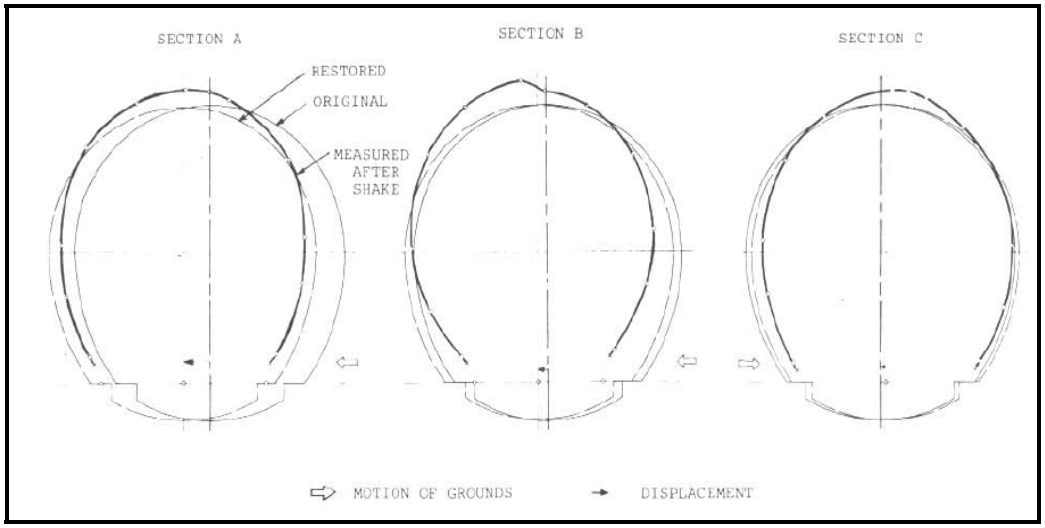

Figure 2.4. Deformation of cross-section, INATORI tunnel (Yoshikawa and Fukuchi, 1984).

As Yoshikawa and Fukuchi (1984) said; it is important for countries where frequent earthquake take place to bear in mind the influence of potential backgrounds so as to maintain or design tunnels. It is hoped that the prediction of large-scale earthquake as well as the risk of earthquake fault in motion, will be put into practice in the future, for the sake of minimizing damages to tunnels and to mankind.

The following three important papers by /Dowding and Rozen, 1978/, by /Sharma and Judd, 1991/, and /Asakura et al, 1998/ will be further expanded. Appendix A, shows previous compilations of damage on underground facilities due to earthquakes. The intention is to present a general empirical background and to extract information of relevance for this particular study.

2.2.4. Dowding and Rozen (1978)

The authors reported 71 cases of tunnel response to earthquake motions. The main characteristics of these case histories are as follows:

- These tunnels served as railway and water links with diameters ranging from 10 feet to 20 feet.
- Most of the tunnels were constructed in rock with variable rock mass quality.
- The construction methods and lining types of these tunnels varied widely. The permanent ground supports ranged from no lining to timber, masonry brick, and concrete linings.

Based on their study, Dowding and Rozen concluded, primarily for rock tunnels, that:

- Tunnels are much safer than above ground structures for a given intensity of shaking.
- Tunnels deep in rock are safer than shallow tunnels.
- No damage was found in both lined and unlined tunnels at surface accelerations up to 0.19g.
- Minor damage consisting of cracking of brick or concrete or falling of loose stones was observed in a few cases for surface accelerations above 0.25g and below 0.4g.

- No collapse was observed due to ground shaking effect alone up to a surface acceleration of 0.5g.
- Severe but localized damage including total collapse may be expected when a tunnel is subject to an abrupt displacement of an intersecting fault.

2.2.5. Sharma and Judd (1991)

The authors extended Owen and Scholl's work and collected qualitative data for 192 reported observations from 85 worldwide earthquake events. They correlated the vulnerability of underground facilities with six factors: overburden cover, rock type (including soil), peak ground acceleration, earthquake magnitude, epicentral distance, and type of support. It must be pointed out that most of the data reported are for earthquakes of magnitude equal to 7 or greater. Therefore, the damage percentage of the reported data may appear to be astonishingly higher than one can normally conceive.

The results are summarized in the following paragraphs. In many cases, the statistic damages, when they are correlated with a certain parameter, may show a trend that violates an engineer's intuition. This could be due to the statistical dependency on other parameters which can be more influential.

- The effects of overburden depths on damage are shown in Figure 2.5A for 132 of the 192 cases. Apparently, the reported damage decreases with increasing overburden depth.
- Figure 2.5B shows the damage distribution as a function of material type surrounding the underground opening. In this figure, the data labeled "Rock (?)" were used for all deep mines where details about the surrounding medium were not known. The data indicate more damage for underground facilities constructed in soil than in competent rock.
- The relationship between peak ground acceleration (PGA) and the number of damaged cases are shown in Figure 2.5C: for PGA values less than 0.15g, only 20 out of 80 cases reported damage. For PGA values greater than 0.15g, there were 65 cases of reported damage out of a total of 94 cases.

- Figure 2.5D summarizes the data for damage associated with earthquake magnitude. The figure shows that more than half of the damage reports were for events that exceeded magnitude M=7.

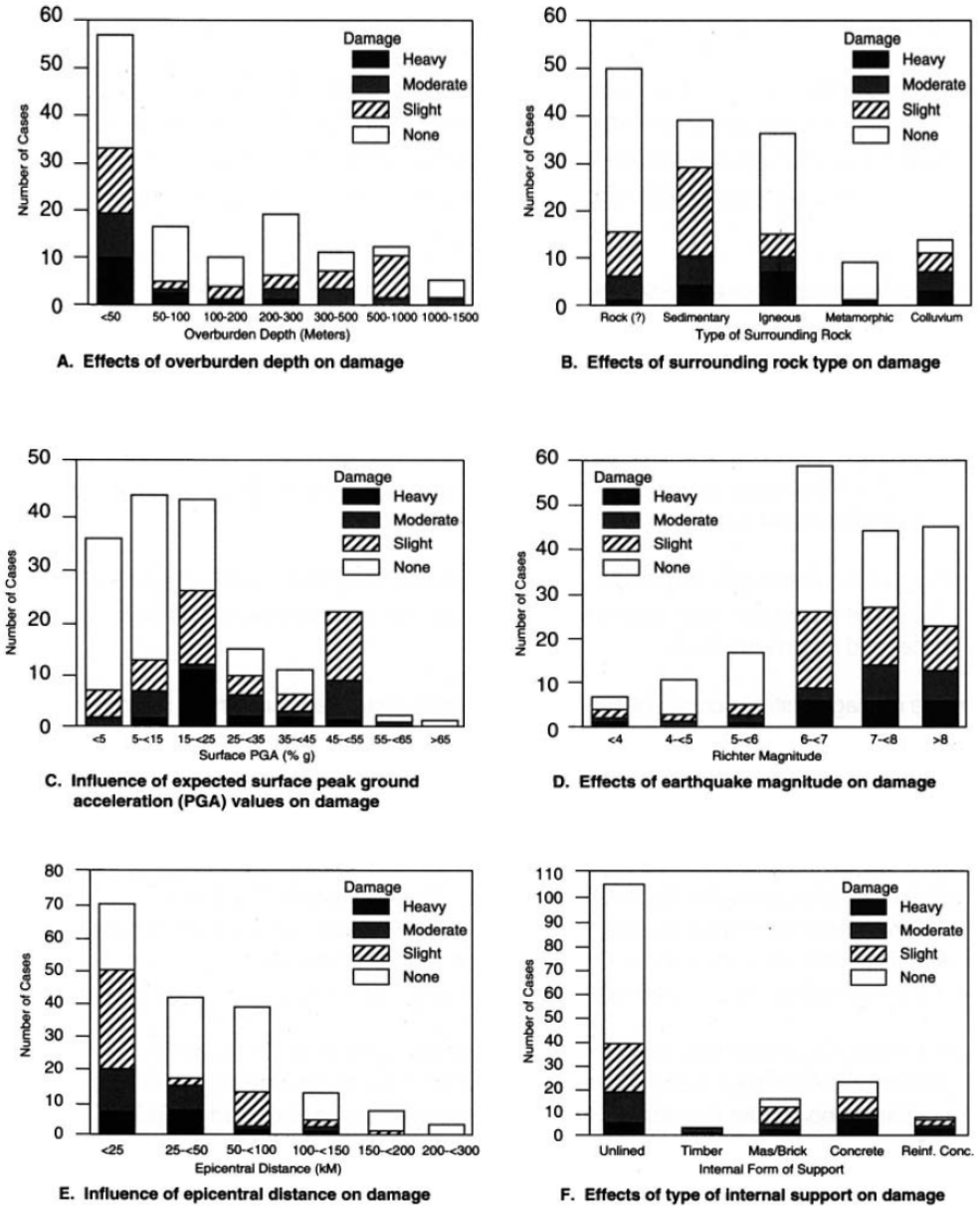

Figure 2.5. Damage statistics (Sharma and Judd, 1991).

- The damage distribution according to the epicentral distance is presented in Figure 2.5E. As indicated, damage increases with decreasing epicentral distance, and tunnels are most vulnerable when they are located within 25 to 50 km from the epicenter.
- Among the 192 cases, unlined openings account for 106 cases. Figure 2.5F shows the statistical damage data for each type of support. There were only 33 cases of concrete-lined openings including 24 openings lined with plain concrete and 9 cases with reinforced concrete linings. Of the 33 cases, 7 were undamaged, 12 were slightly damaged, 3 were moderately damaged, and 11 were heavily damaged.

It is interesting to note that, according to the statistical data shown in Figure 2.5F, the proportion of damaged cases for the concrete and reinforced concrete lined tunnels appears to be greater than that for the unlined cases. Sharma and Judd attributed this phenomenon to the poor ground conditions that originally required the openings to be lined. Richardson and Blejwas (1992) offered two other possible explanations:

- Damage in the form of cracking or spalling is easier to identify in lined openings than in unlined cases.
- Lined openings are more likely to be classified as damaged because of their high cost and importance.

2.2.6. Asakura and Sato (1998)

The paper of Asakura and Sato (1998), provides an excellent compilation of past earthquake damage to Japanese tunnels and also a description of damage due to the 1995 Hyogoken-Nanbu (Kobe) earthquake. They reported the following findings concerning past earthquakes:

- Less influence sub-surface than at surface.
- Large part of damage locations coincided with locations of existing faults and fracture zones that had been identified during construction.

- Mountain tunnels in sound rock and lined without material and structural defects are less affected by an earthquake even if it is very large.
- Mountain tunnels may suffer some damage if the tunnel is located near the epicenter of the earthquake fault, when the tunnel has special geological or construction conditions, such as poor slope stability around tunnel portal, crossing existing faults or fracture zones, or if collapse or water inflow trouble occurred during construction.

2.3. Characterization of Rock Mass

There are geological conditions favorable to earthquake damage to shallow and deep-lying underground structures:

- Fault zones which could be activated by earthquake crossing the structure.
- Sudden changes in geological conditions with major contrasts in physical and mechanical properties.
- Potentially liquefiable soils.
- Pore fluids.
- Marked anisotropy in the local stress field combined with steeply dipping joints sets.

The cause of damage in underground structures is due chiefly to irreversible displacement along faults, heavy water inflows, mechanical instability at tunnel portals and soil settlement and rupture due to liquefaction. It is commonly known that the location of other damage coincides with fracture zones encountered during the construction of the tunnel.

The presence of a liquid phase under pressure in the rock mass is a negative factor for any damage which might be sustained by underground structures in a seismic context:

- In soils, the risk of liquefaction related to saturation of the pores is the best illustration of this.
- In rock, significant changes in hydraulic conditions caused by a major earthquake event have been reported but the extent of these effects and their consequences on the structures are difficult to predict through lack of sufficiently well documented reports, and the scale of the processes to be modeled.

2.3.1. Rock Mass Classification

The AFTES (2001) suggest for rock mass classification the use of the information given in table 2.2. This shows additional rock parameters, concerning rock fracturing in particular, i.e. the Rock Quality Designation (RQD) and ID parameter, a discontinuity density index (AFTES Guidelines 1993).

According to AFTES (2001), this classification system must not be substituted for geotechnical investigations suited to the size and purpose of the underground structure. It is strongly recommended that the system must be used only as a general indicator. Besides the addition of columns for RQD and ID, the differences between this classification and the system in the NF standard are:

- There is more detailed discrimination according to the degree of fracturing or weathering of the rock.
- There are different category names for group a cohesive soils and group b moderately cohesive soils.
- The tem rock has been removed from group c.

Table 2.2. Rock Mass classification according to AFTES 2001.

HOST MATERIAL		CPT	SPT	Pressuremeter		Rc*	Vs	Vp		RQD	ID
		Q_c	N	EM	Pl - po			Below w/t	Above w/t		
		(MPa)		(MPa)	(MPa)	(MPa)	(m/s)	(m/s)	(m/s)	(%)	(cm)
Sound, unweathered, unfracture rock		/	/	(see C2.3c)		>10	>800	/	>2500	>75	>60
Group a	Weathered or fractured rock	/	/	50 to 100	2.5 à 5	6 to 10	500 à 800	/	1000 à 2500	50 to 75	20 to 60
	Cohesive soil (stiff clay or marl	>5	/	>25	>2	>0.4	>400	/	>1800	/	/
	Compact granular soil	>15	>30	>20	>2	/	>400	>1800	>800	/	/
Group b	Decomposed or severely fractured rock	/	/	50 to 100	2.5 to 5	1 to 6	300 to 500	/	400 to 1000	<50	<20
	Moderately compact granular soft	5 to 15	10 to 30	6 to 20	1 to 2	/	150 to 400	1500 to 1800	500 to 800	/	/
	Moderately consistent cohesive soil and very soft rock	1.5 to 5	/	5 to 25	0.5 to 2	0.1 to 0.4	150 to 400	/	1000 to 1800	/	/
Group c	Loose granula soil	<5	<10	<6	<1	/	<150	<1500	<500	/	/
	Soft cohesive soil (soft clay or mud)	<1.5	<2	<5	<0,5	<0.1	<150	<1500	<500	/	/

R_C is the unconfined compressive strength (UCS or F_C).

It is recommended characterize the deformability of sound rock from dilatometer tests. This type of test can also be used for rock formations of lesser quality.

2.3.2. Special Recommendation

In rock, special attention have to be given for describing the interfaces between different geological formations crossed by the structure, which may be potential shear zones under seismic loading. If the Norwegian Geotechnical Institute is used, they recommend halving the value of Q classification determined according to standard rock mechanics practice. This change in the Q index is due to the doubling of the Stress Reduction Factor (SRF) by reason of the seismic context (N. Barton 1984).

2.3.3. Additional geotechnical properties to take account in seismically-active areas

It is assumed that the mass density representative of each formation crossed by the underground structure and the hydrogeological site conditions are known. For all rock mass (soil or rock), if the ground-structure interaction is considered, the calculation of longitudinal and transverse dynamic stiffness coefficients requires that the shear stiffness modulus G and Poisson's ratio ν have to be known.

In case where the underground structure passes through fault zones specific seismotectonic study have to be done in order to estimate the orientation of the discontinuities, and the direction and extent of relative displacements between the walls of the faults. Dowding (1979) suggests that strong high-frequency (30-60 Hz) accelerations are probably capable of causing differential movements of rock blocks such as to large excavations.

2.3.4. Special considerations for earthquake design of underground structures

The shear stiffness modulus G and Poisson's ratio ν can be determined by measuring the velocity of the compression wave V_P and shear wave V_S. This can be done in laboratory by using samples or in situ by using sonic surveys, cross hole test or applying other method which yields velocities for waves commensurate with the structure.

Shear wave V_S can be measured from ground level by Spectral Analysis of Surface Waves method for underground structures less than 20m deep and for example by cross hole tests for structures up to depths of 100m below ground level.

The SAWS's method is based on the use of the scattering of Rayleigh waves generated on the surface in harmonic or pulse from (Nazarian & Stoke 1994, Mathews et al 1996). Cross hole tests (ASTM D44-28) are dynamic in situ seismic

transmission tests by using boreholes equipped to measured the P and S wave velocities. The seismic source and pick-ups are set at the same depth in the same borehole.

C. Louis (1974) found a way to relate the ratio between compression wave velocities measured in the situ V_P and on laboratory samples V_{Pl} to RQD as follows:

RQD (%)	0	25	50	75	90	100
Vp / Vpl	0	0.2	0.4	0.6	0.8	1

N. Barton et al, instead, propose a relationship between compression wave velocity V_P and the Q index as follows:

Q	0.001	0.01	0.1	1	10	100	1000
Vp (m/s)	500	1500	2500	3500	4500	5500	6500

Adme Zaneta (2004), on his work "Analysis of NATM tunnel responses due to earthquake loading in various soils" selected some sites according to four basic criteria (history of the city, population of the city, type of tunnel and variance of the soils), to formulate the properties of rock mass (see Table 2.3). This represents another solution respect to AFTES 2001.

Table 2.3. Soil properties (Adme, 2004).

	Soil Type	Mass Density (kg/m^3)	Elastic Modulus (Pa)	Poisson's Ratio	Internal Friction Angle (deg.)	Cohesion (Pa)
Gravel	Uniform	1600	4.00E+07	0.25	34	0
	Sandy w/ few fines	2100	4.00E+07	0.25	35	0
	Sandy w/ silt or clay	2100	4.00E+07	0.25	35	1000
	Mixture of gravel and sand	2000	1.50E+07	0.25	38	3000
Sand	Uniform, fine	1600	1.50E+07	0.25	32	0
	Uniform, coarse	1600	2.50E+07	0.25	34	0
	Uniform, well-graded	1800	2.00E+07	0.25	33	0
Silt	Low plasticity	1750	4.00E+06	0.25	28	2000
	Medium to high plasticity	1700	3.00E+06	0.25	25	3000
Clay	Low plasticity	1900	2.00E+06	0.28	24	6000
	Medium plasticity	1800	1.00E+06	0.25	20	8000
	High plasticity	1650	6.00E+05	0.25	17	10000
	Organic	1550	5.00E+05	0.25	20	7000
Rock	Granite	2700	7.40E+10	0.25	51	5.51E+07

2.4. Seismic Action

The seismic soil vibration is characterized by an ensemble of translational ground motions due to the propagation of P, S, Rayleigh and Love waves. For design purposes, the seismic action can be defined by means of a number of different models, whose complexity should be appropriate to solve the problem.

In the other hand, earthquake damages on underground structures can be grouped into two categories: ground failure as liquefaction, fault displacement and slope instability and ground shaking. Ground failures are the result of seismic shaking. This is particularly prevalent at tunnel portals and in shallows tunnels. Ground shaking corresponds to the deformation of the ground produced by seismic waves propagating

through the surface. The major factors that influence shaking damage are (Dowding and Rozen, 1978; St. John and Zahrah, 1987):

- The shape, dimensions and depth of the structure.
- The properties of the surrounding soil or rock.
- The properties of the structure and the severity of the ground shaking.

The behavior of a tunnel is sometimes approximated to that of an elastic beam subject to deformations imposed by the surrounding ground. According to Owen and Scholl (1981) there are three types of deformations that express the response of underground to seismic motions: axial compression and extension, longitudinal bending and ovaling/raking (Figure 2.6).

The study of underground structure seismic response requires an understanding of the anticipated ground shaking as well as an evaluation of the response of the ground and the structure to such shaking. One of the steps that correspond an approach for evaluating the seismic response of underground structures is the knowledge of the seismic environment.

This can be done by defining a ground motion by characterizing the amplitudes and characteristics of expected ground motions and their expected return frequency (Kramer, 1996). By using a seismic hazard analysis it could possible to characterize the potential for strong motions, the potential fault motion and the frequency in which the faults release stored energy. There are two methods of analysis: (1) the deterministic hazard analysis (DSHA); and (2) the probabilistic seismic hazard analysis (PSHA).

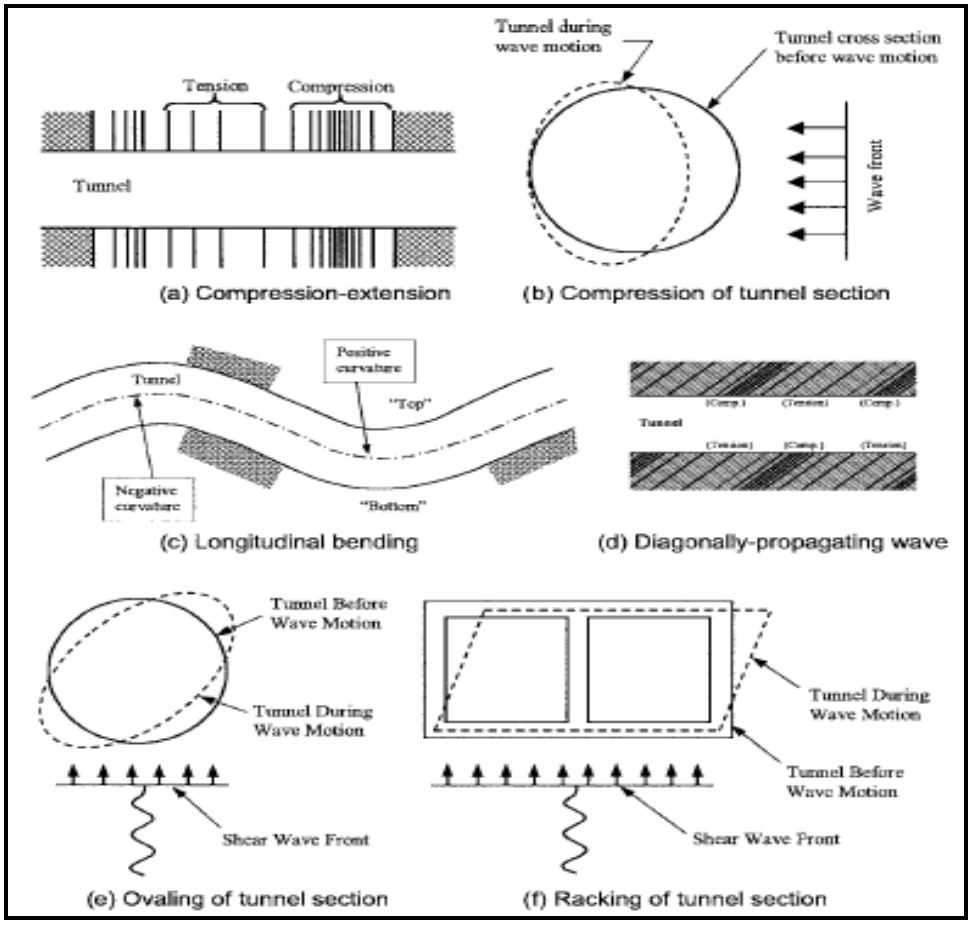

Figure 2.6. Deformations models of tunnels due to seismic waves (after Owen and Scholl, 1981).

2.4.1. Deterministic seismic hazard analysis (DSHA)

A deterministic seismic hazard analysis involves the development of a seismic scenario to summarize the ground motion hazard at a site. This scenario requires the "postulate occurrence" of a particular size of earthquake at a particular location. Reiter (1990) outlines the following four-step (see Figure 2.7).

1. Identification and characterization of all earthquake sources capable of producing significant ground motion at the site, including definition of the geometry and earthquake potential. The most obvious feature delineating a seismic zone is typically the presence of faulting. However, the presence of

fault doesn't mean a potential earthquake hazard, the fault must be active to present a risk.

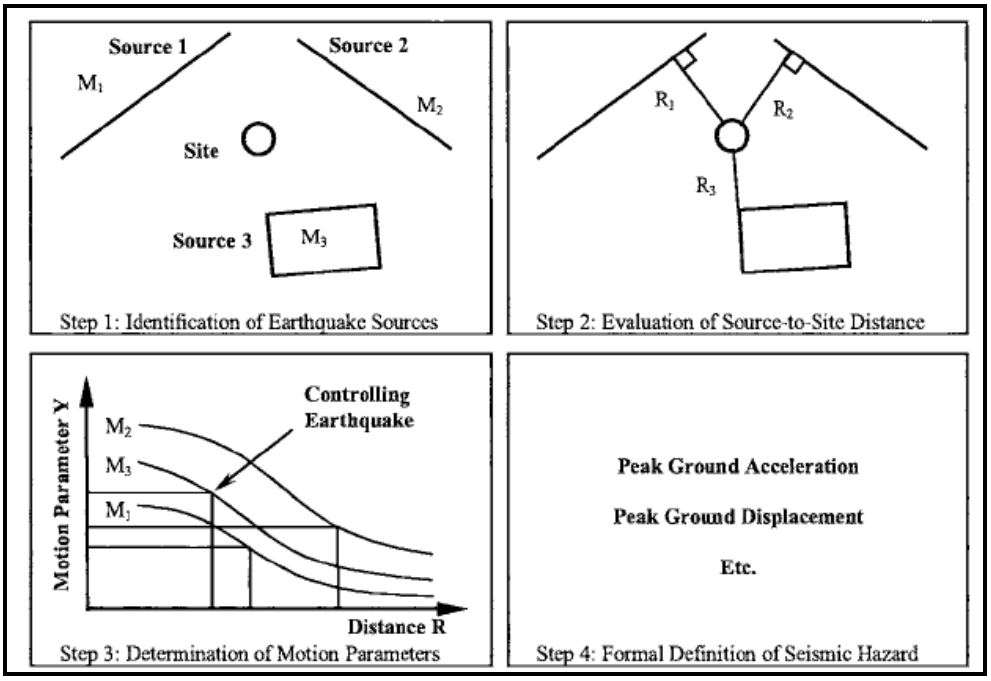

Figure 2.7. Deterministic seismic hazard analysis procedure (after Reiter, 1990).

2. Selection of a source to site distance parameter for each source. This distance is the shortest respect to the fault source.

3. Selection of a controlling earthquake, generally expressed in terms of a ground motion parameter at the site. Attenuation relationships are typically used to determine these site specific parameters from data recorded at nearby locations.

4. Formal definition of the seismic hazard at the site in terms of the peak acceleration, velocity and displacement, response spectrum ordinates, and ground motion time history of the maximum credible earthquake. Design fault displacements should also be defined, if applicable.

A DSHA provides a straightforward framework for the evaluation of worst-case scenarios at a site. However, it does not provide information about likelihood or frequency of occurrence of the controlling earthquake.

Another definition of deterministic approach says that specific earthquake events associated with particular faults are identified, and the sizes (magnitudes, epicentral intensities, etc.) and source-site distances associated with events are used for the development of the response spectra. Standard ground motion versus distance attenuation curves derived from statistical regression analysis are used to establish the general levels of shaking at the site. These ground shaking levels are used to derive response spectra by scaling standardized spectrum shapes.

Standardized spectrum shapes are developed from statistical analysis of response spectra with different levels of damping for an ensemble of measured ground motion records, either for a variety of geologic settings or one specific type of geologic setting.

2.4.2. Probabilistic seismic hazard analysis (PSHA)

A probabilistic seismic hazard analysis provides a framework in which uncertainties in the size, location, and recurrence rate of earthquake can be identified, quantified, and combined in a rational manner. For this type of analysis, future earthquake events are assumed spatially and temporally independent. Reiter (1990) outlined four steps in PSHA (see Figure 2.8).

1. Identification and characterization of earthquake sources, including the probability distribution of potential rupture locations within the source zone. These distributions are combined with the source geometry to obtain the probability distribution of source to site distances.

2. Characterization of the seismicity or temporal distribution of earthquake recurrence. Information obtained from historical data and paleoseismological studies can help to develop a recurrence relationship that describes the average rate at which an earthquake of some magnitude will be exceeded.

3. Determination of the ground motion produced at the site by any size earthquake occurring at any source zone using attenuation relationships. The uncertainty related to in the predictive relationship is also considered.

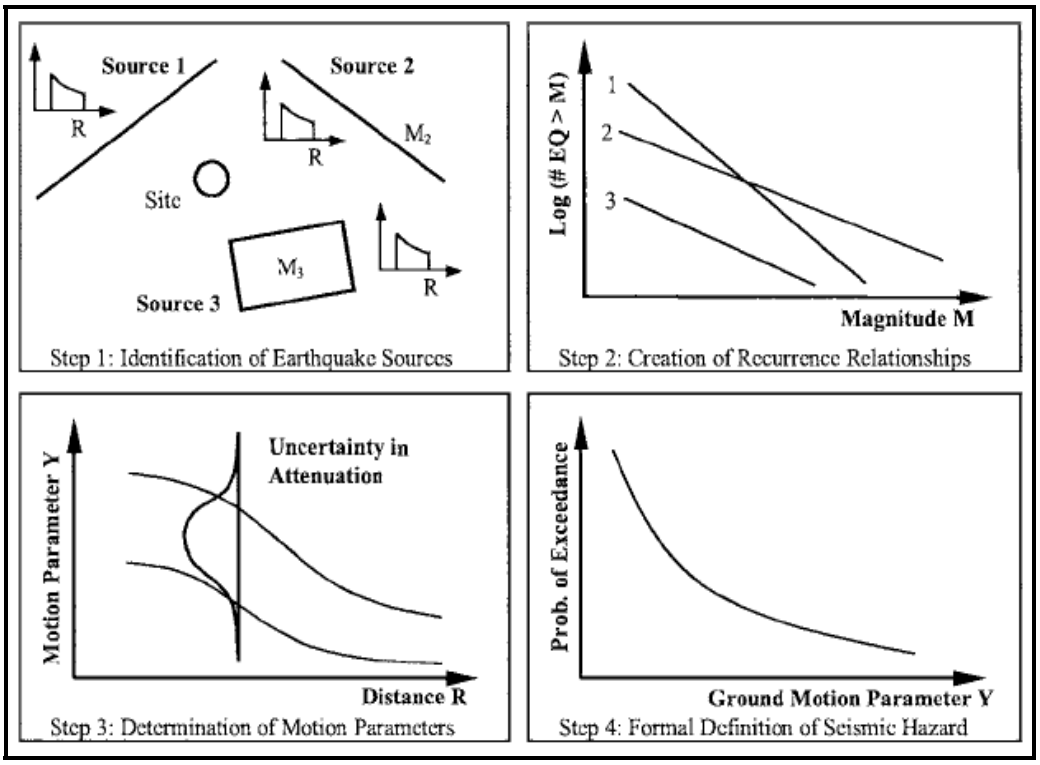

Figure 2.8. Probabilistic seismic hazard analysis procedure (after Reiter, 1990).

4. Combination of the uncertainties to obtain the probability that a given ground motion parameter will be exceeded during a given time period.

The probabilistic approach incorporates the uncertainties in source to site distance, magnitude, rate of recurrence and the variation of ground motion characteristic into the analyses. In areas where no active faults can be readily identified it may be necessary to rely on a purely statistical analysis of historic earthquakes in the region.

Another definition is given by C. M. St John and T. F. Zahrah (1987). This method uses simple probabilistic models as tools for estimating effects of uncertainties in the occurrence of earthquakes and in the attenuation relationships. The occurrence of earthquakes events in time and space within each potential earthquake source is represented using a simple probabilistic model. Most commonly, it is assumed that the future earthquake events are spatially and temporally independent.

In its simplest form, the current practice is, typically, to use peak ground acceleration as the single measure of the strength of shaking at the site. Peak acceleration versus probability curves are developed and are entered at a selected probability level in order to define the peak ground acceleration. This acceleration is then used to scale a fixed spectrum shape in order to obtain the site design response spectra.

Another way to quantify the type of deformation that the underground structure can suffer is necessary, first, know the different earthquakes actions in an underground engineering context. This derives from that used in surface structure construction, defined in regulations and/or contract specifications.

This and several alternative approaches can be used for defining seismic action. Another of these approaches consists in to specify ground motion time histories. This method allows engineers to outline the track active faults and their release of seismic potential energy. In this case an ensemble of motion time histories, rather than a single time history, should be specified. The family of motions should have the same overall intensity and frequency content, and should be representative of the anticipated shaking at the significant potential earthquake sources in the vicinity of the site. The procedure used to select the motion time histories is described by Werner (1985).

An alternative approach involves the use of seismic regionalization maps of the type used in the seismic design guidelines suggested by the Applied Technology Council (ATC 1978). These are planned to provide representative intensities of shaking for the regions under consideration, based on their seismologic and geologic characteristics. This intensity factor is used, together with a numerical factor R, in order to incorporate the influence of the seismic environment in the computation of equivalent forces upon which the seismic design of the structure is based (Berg 1982).

2.5. Seismic Design Analysis in Underground Structures

Although sophisticated methods to investigate the dynamic responses of underground structures to seismic loading are available, design tools remain relatively simple. Simple procedures to facilitate identification of factors important to design, to define design loads, and to verify design adequacy are going to be shown below. These, or similar procedures, should always be used as a starting point for any analyses of subsurface excavations and their ground support system, and underground structures (C. M. St John and T. F. Zahrah, 1987).

2.5.1. Design against fault displacement

It is necessary to take into account for a tunnel design the potential offset at an active fault. These features that mitigate the effect of the offset and facilitate post-earthquake repairs consist in the excavation of an oversize section through support system; or in incorporating a flexible coupling, if the tunnel is lined.

The design of flexible couplings, or joints, has received considerable attention because they also require at interfaces between different geologic media and between sections of an underground structure that will respond differently to seismic loading. For example, Hradilek (1977) offers recommendations for the design of reinforced concrete conduits crossing a known active fault zone. However, the design objective

is to achieve the necessary flexibility in the liner, or conduit, to permit the relative motion without major damage. How this objective is achieved will be site specific and project specific (C. M. St John and T. F. Zahrah, 1987).

2.5.2. Design of portals and very shallow tunnels

It is known that tunnel portals appear to be particularly susceptible to damage. This could be due to occurrence of superficial failures that may be entirely unrelated to the tunnel. The site investigation required to determine the potential for superficial failures even is beyond of the study. However, it is appropriate to note that the principal failure modes of concern are slope instability, soil liquefaction and differential settlement. Particular precautions should be taken if portal structure also acts as a soil retaining wall.

As noted, the primary objective is to increase the flexibility so that differential motion can be survived without significant damage (C. M. St John and T. F. Zahrah, 1987). For tunnels in soil or rock, such flexibility is best provided by closely spaced steel sets, or ribs. Static design procedures for this type of support are relatively well established.

2.5.3. Design against ground shaking

Simplified models are considered in order to estimate the stresses and strains that an underground structure could be subjected to ground shaking during an earthquake, and the resulting additional dynamic loads that will be applied to a support system. These models are appropriate include lined and unlined tunnels in soil and rock, subaqueous tunnels and cut and cover construction.

The distinction between the many types is drawn not upon the basis of the function that the excavation serves but upon: (a) the nature of the geologic medium; (b) the extent to which any support system may resist the ground motion in the medium; and (c) the method of construction.

An example of simple model corresponds to a compressional wave propagating parallel to the axis of a subsurface excavation (Figure 2.6a). For practical purpose,

interaction between the wave and the excavation can be ignored, although the changes in axial stress will cause some closure or enlargement of the cross section as the rock or soil respond to the applied loads (C. M. St John and T. F. Zahrah, 1987).
For the case of a wave propagating normal to the tunnel axis (Figure 2.6b), the stress induces a deformation of the cross-section. The type of asymmetric deformation of the cross-section in the figure will be observed only if the wavelength is short relative to the tunnel diameter. In the more general cases, the wave induce curvature of the structure (Figure 2.6e). This phenomenon will induce alternate regions of compression and tension along the tunnel.

2.5.4. Simple models for design

Considerable attention has been devoted to studying stress concentrations around lined and unlined tunnels subjected to both simple harmonic or transient loading. Mow and Pao (1971), for example, studied the interaction of steady-state P waves in tunnels where the propagation direction is normal to the longitudinal axis (figure 2.6a). As a result, it has been concluded that the peak stress concentration due to harmonic loading may exceed the static values by 10 – 15% for P waves and 5% for S waves.

Stress concentration factors alone are insufficient for design an underground structure. The designer needs to be able to predict, at least in an approximate manner, the stress distribution in the medium and the liner thrust and bending moment that will be experienced as a result of any given ground motion. Such predictions generally require application of numerical models, based on finite element or finite difference techniques (St. John & Zahrah, 1984).

When such calculations are performed, it is found that there is remarkably little difference between the stresses in the medium and liner between the transient and static cases, provided that the wavelength of the incident wave is relatively long. Figure 2.9 shows the radial and circumferential stresses for a tunnel supported by a

thin liner. In the dynamic case, the tunnel has been fully engulfed by a dilatational wave.

In this figure, the free field stresses correspond to a vertically propagating dilatational wave (P wave). The stresses have been normalized so that the peak horizontal and vertical stresses in the free field are respectively 1.0 and 0.333. The close parallel between the static and dynamic solutions allows simple "static" design models to be used to predict the consequences of dynamic loading having relatively long wavelengths (St. John & Zahrah, 1984).

Models like this are used to calculate circumferential stress, thrusts bending moments in a liner once the applied loads have been estimated. A tunnel liner must be designer to withstand those loads, in addition to the pre-existing static loads. It must also take into account the axial and shear loads, and bending stresses due to curvature (see figure 2.10). Each must be estimated in order to select the appropriate tunnel section or predict the consequence of seismic loading St. John & Zahrah, 1984).

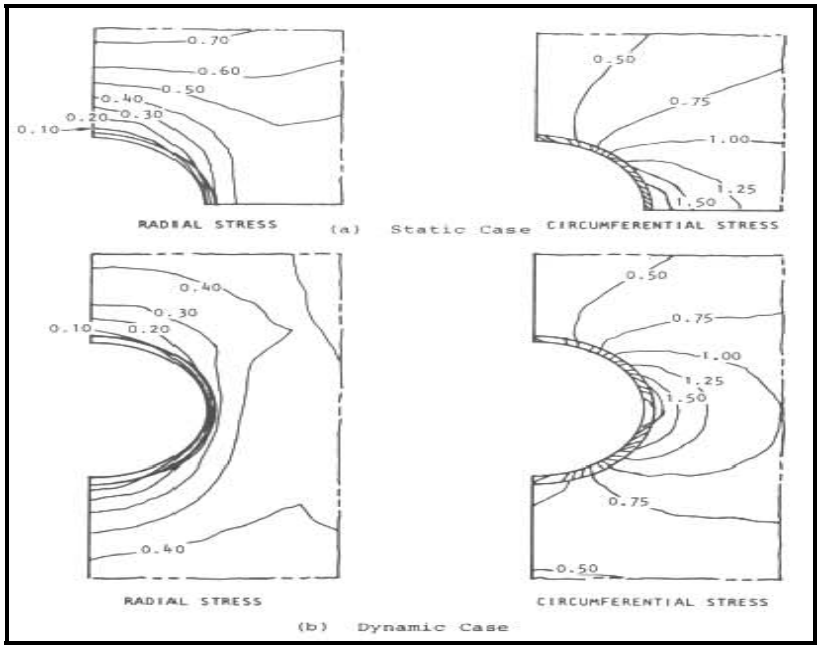

Figure 2.9. Radial and circumferential stresses in a tunnel lining and surrounding medium (St. John & Zahrah, 1984).

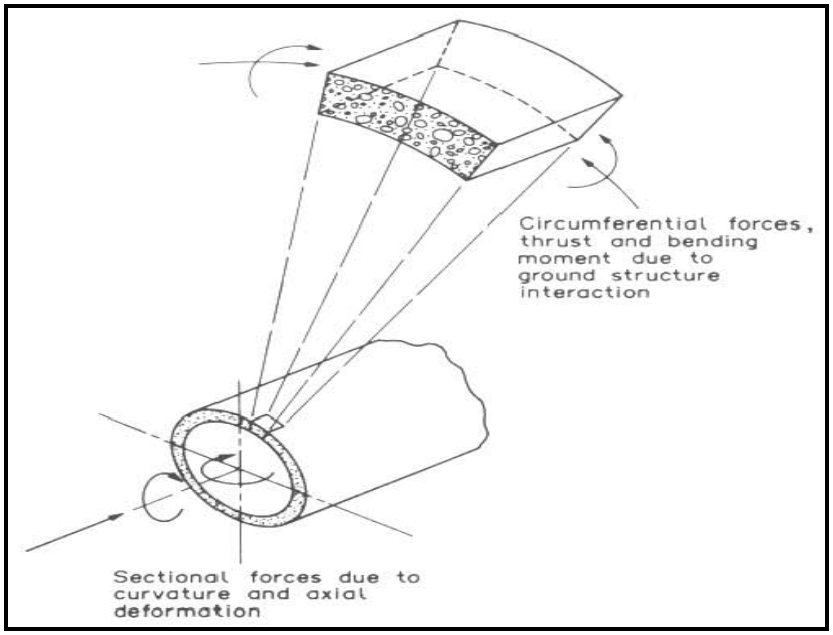

Figure 2.10. Identification of design parameters

for a tunnel section (Modified from Owen and Scholl, 1981).

2.5.5. Seismic design loading criteria

Design loading criteria for underground structures has to incorporate the additional loading imposed by ground shaking and deformation (Hashash, Hook, Schmidt and Yao, 2001). Once the ground motion parameters for the maximum and operational design earthquakes have been determined, load criteria are developed for the underground structure using the load factor design method. This criteria is explained as follow:

- *Loading criteria for maximum design earthquake (MDE):* The MDE is defined as the maximum level of shaking that can be experienced at the site for Deterministic Seismic Hazard Analysis (DSHA) instead for Probabilistic Seismic Hazard Analysis (PSHA) is defined as an event with a small probability of exceedance during the life of the facility. However, the MDE design goal is that public safety shall be maintained during and after the event.

In this case the loading criteria is applied for cut and cover tunnel structures and for bored or mined tunnel lining, the required structural strength (U) is calculated.

- *Loading criteria for opening design earthquake (ODE):* The ODE is an earthquake event that can be reasonably expected to occur at least once during the design life of the facility. In an ODE analysis, the seismic design loading depends on the structural performance requirements of the structural members. Since the goal is that overall system shall continue operating during and after an ODE and experience little or no damage, inelastic deformations must be kept to a minimum (Hashash, Hook, Schmidt and Yao, 2001). For the loading criteria, the seismic design loading combination depends on the performance requirements of the structural members. Also for this case the required structural strength (U) is calculated for cut and cover tunnel structure and for bored or mined tunnel lining.

2.6. Concluding remarks

This chapter represents a summary of the current state of seismic analysis and design for underground structures. As one may see in the section about **Earthquake damage on Underground structures**, examples of earthquake damages were presented together with the previous to be taken in order to prevent major catastrophe in some countries where the seismic activities are very frequent. Sharma and Judd (1991) concluded a series of important consideration for the design of underground structures like depth and geometry of the tunnel, and type of rock mass from a seismic point of view.

Taking a look of the Loma Prieta Earthquake in San Francisco, USA, it is possible to see the two faces of the effects in an underground structure with and without seismic design criteria. In the BART system, the structure did not suffer any damage. This has

permitted the normal use of the activities in the structure after the earthquake and the safeguard of life. In the other hand, the Alameda Tubes suffered damage that affected the systems of the structure and, therefore, the impossibility of the traffic circulation. In this order, it is important in countries where frequent earthquake take place to have in mind the influence of potential backgrounds to maintain or design safe tunnel.

When an earthquake is produced the presence of water in the rock mass inflows in the mechanical instability at tunnel portals, soil settlement and rupture due to liquefaction. Performing a geotechnical analysis implies the appropriate characterization of the rock mass. If the quality of the rock mass is not good enough, rock mass reinforcements strategies have to be applied.

Seismically active regions should incorporate the use of thin flexible liners of fibre or mesh reinforced shotcrete and systematic rock bolting, to increase the modulus of the surrounding ground. In case where is detected the presence of faults, important consideration have to be done in order to prevent the rupture of the tunnel in the interface when this traverses the fault.

Depending on the medium and the shape of the ground structure, the kind of deformation due to seismic waves (Figure 5) can vary. This of course generates compression and tension zones inside the tunnel that affect its stability. In this manner, appropriate structural analysis has to be applied by, first, performing seismic hazard analysis.

It is important the development of improved numerical models to simulate the dynamic soil structure interaction problem of tunnels, as well as portal and subway structures. These allow the study of the effect of high velocity pulses generated near fault sources on underground structures (Hashash et al., 1998).

Finally, as St John and Zahrah (1987) said, different seismic design criteria, have to be taken into account just as a starting point for any analyses of subsurface excavations and their ground support system, and underground structures.

CHAPTER III

ANALYTICAL APPROACH APPLIED TO UNDERGROUND STRUCTURES

3.1. Introduction

This chapter describes procedures used to compute deformations and forces corresponding to three deformation modes: compression-extension, longitudinal bending and ovalling, as shown below. A second part of this chapter shows the analytical approach due to Corigliano et. al. (2006); in general it is possible to see the description of the analysis of transverse response (ovaling deformation).

Appendix B describes the analytical approach applied by Marchant and Weir (2004) in New Zealand using an empirical relation from seismology to relate earthquake magnitude, distance from the epicenter and the peak ground acceleration resulting from the seismic wave in order to estimate the likely damage at the mine site. On appendix C, the analytical approach due to Richardson and Blejwas for an underground repository located in a seismic region in USA is described, taking special attention to in the design and performance of lined openings in a seismic environment.

3.2. Free field deformation approach

The term “Free field deformations” describes ground strains caused by seismic waves in the absence of structures or excavations. These deformations ignore the interaction between the underground structure and the surrounding ground, but can provide a first order estimate of the anticipated deformation of the structure. The analytical

procedure for estimating these strains and stresses is based on the theory of wave propagation in homogeneous, isotropic elastic media.

3.2.1. Closed form elastic solutions

Simplified, closed form solutions are useful for developing initial estimates of strains and deformations in a tunnel. These simplified methods assume the seismic wave field to be that of plane waves with the same amplitudes at all locations along the tunnel, differing only in their arrival time.

Newmark (1968) and Kuesel (1969) proposed a simplified method for calculating free field ground strains caused by a harmonic wave propagating at a given angle of incidence in a homogeneous, isotropic, elastic medium (Fig. 3.1).

The most critical incident angle yielding maximum strain is typically used as a safety measure against the uncertainties of earthquake prediction.

Newmark's approach provides an order of magnitude estimate of wave-induced strains while requiring a minimal input, making it useful as both as initial design tool and a method of design verification (Wang, 1993).

Figure 3.1 shows the behavior of a transversal displacement (u_y) end the axial displacement (u_x) for a tunnel exposed to the Newmark's approach with a wavelength L and amplitude D.

St. John and Zahrah (1987) used Newmark's approach to develop solutions for free-field axial and curvature strains due to compression, shear and Rayleigh waves. Solutions for all three types are shown in Table 3.1, though S-waves are typically associated with peak particle accelerations and velocities (Power et al., 1996).

The seismic waves causing the strains are shown in Fig. 3.2. It is usually difficult to determine which type of wave will dominate a design. Strains produced by Rayleigh waves tend to govern only in shallow structures and at sites far from the seismic source (Wang, 1993).

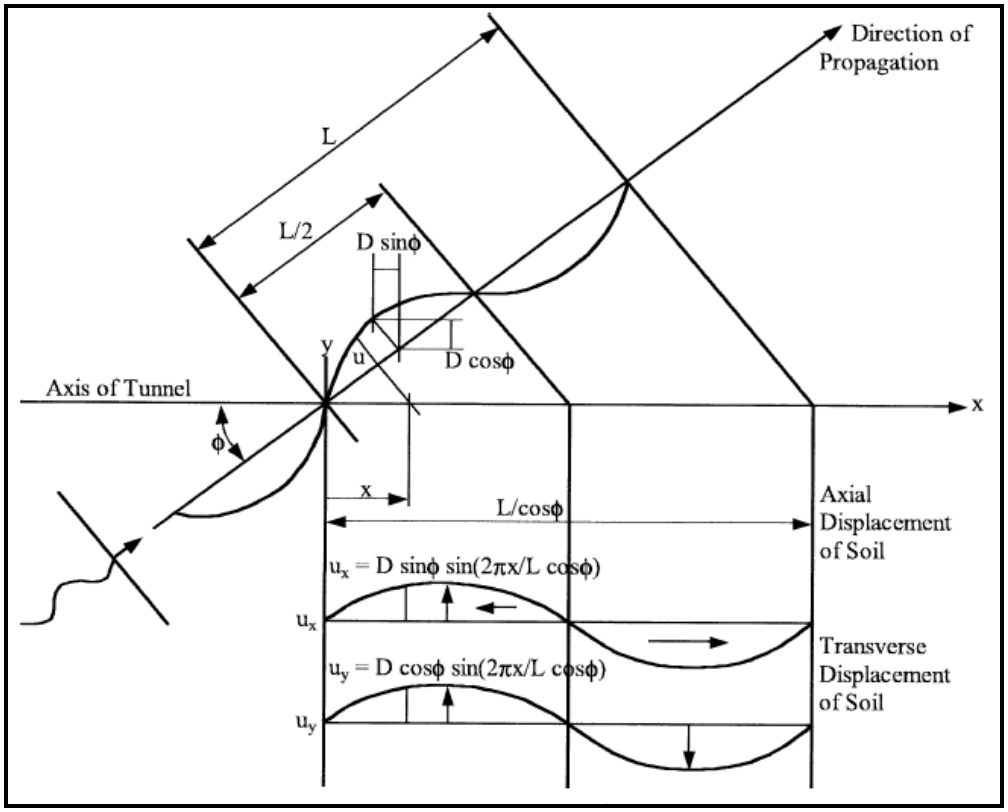

Figure 3.1. Simple harmonic wave and tunnel (after Wang, 1993).

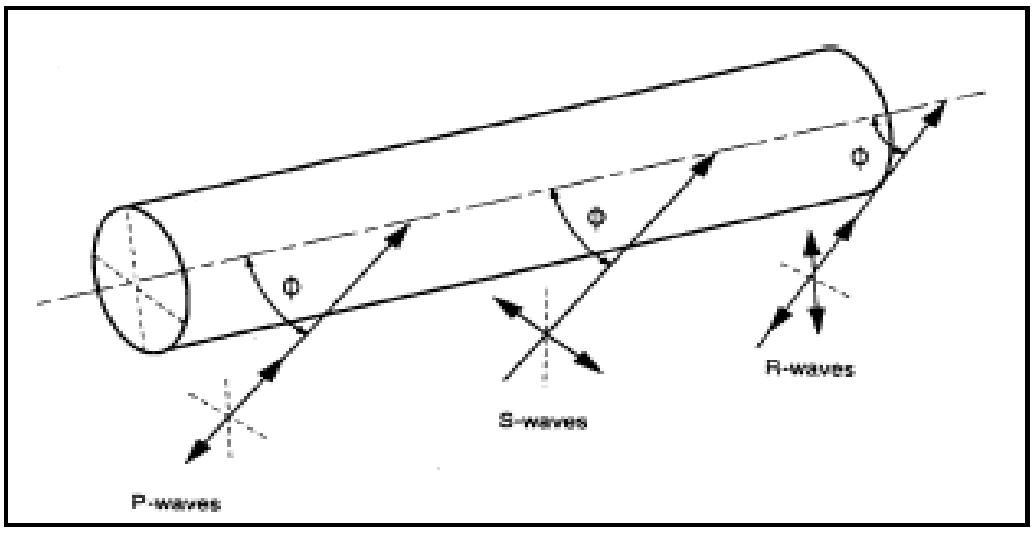

Figure 3.2. Seismic wave causing longitudinal axial and bending strains (Power et al., 1996).

Assuming that a tunnel, whether lined or unlined, conforms to the ground deformation, the total axial strain will be the combined effect of axial deformation and bending.

$$\varepsilon^{ab} = \left[\frac{V_P}{C_P}cos^2\phi + r\frac{a_P}{C_P^2}sin\phi cos^2\phi\right] \quad (3.1)$$

for P – waves

$$\varepsilon^{ab} = \left[\frac{V_S}{C_S}cos\phi sin\phi + r\frac{a_S}{C_S^2}cos^3\phi\right] \quad (3.2)$$

for S – waves

$$\varepsilon^{ab} = \left[\frac{V_R}{C_R}cos^2\phi + r\frac{a_R}{C_R^2}sin\phi cos^2\phi\right] \quad (3.3)$$

for Rayleigh – waves (compressional component)

where:

r: radius of circular tunnel or half height of a rectangular tunnel.

a_P: peak particle acceleration associated with P – wave.

a_S: peak particle acceleration associated with S – wave.

a_R: peak particle acceleration associated with Rayleigh – wave.

φ: angle of incidence of wave with respect to tunnel axis.

ν_l: Poisson's ratio of tunnel lining material.

V_P: peak particle velocity associated with P – wave.

C_P: apparent velocity of P – wave propagation.

V_S: peak particle velocity associated with S – wave.

Table 3.1. Strain and curvature due to the body and surface waves (after St. John and Zahrah, 1987).

Wave type	Longitudinal strain	Normal strain	Shear strain	Curvature
P-wave	$\varepsilon_l = \frac{V_p}{C_p}\cos^2\phi$	$\varepsilon_n = \frac{V_p}{C_p}\sin^2\phi$	$\gamma = \frac{V_p}{C_p}\sin\phi\cos\phi$	$\frac{1}{\rho} = \frac{a_p}{C_p^2}\sin\phi\cos^2\phi$
	$\varepsilon_{lm} = \frac{V_p}{C_p}$ for $\phi = 0°$	$\varepsilon_{nm} = \frac{V_p}{C_p}$ for $\phi = 90°$	$\gamma_m = \frac{V_p}{2C_p}$ for $\phi = 45°$	$\frac{1}{\rho_{max}} = 0.385\frac{a_p}{C_p^2}$ for $\phi = 35°16'$
S-wave	$\varepsilon_l = \frac{V_s}{C_s}\sin\phi\cos\phi$	$\varepsilon_n = \frac{V_s}{C_s}\sin\phi\cos\phi$	$\gamma = \frac{V_s}{C_s}\cos^2\phi$	$K = \frac{a_s}{C_s^2}\cos^3\phi$
	$\varepsilon_{lm} = \frac{V_s}{2C_s}$ for $\phi = 45°$	$\varepsilon_{nm} = \frac{V_s}{2C_s}$ for $\phi = 45°$	$\gamma_m = \frac{V_s}{C_s}$ for $\phi = 0°$	$K_m = \frac{a_s}{C_s^2}$ for $\phi = 0°$
Rayleigh wave Compressional component	$\varepsilon_l = \frac{V_{RP}}{C_R}\cos^2\phi$	$\varepsilon_n = \frac{V_{RP}}{C_R}\sin^2\phi$	$\gamma = \frac{V_{RP}}{C_R}\sin\phi\cos\phi$	$K = \frac{a_{RP}}{C_R^2}\sin\phi\cos^2\phi$
	$\varepsilon_{lm} = \frac{V_{RP}}{C_R}$ for $\phi = 0°$	$\varepsilon_{nm} = \frac{V_{RP}}{C_R}$ for $\phi = 90°$	$\gamma_m = \frac{V_p}{2C_R}$ for $\phi = 45°$	$K_m = 0.385\frac{a_{RP}}{C_R^2}$ for $\phi = 35°16'$
Shear component		$\varepsilon_n = \frac{V_{RS}}{C_R}\sin\phi$	$\gamma = \frac{V_{RP}}{C_R}\cos\phi$	$K = \frac{a_{RS}}{C_R^2}\cos^2\phi$
		$\varepsilon_{nm} = \frac{V_{RS}}{C_R}$ for $\phi = 90°$	$\gamma_m = \frac{V_{RS}}{C_R}$ for $\phi = 0°$	$K_m = \frac{a_{RS}}{C_R^2}$ for $\phi = 0°$

The Poisson's ratio and dynamic modulus of a soil deposit can be computed from measured P- and S-wave propagation velocities in an elastic medium: $v_m = \frac{1}{2}\frac{(C_p/C_s)^2 - 2}{(C_p/C_s)^2 - 1}$ or $C_p = \sqrt{\frac{2(1-v_m)}{(1-v_m)}}C_s$; $E_m = \rho C_p^2\frac{(1+v_m)(1-2v_m)}{(1-v_m)}$; and $G_m = \rho C_s^2$, respectively.

C_S: apparent velocity of S – wave propagation.

V_R: peak particle velocity associated with Rayleigh – wave.

C_R: apparent velocity of Rayleigh – wave propagation.

Having evaluated the strains resulting from seismic waves, the induced stresses are considered, since those are the more common boundary conditions for any design models. The stresses in the medium can be determined from the constitutive relationship for a linear elastic isotropic material:

$$\sigma_x = \frac{E}{(1+\nu)(1-2\nu)}\left((1-\nu)\varepsilon_x + \nu(\varepsilon_x + \varepsilon_z)\right) \quad (3.4)$$

And

$$\tau_{xy} = G\gamma_{xy} \quad (3.5)$$

In which σ_x and τ_{xy} are, respectively, the normal and the shear stresses and E and G the elastic modulus and shear modulus. From equation (3.4) and Table 3.1, the maximum normal stress due to P – wave occurs when the wave propagates parallel to the axis of the tunnel and is equal to:

$$\sigma_p = \frac{(1-\nu)E}{(1+\nu)(1-2\nu)}\frac{V_p}{C_p} \quad (3.6)$$

A similar procedure can be used to derive expressions for the maximum normal and shear stresses for the P and S –waves. These, along with the critical angle of incidence are summarized in Table 3.2.

If simple continuum models of the tunnel structure are used as a basis for design, these stresses are the "remote" boundary conditions. If, instead, the tunnel structure is treated as a simple beam, then the design strains and curvatures are given directly by Table 3.1.

Table 3.2. Maximum stresses resulting from body waves (after St. John and Zahrah, 1984).

	Maximum normal stress		Maximum shear stress
P-Wave	$\frac{(1-\nu)E}{(1+\nu)(1-2\nu)}$	$\frac{V_p}{c_p}$	$\frac{G\,V_p}{2c_p}$
	$\theta = 0$		$\theta = 45°$
S-wave	$\frac{E}{(1+\nu)(1-2\nu)}$	$\frac{V_s}{2c_s}$	$\frac{G\,V_s}{c_s}$
	$\theta = 45°$		$\theta = 0$

In general, as the radius increases, the contribution of curvature deformation to axial strain increases. However, as it is possible see on table 1 the bending component of strain is, relatively, small compared to axial strains for tunnels under seismic loading.

According to Wang (1993), the cyclic nature of the axial strains should also be noted – although a tunnel lining may crack in tension, this cracking is usually transient due to the cyclic nature of the incident waves. The reinforcing steel in the lining will close these cracks at the end of the shaking.

Even unreinforced concrete linings are considered adequate as long as the cracks are small, uniformly distributed, and do not adversely affect the performance of the lining.

Data from Power et al., 1996, specify an apparent S – wave velocities fall in the range of 2 – 4 km/s while apparent P – wave velocities fall in the range of 4 – 8 km/s.

3.2.2 Ovaling deformation of circular tunnels

Ovaling deformations are developed when waves propagate perpendicular to the tunnel axis (typically under two-dimensional, plane-strain conditions).

Studies have suggested that, while ovaling may be caused by waves propagating horizontally or obliquely, vertically propagating shear waves are the predominant form of earthquake loading that causes these types of deformations (Wang, 1993).

Ground shear distortions can be defined in two ways (see Fig. 3.3). In the non-perforated ground, the maximum diametric strain is a function of maximum free-field shear strain only:

$$\frac{\Delta d}{d} = \pm \frac{\gamma_{max}}{2} \tag{3.7}$$

The diametric strain in a perforated ground is further related to the Poisson's ratio of the medium:

$$\frac{\Delta d}{d} = \pm 2\gamma_{max}(1 - \upsilon_m) \tag{3.8}$$

Both of these equations assume the absence of the lining, therefore ignoring tunnel-ground interaction. In the free-field, the perforated ground would yield a much greater distortion than the non-perforated, sometimes by a factor of two or three.

This provides a reasonable distortion criterion for a lining with little stiffness relative to the surrounding soil, while the non-perforated deformation will be appropriate when the lining stiffness is equal to that of the medium. A lining with large relative stiffness should experience distortion even less than those given by Eq. (3.7) (Wang, 1993).

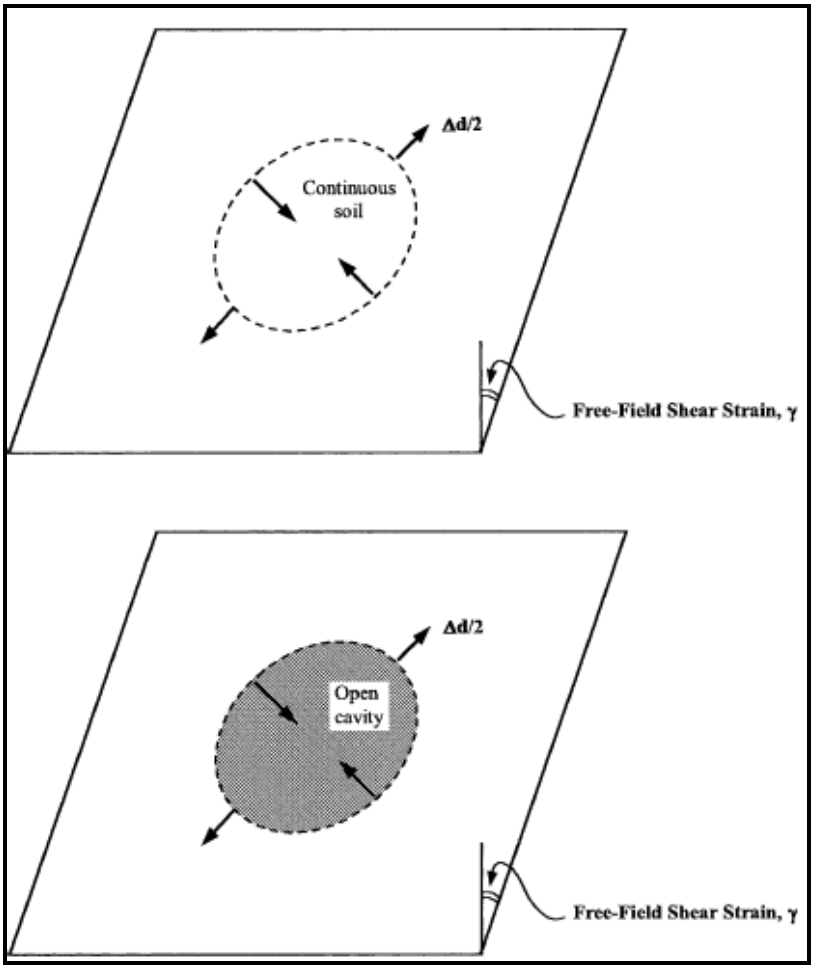

Figure 3.3. Free-field shear distortion of perforated and non-perforated ground, circular shape (after Wang, 1993).

3.3. Soil structure interaction approach

The presence of underground structure modifies the free field ground deformations. The analytical procedure for estimating strains and stresses is based on the theory of wave propagation in an infinite, homogeneous, isotropic, elastic medium, and the theory for an elastic beam on an elastic foundation. The beam theory is necessary to account for the effects of interaction between the soil and the tunnel structure.

The effects of first transverse horizontal shear waves and subsequently vertical shear waves are considered. The approach used to evaluate the effect of shear waves is also applicable to the case of compressional waves.

3.3.1. Closed form solution for circular tunnels, axial force and moment

The beam theory is used to model soil-structure interaction effects. The solutions ignore dynamic (inertial) interaction effects. Under seismic loading, the cross-section of a tunnel will experience axial bending and shear strains due to free field axial, curvature, and shear deformations. The maximum structural strains are (after St. John and Zahrah, 1987):

$$\varepsilon_{max}^{a} = \frac{\left(\frac{2\pi}{L}\right)A}{2+\frac{E_l A_c}{K_a}\left(\frac{2\pi}{L}\right)^2} \leq \frac{fL}{4E_l A_c} \qquad (3.9)$$

Where:

L: wavelength of an ideal sinusoidal shear wave.

K_a: longitudinal spring coefficient of medium (in force per unit deformation per unit length of tunnel).

A: free-field displacement response of an ideal sinusoidal shear wave.

A_c: cross-sectional area of tunnel lining.

E_l: elastic modulus of the tunnel lining.

f: ultimate friction force (per unit length) between tunnel and surrounding soil.

The forces and moments in the tunnel lining due to seismic waves propagating along the tunnel axis are shown in Fig. 3.4a. The maximum frictional forces that can be developed between the lining and the surrounding soils limit the axial strain in the lining. This maximum frictional force, $(Q_{max})_f$, can be estimated as the ultimate frictional force per unit length time one-quarter the wavelength, as shown in Eq. (3.9) (Sakurai and Takahashi, 1969).

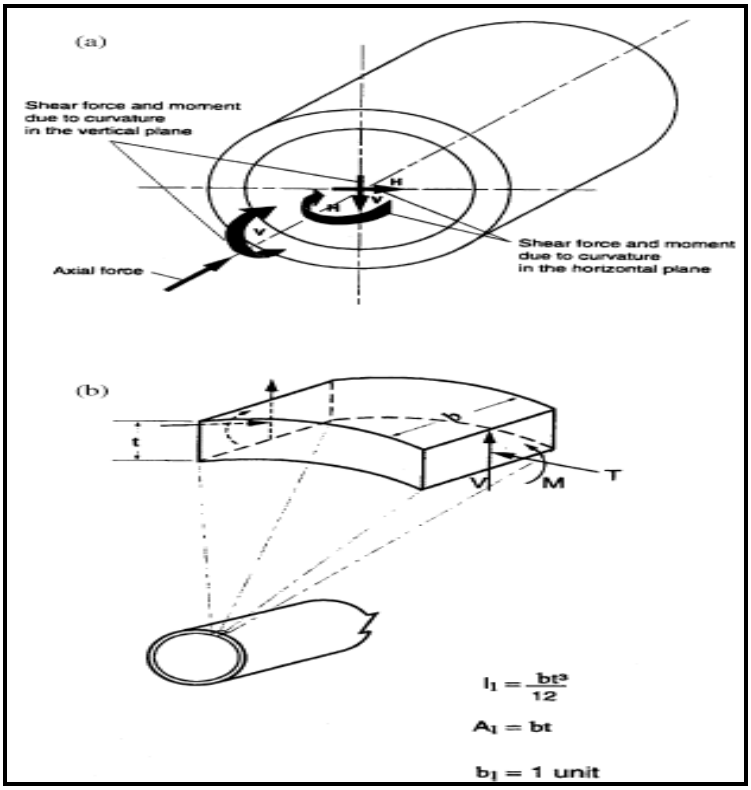

Figure 3.4. Induce forces and moments caused by seismic waves (Power et al., 1996), (a) Induced forces and moments caused by waves propagating along tunnel axis, (b) Induced circumferential forces and moments caused by waves propagating perpendicular to tunnel axis.

The maximum bending strain, caused by 0° incident shear wave is:

$$\varepsilon_{max}^{b} = \frac{\left(\frac{2\pi}{L}\right)A}{1+\frac{E_l I_c}{K_t}\left(\frac{2\pi}{L}\right)^4} r \qquad (3.10)$$

Where:

I_c: moment of inertia of the tunnel section.

K_t: transverse spring coefficient of the medium (in force per unit deformation per unit length of tunnel), equal to K_a.

r: radius of circular tunnel or half height of a rectangular tunnel.

A conservative estimate of the total axial strain and stress is obtained by combining the strains from the axial and bending forces (modified from Power et al., 1996):

$$\varepsilon^{ab} = \varepsilon_{max}^{a} \mid \varepsilon_{max}^{b} \qquad (3.11)$$

For Wang (1993), these equations are necessary only for structures built in soft ground, as structures in rock or stiff soils can be designed using free-field deformations. It should be noted that increasing the structural stiffness and the strength capacity of the tunnel may not result in reduced forces – the structure may actually attract more force.

3.3.2. Ovaling deformations of circular tunnels

In early studies of ovaling deformations closed-form solutions were proposed in terms of thrust, bending moments, and displacements under external loading conditions. The response of a tunnel lining is a function of the compressibility and flexibility ratios of the structure, and the in-situ overburden pressure ($\gamma_t h$) and at-rest coefficient of earth pressure (K_o) of the soil.

The stiffness of a tunnel relative to the surrounding ground is quantified by the compressibility and flexibility ratios (C and F), which are measures of the extensional stiffness and the flexural stiffness (resistance to ovaling) (Merritt et al., 1985):

$$C = \frac{E_m(1-v_l^2)r}{E_l t(1+v_m)(1-2v_m)} \tag{3.12}$$

$$F = \frac{E_m(1-v_l^2)R^3}{6E_l I(1+v_m)} \tag{3.13}$$

Where E_m = modulus of elasticity of the medium, I = moment of inertia of the tunnel lining (per unit width) for circular lining R, and t =radius and thickness of the tunnel lining.

Assuming full-slip conditions, without normal separation and therefore, no tangential shear force, the diametric strain, the maximum thrust, and bending moment can be expressed as (Wang, 1993):

$$\frac{\Delta d}{d} = \pm\frac{1}{3}K_1 F\gamma_{max} \tag{3.14}$$

$$T_{max} = \pm\frac{1}{6}K_1\frac{E_m}{(1+\upsilon_m)}r\gamma_{max} \tag{3.15}$$

$$M_{max} - \pm\frac{1}{6}K_1\frac{E_m}{(1+\upsilon_m)}r^2\gamma_{max} \tag{3.16}$$

Where:

$$K_1 = \frac{12(1-\upsilon_m)}{2F+5-6\upsilon_m} \tag{3.17}$$

These forces and moments are illustrated in Fig. 3.4b. The relationship between the full-slip lining response coefficient (K_1) and flexibility ratio is shown in Fig. 3.5.

According to various studies, slip at the interface is only possible for tunnels in soft soils or cases of severe seismic loading intensity. For most tunnels, the interface condition is between full-slip and no-slip, so both cases should be investigated for critical lining forces and deformations. However, full-slip assumptions under simple shear may cause significant underestimation of the maximum thrust, so it has been recommended that the no-slip assumption of complete soil continuity be made in assessing the lining thrust response (Hoeg, 1968; Schwartz and Einstein, 1980):

$$T_{max} = \pm K_2\tau_{max}r = \pm K_2\frac{E_m}{2(1+\upsilon_m)}r\gamma_{max} \tag{3.18}$$

Where:

$$K_2 = 1 + \frac{F\left[(1-2\upsilon_m)-(1-2\upsilon_m)C-\frac{1}{2}(1-2\upsilon_m)^2\right]+2}{F[(3-2\upsilon_m)-(1-2\upsilon_m)C]+C\left[\frac{3}{2}-8\upsilon_m+6\upsilon_m^2\right]+6-8\upsilon_m} \tag{3.19}$$

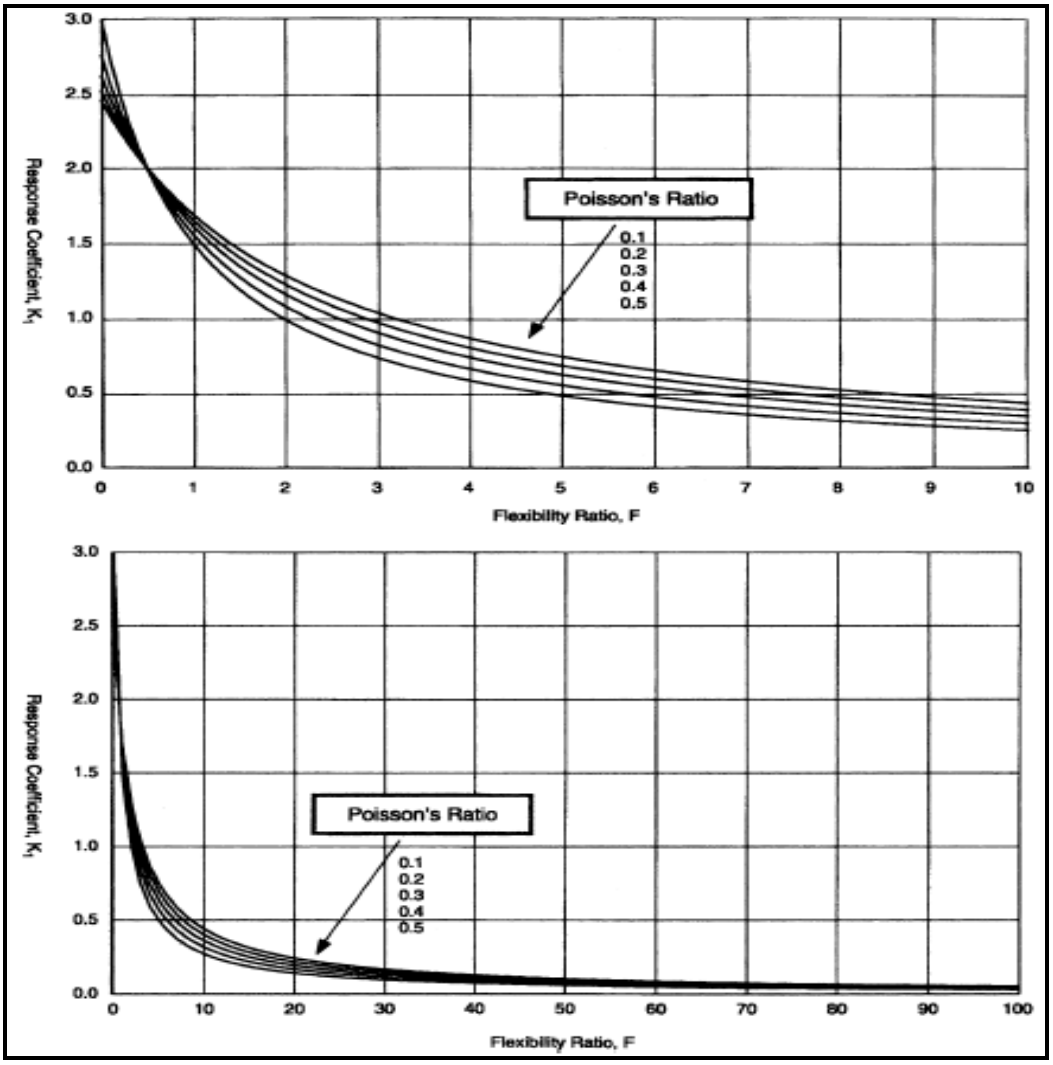

Figure 3.5. Lining response vs. flexibility ratio, full-slip interface, and circular tunnel (Wang, 1993).

As shown in Fig. 3.6, seismically-induced thrust increase with decreasing compressibility and flexibility ratios when the Poisson's ratio of the surrounding ground is less than 0.5.

As Poisson's ratio approaches 0.5 (i.e. saturated undrained clay), the thrust response is independent of compressibility because the soil is considered incompressible (Wang, 1993).

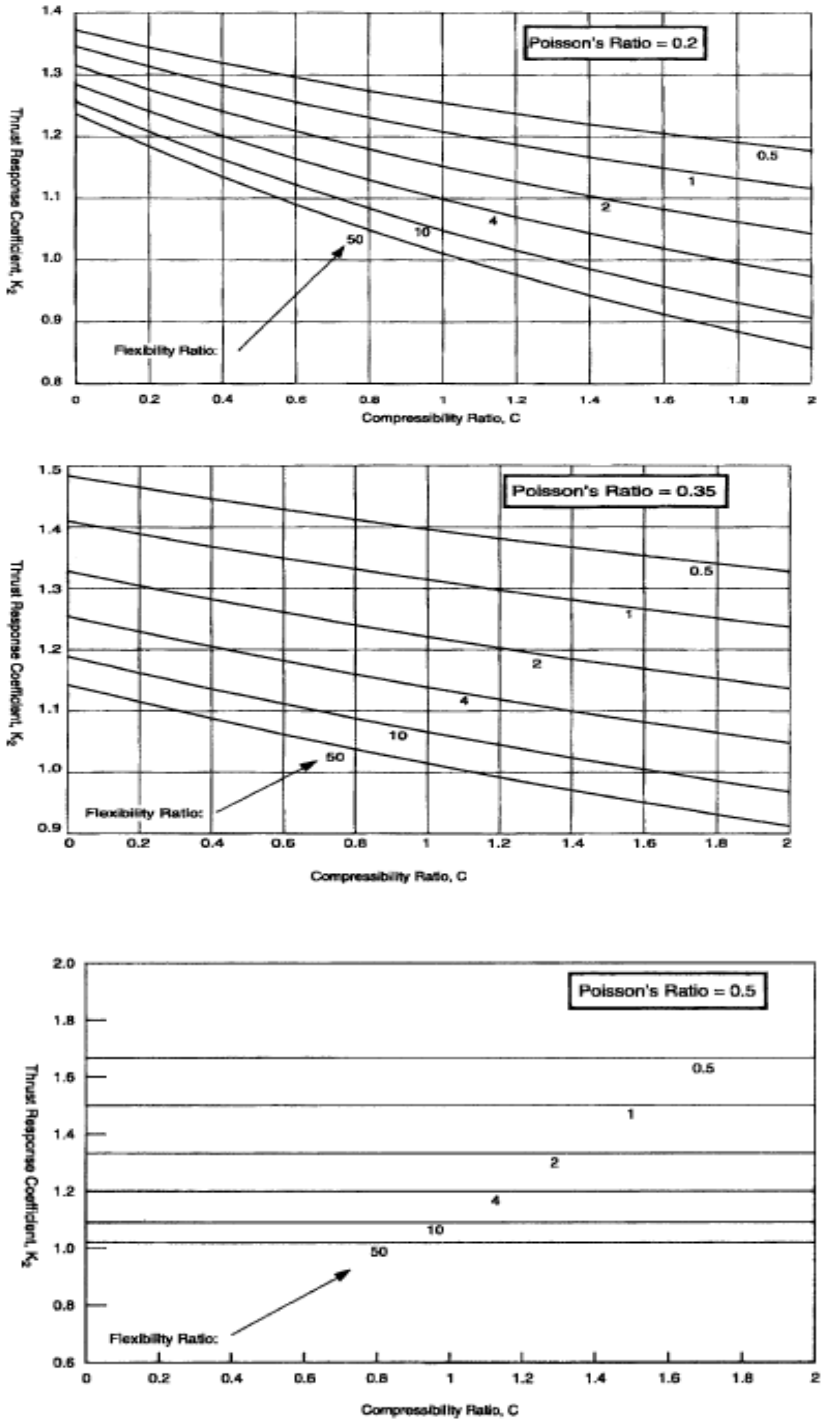

Figure 3.6. Lining (thrust) response coefficient vs. compressibility ratio, no-slip interface and circular tunnel (Wang, 1993).

The normalized lining deflection provides an indication of the importance of the flexibility ratio in lining response, and is defined as (Wang, 1993):

$$\frac{\Delta d_{lining}}{\Delta d_{free-field}} = \frac{2}{3} K_1 F \qquad (3.20)$$

According to this equation and Fig. 3.7, when the flexibility is less than one a tunnel lining will deform less than the free field (i.e. stiff lining in soft soil). As the flexibility ratio increases, the lining deflects more than the free field and may reach an upper limit equal to the perforated ground deformations. This condition continues as the flexibility ratio becomes infinitely large (i.e. perfectly flexible lining).

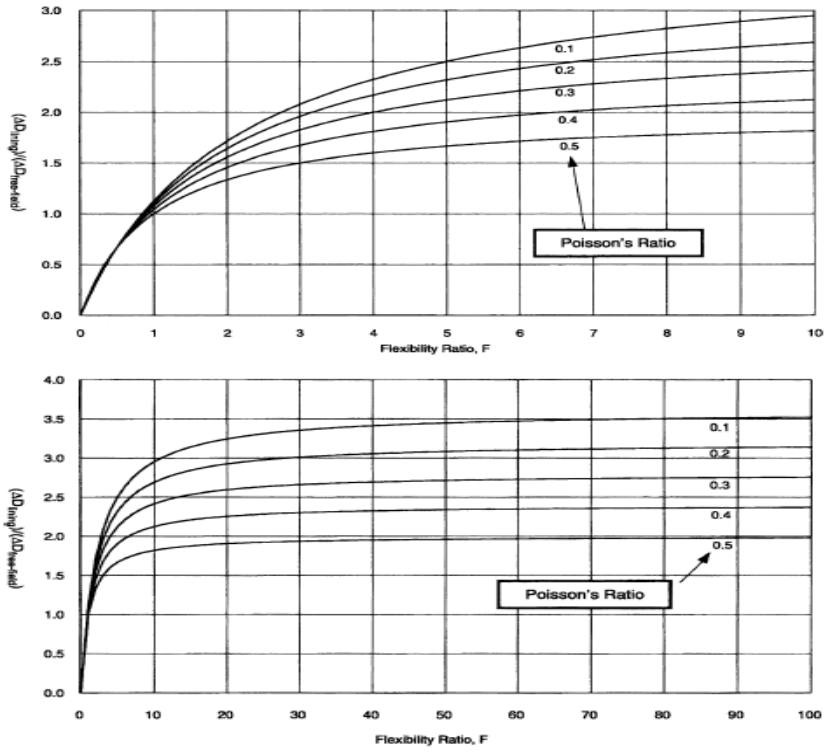

Figure 3.7. Normalized lining deflection vs. flexibility ratio, full slip interface, and circular lining (Wang, 1993).

3.4. The Corigliano's approach

Corigliano, Lai and Barla (2006), in their work titled "Seismic response of rock tunnels in near-fault conditions" proposed a simplified approach for studying the seismic response of tunnels this takes into account the interaction of the underground structure with the surrounding ground and at the same time adequately considers the features of near-fault ground motion.

3.4.1. Axial and bending deformation (Analysis of longitudinal response)

To study the tunnel response along the longitudinal direction (which involves axial and bending deformation), they developed a finite element *stick* model by subdividing the tunnel into a finite number of frame elements with lumped mass, connecting to the surrounding ground by a series of frequency-dependent springs and dashpots in parallel (i.e. Kelvin-Voigt model, see Figure 3.8). These represent the effects of ground deformability and energy dissipation (though *Sommerfield* radiation and material damping).

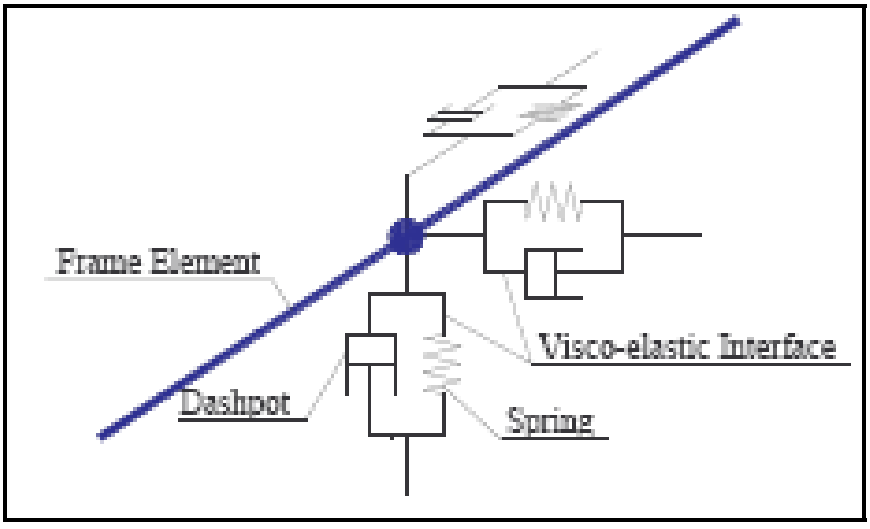

Figure 3.8. Spatial frame element model connected with Kelvin-Voigt elements to the surrounding ground (Corigliano, Lai and Barla, 2006).

Wave scattering is not accounted for and thus this model can be ascribed to the class of simplified dynamic methods to analyze underground structures. The seismic excitation is inputted at the external nodes of the Kelvin-Voigt model through appropriate three component free-field displacement and velocity time-histories.

3.4.2. Ovaling deformation (Analysis of transversal response)

The analysis of the transversal response is performed by considering a lined circular tunnel in plane strain conditions. The earthquake loading is modeled as a uniform quasi-static strain field simulating a pure shear deformation (see Figure 3.9).

The relations for displacements, bending moment, thrust and shear forces are derived following the same approach used by Einstein and Schwartz (1979). The solution has been derived for two contact conditions at the structure-rock interface: *full-slip* and *no-slip.*

For the sake of brevity, only the relationships for bending moment M and the thrust T in the tunnel lining for seismic design associated to the no-slip condition are reported in the following.

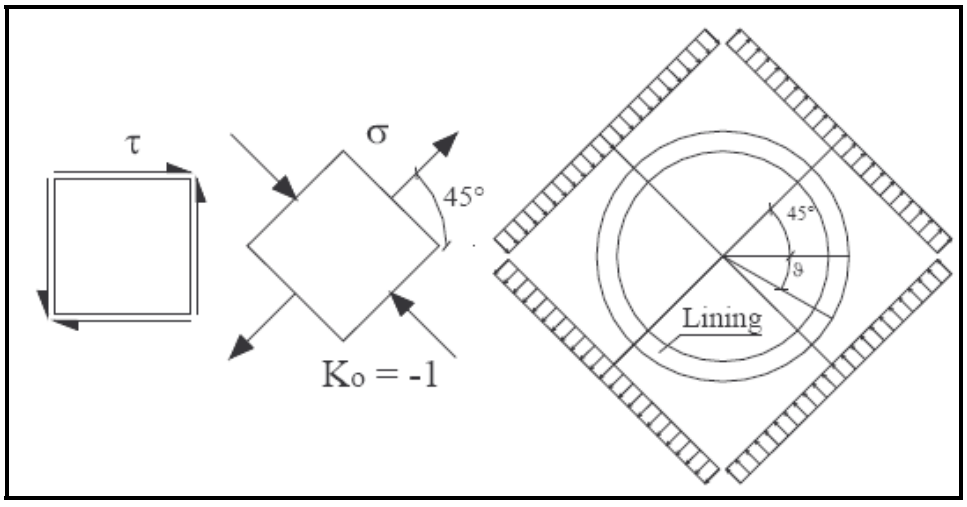

Figure 3.9. State of stress corresponding to a uniform, pure shear deformation.

$$T = \frac{E_g}{2(1+v)} \gamma_{ffmax} r \left(1 - \frac{\delta}{3}\right) cos2\left(\vartheta + \frac{\pi}{4}\right) \quad (3.21)$$

$$M = \frac{1}{2} \frac{E_g}{2(1+v)} \gamma_{ffmax} r \left(1 - \frac{\delta}{3} + \varepsilon\right) cos2\left(\vartheta + \frac{\pi}{4}\right) \quad (3.22)$$

Where:

$$\varepsilon = \frac{{}^{3C^*}/_{F^*}([C^*(1-v)-2]-3[C^*(1-v)+2])+([C^*(1-v)-2]+[C^*(1-v)+2])[1+C^*(1-v)]}{C^*(1-v)([C^*(1-v)+4v]-2[C^*(1-v)+2])+{}^{3C^*}/_{F^*}\beta+[C^*(1-v)+4v]-2v[C^*(1-v)+2]} \quad (3.23)$$

$$\delta = \frac{[C^*(1-v)-2]-[C^*(1-v)+4v]\varepsilon}{[C^*(1-v)+2]} \quad (3.24)$$

$$\beta = [C^*(1-v)+4v] - 6[C^*(1-v)+2](1-v) \quad (3.25)$$

$$C^* = \frac{E_m r(1-v_l^2)}{E_l A_l(1-v_m^2)} \quad , \quad F^* = \frac{E_m r^3(1-v_l^2)}{E_l I_l(1-v_m^2)} \quad (3.26)$$

It is possible to find the value of the imposed loading knowing the shear string by:

$$\sigma = \tau = \frac{E_m}{2(1-\upsilon_m)} \gamma_{ffmax} \quad (3.27)$$

Where γ_{ffmax} is the maximum shear strain (in absolute terms) evaluated in free-field conditions.

The true contact conditions at the ground-structure interface are known and the *full* and *no-slip* conditions simply represent the two extreme cases in which the real situation is bounded.

The *full slip* contact condition is usually adopted to obtain the extreme values of the bending moment and shear in the tunnel lining whereas the *no-slip* assumption is used to find the maximum values of the thrust acting on the lining (Wang, 1993).

A key parameter for definition of the state if stress in the tunnel lining is the maximum shear strain evaluated in free-field conditions. For shallows tunnels the shear strain profile can be easily obtained by considering a horizontally layered system and using one-dimensional wave propagation theory (Wang, 1993).

In near-fault conditions the assumptions of the previous approach are no longer valid (i.e. one-dimensional wave propagation theory with the wave front impinging in the vertical direction). If the direction along the tunnel axis is denoted as "*x*", the shear strain γ_{xz} may be computed as follows:

$$\gamma_{xz} = \frac{\partial v}{\partial z} + \frac{\partial w}{\partial y} \approx \frac{1}{2\Delta z}[v(y_0, z_0 + \Delta z) - v(y_0, z_0 - \Delta z)] + \frac{1}{2\Delta z}[w(y_0, z_0 + \Delta z) - w(y_0, z_0 - \Delta z)] \quad (3.28)$$

In which the partial derivates are evaluated using the two-point-central finite difference operators.

CHAPTER IV

DISCONTINUUM ROCK MASS ANALYSIS

4.1. Introduction

A first criterion for the analysis of an underground structure consists in assuming the structure immersed in an isotropic, elastic and continuum medium; even if geology includes fractures and faults, when sufficiently large length scales are considered a continuum may be sufficient. However from the engineering point of view, large classes of problems exist where the structures of interest have sizes comparable with the block sizes.

In addition, it is possible that while the structure may be subjected to loads that do not induce damage to individual blocks, some joints may fail. The use of a continuum analysis is usually inappropriate.

Many underground structures in a discontinuum medium are stable in usual conditions, but become unstable, or even fail under seismic loading or when significant groundwater is present (Tao and Chang 2000). Groundwater flows in the discontinuities in the rock. Joint deformation will change the hydraulic aperture of the joint and influence the joint permeability. Groundwater flow will influence the pore pressure and the mechanical properties of the joint.

Besides groundwater, seismic activity is an important factor that has to be taken into consideration for the analysis of stability of the jointed rock. The dynamic reaction and deformation (or failure mechanism) of the underground excavation under seismic loading follows its particular rule and the success of the underground facilities directly depends on the stability of the jointed rock.

In this order, the use of numerical methods represents an useful tool for obtaining appropriate solutions to tunnel engineering problems in the framework of discontinuum approach.

4.2. Distinct element method (DEM)

The distinct element method (DEM) is an alternative mesh free approach. In the DEM the rock mass is represented as a whole of discrete blocks which may be considered either "not deformable" or "deformable". Joints and discontinuities are viewed as interfaces between distinct bodies.

In order to apply the distinct element method to the solution of tunnel problems, there are two crucial issues which include the joint geometry data and the material properties assigned to the joints. The first issue relates to the introduction in the model of those joints which are most critical to the response of the rock mass. The second issue is closely connected with the need to assign to the joints in the model the stiffness and strength properties of the real joints in situ (Barla & Barla, 1999).

The lagrangian nature of the DEM simplifies tracking of material properties as blocks of material move. It is also possible to guarantee exact conservation of linear and angular momentum. Furthermore, by using an explicit integration scheme, the joint constitutive model can be very flexible. In particular, the joint constitutive model can incorporate experimentally observed effects such as, cohesion, joint dilation, and friction angle.

The Distinct Element Method (DEM) is used to analyze the influence of the peak velocity and frequency spectrum which are the primary factors in the analysis of the seismic wave commonly induced by an earthquake.

4.3. The universal distinct element code (UDEC)

The Universal Distinct Element Code (*UDEC*) is a two-dimensional numerical program based on the distinct element method for discontinuum modeling. *UDEC* simulates the response of discontinuous media (such as a jointed rock mass) subjected to either static or dynamic loading. The discontinuous medium is represented as an assemblage of discrete blocks. The discontinuities are treated as boundary conditions between blocks; large displacements along discontinuities and rotations of blocks are allowed.

Individual blocks behave as either rigid or deformable material. Deformable blocks are subdivided into a mesh of finite-difference elements, and each element responds according to a prescribed linear or non-linear stress-strain law. The relative motion of the discontinuities is also governed by linear or non-linear force-displacement relations for movement in both the normal and shear directions.

UDEC has several built-in material behavior models, for both the intact blocks and the discontinuities, which permit the simulation of response representative of discontinuous geologic or similar, materials. *UDEC* is based on a "Lagrangian" calculation scheme that is well-suited to model the large movements and deformations of a blocky system.

UDEC is primarily intended for analysis in rock engineering projects, ranging from studies of the progressive failure of rock slopes to evaluations of the influence of rock joints, faults, bedding planes, etc. on underground excavations and rock foundations. *UDEC* is ideally suited to study potential modes of failure directly related to the presence of discontinuous features.

4.3.1. Numerical Formulation

In the distinct element method, a rock mass is represented as an assembly of discrete blocks. Joints are viewed as interfaces between distinct bodies (i.e., the discontinuity is treated as a boundary condition).

The contact forces and displacements at the interfaces of a stressed assembly of blocks are found through a series of calculations which trace the movements of the blocks.

Movements result from the propagation through the block system of disturbances caused by applied loads or body forces. This is a dynamic process in which the speed of propagation depends on the physical properties of the discrete system.

The dynamic behavior is represented numerically by a timestepping algorithm in which the size of the timestep is limited by the assumption that velocities and accelerations are constant within the timestep.

The distinct element method is based on the concept that the timestep is sufficiently small that, during a single step, disturbances cannot propagate between one discrete element and its immediate neighbors. This corresponds to the fact that there is a limited speed at which information can be transmitted in any physical medium.

The timestep restriction applies to both contacts and blocks. For rigid blocks, the block mass and interface stiffness between blocks define the timestep limitation; for deformable blocks, the zone size is used, and the stiffness of the system includes contributions from both the intact rock modulus and the stiffness at the contacts.

The calculations performed in the distinct element method alternate between application of a force-displacement law at all contacts and Newton's second law at all blocks. The force-displacement law is used to find contact forces from known (and fixed) displacements.

Newton's second law gives the motion of the blocks resulting from the known (and fixed) forces acting on them. If the blocks are deformable, motion is calculated at the gridpoints of the triangular finite-strain elements within the blocks.

Then, the application of the block material constitutive relations gives new stresses within the elements. Figure 4.1 shows schematically the calculation cycle for the distinct element method. The equations in this figure are described in the following sections.

4.3.2. Equations of motion

The motion of and individual block is determined by the magnitude and direction of resultant out-of-balance moment and forces acting on it. Considering the one-dimensional motion of a single mass acted on by a varying force, *F(t)*. Newton's second law of motion can be written in the form:

$$\frac{d\dot{u}}{dt} = \frac{F}{m} \tag{4.1}$$

Where $\dot{u}$ = velocity

t = time

m = mass.

The central difference scheme for the left-hand side of Eq. (4.1) at time t can be written as:

$$\frac{d\dot{u}}{dt} = \frac{\dot{u}^{(t+\Delta t/2)} - \dot{u}^{(t-\Delta t/2)}}{\Delta t} \tag{4.2}$$

Substituting Eq. (4.2) in Eq. (4.1) and re-arranging yields

$$\dot{u}^{(t+\Delta t/2)} = \dot{u}^{(t-\Delta t/2)} + \frac{F^t}{m}\Delta t \tag{4.3}$$

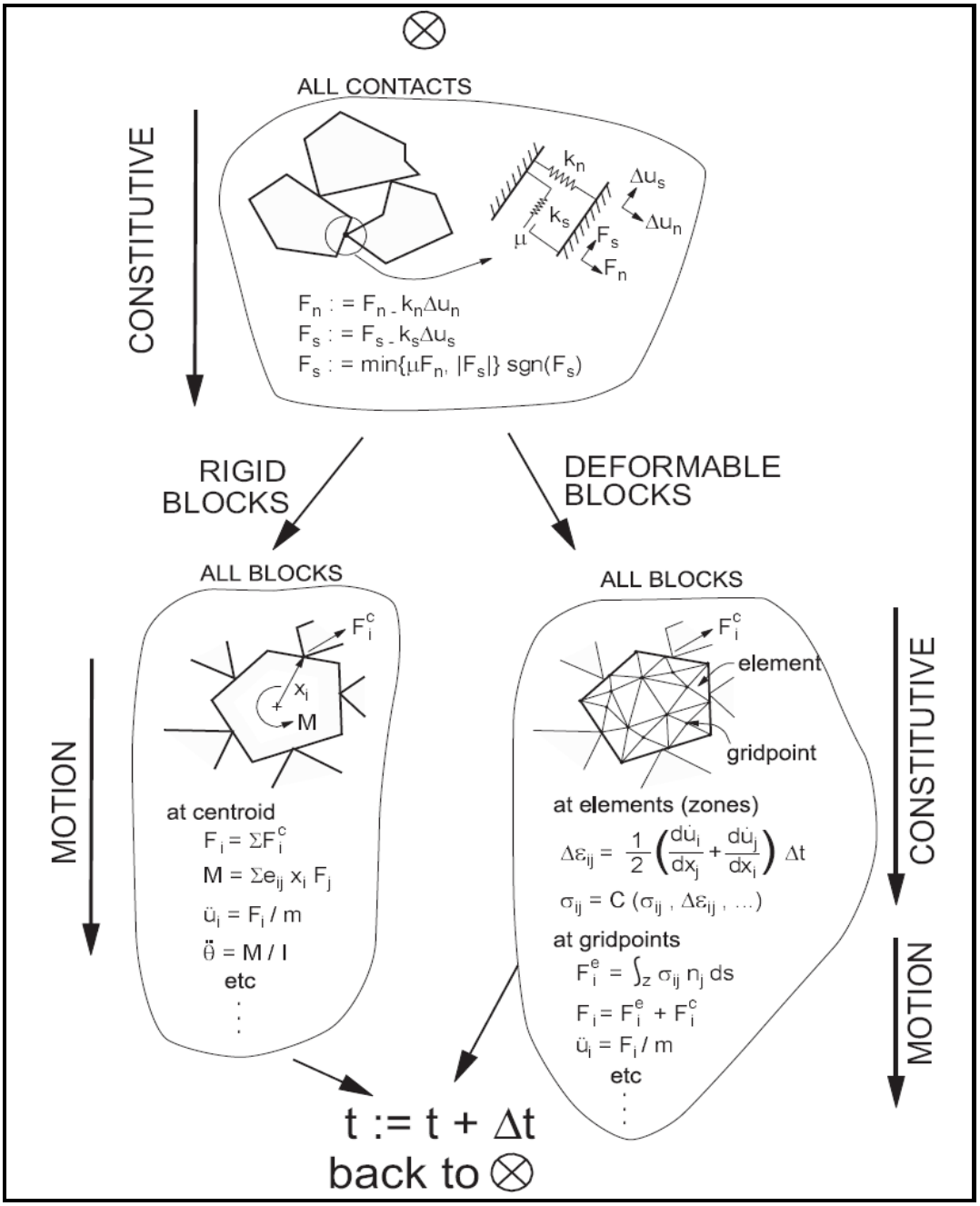

Figure 4.1. Calculation cycle for the distinct element method (ITASCA, 1999).

With velocities stored at the half-timestep point, it is possible to express displacement as

$$u^{(t+\Delta t)} = \dot{u}^{(t+\Delta t/2)}\Delta t + u^{t} \tag{4.4}$$

Because the force depends on displacement, the force/displacement calculation is done at one time instant. Figure 4.2 illustrates the central difference scheme with the order of calculation indicated by the arrows. The central difference scheme is "second-order accurate" – i.e., first-order error terms vanish from the solution. This is an important characteristic that prevents long-term drift in a distinct element simulation.

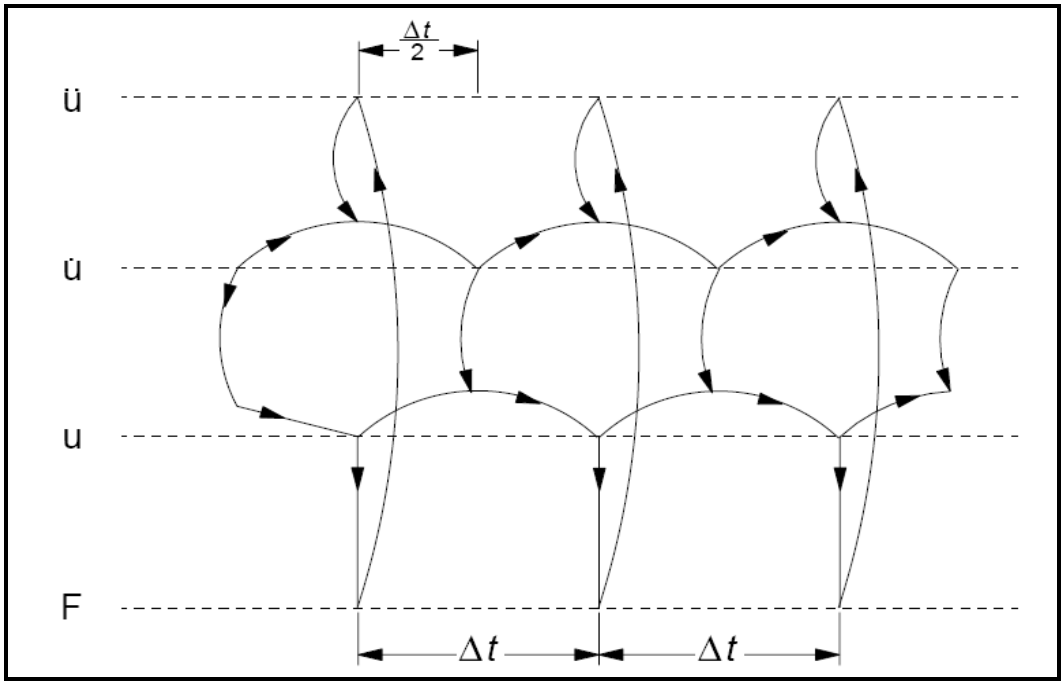

Figure 4.2. Interlaced nature of the calculation cycle used in distinct element formulation (ITASCA, 1999).

For blocks in two dimensions that are acted upon by several forces as well as gravity, the velocity equations become:

$$\dot{u}_t^{(t+\Delta t/2)} = \dot{u}_t^{(t-\Delta t/2)} + \left(\frac{\Sigma F_i^{(t)}}{m} + g_i \right) \Delta t$$

$$\dot{\theta}^{(t+\Delta t/2)} = \dot{\theta}^{(t-\Delta t/2)} + \left(\frac{\Sigma M^{(t)}}{I} \right) \Delta t \qquad (4.5)$$

Where $\dot{\theta}$ = angular velocity of block about centroid

I = moment of inertia of block

ΣM = total moment acting on the block

$\dot{u}_i$ = velocity components of block centroid

g_i = components of gravitational acceleration (body forces)

In Eq. (4.5) and those that follow, indices i denote components in a Cartesian coordinate frame, and summation is implied for repeated indices in an expression.

The new velocities in Eq. (4.5) are used to determine the new block location according to:

$$x_i^{(t+\Delta t)} = \dot{u}_i^{(t+\Delta t/2)} \Delta t + x_i^{(t)}$$

$$\theta_i^{(t+\Delta t)} = \dot{\theta}_i^{(t+\Delta t/2)} \Delta t + \theta^{(t)} \qquad (4.6)$$

Where θ = rotation of block about centroid

x_i = coordinates of block centroid

Note that rotations are not stored; incremental rotations are used to update the positions of block vertices. In summary, each timestep produces new block positions that generate new contact forces. Resultant forces and moments are used to calculate linear and angular accelerations of each block.

Block velocities and displacements are determined by integration over increments in time. The procedure is repeated until a satisfactory state of equilibrium failure results.

4.3.3. Conservation of Momentum and Energy in the Distinct Element Formulation

Many continuum-based computer programs start with a statement of the conservation laws and then derive the necessary equations from these for the formulation of the numerical schemes. This approach is used to demonstrate that these codes satisfy conservation of momentum and energy in their dynamic simulation.

The equations used in *UDEC* are based on the interaction of bodies by means of springs and the responses of the bodies to applied forces (see Figure 4.1).

4.3.3.1. Momentum Balance

Consider two bodies (denoted by subscript a and b) in contact for a period, T. By Newton's laws, a common force, F, acts in opposite directions on the two bodies, which accelerate in proportion to the forces:

$$m_a \ddot{u}_a = F$$

$$m_b \ddot{u}_b = -F \qquad (4.7)$$

By combining these equations and integrating,

$$\int_0^T m_a \ddot{u}_a dt = -\int_0^T m_b \ddot{u}_b dt \tag{4.8}$$

$$m_a\left(\dot{u}_a^{(T)} - \dot{u}_a^{(0)}\right) = -m_b\left(\dot{u}_b^{(T)} - \dot{u}_b^{(0)}\right) \tag{4.9}$$

$$m_a\dot{u}_a^{(T)} + m_b\dot{u}_b^{(T)} = m_a\dot{u}_a^{(0)} + m_b\dot{u}_b^{(0)} \tag{4.10}$$

Eq. (4.10) indicates that the total momentum at the end of an arbitrary time period is equal to that at the beginning.

4.3.3.2. Energy balance

Suppose a body with initial velocity v_o is brought to a final velocity of v in a distance S by a constant force F:

$$m\dot{v} = F \tag{4.11}$$

Using the identity $\dot{v} = v\,dv/ds$

$$m\int_{v_o}^{v} v dv = \int_0^S F ds \tag{4.12}$$

$$\frac{1}{2}m(v^2 - v_o^2) = FS \tag{4.13}$$

Eq. (4.13) expresses the fact that the work done by the force is equal to the change in kinetic energy of the body. If the force opposing motion is related to the displacement by the equation (F=-Ks), where K denotes the spring stiffness, then Eq. (4.12) is replaced by:

$$m\int_{v_o}^{v} vdv = -\int_{0}^{S} Ksds \tag{4.14}$$

Hence,

$$\frac{1}{2}m(v^2 - v_o^2) = \frac{1}{2}KS^2 \tag{4.15}$$

In this case, the decrease in kinetic energy equals the energy stored in the spring. The same argument may be used in inverse to show that the kinetic acquired by a body is equal to the decrease in energy stored in a spring. Hence, the kinetic energy of a body after an elastic collision is equal to the kinetic energy before the collision.

4.4. Dynamic analysis in UDEC

Dynamic analysis in *UDEC* permits two-dimensional, plane-strain or plane-stress, fully dynamic analysis. The calculation is based on the explicit finite difference scheme to solve the full equations of motion, using real rigid-block masses, or lumped gridpoint masses derived from the real density of surrounding zones (rather than scaled masses used for static solution).

This formulation can be coupled to the structural element model, thus permitting analysis of rock-structure interaction brought about by ground shaking. The dynamic feature can also be coupled to the model for fluid flow in joints; this permits, for example, analyses of the effect of dynamic loading of saturated joints.

The dynamic model can likewise be coupled to the optional thermal model in order to calculate the combined effect of thermal and dynamic loading. The dynamic facility expands *UDEC*'s analysis capability to a wide range of dynamic problems in disciplines such as earthquake engineering, seismology and mine rockbursts.

There are three aspects to preparing a *UDEC* model for a dynamic analysis. These are: (1) dynamic loading and boundary conditions; (2) mechanical damping; and (3) wave transmission through the model. This section provides guidance on addressing each aspect when preparing a *UDEC* data file for dynamic analysis.

4.4.1. Dynamic loading and boundary conditions

UDEC models a region of jointed material subjected to external and/or internal dynamic loading by applying a dynamic input boundary condition at either the model boundary or to internal blocks.

Wave reflections at model boundaries are minimized by specifying either quiet (viscous) or freefield boundary conditions. The types of dynamic loading and boundary conditions are shown schematically in Figure 4.3.

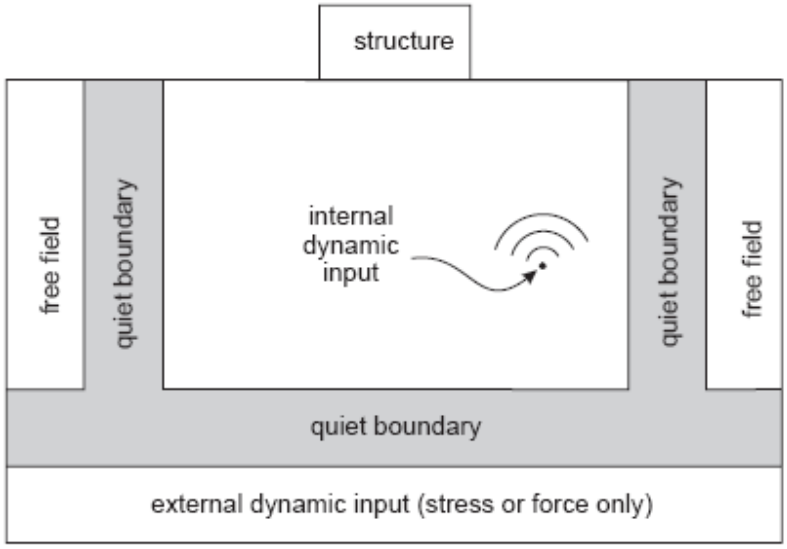

(a) Flexible base

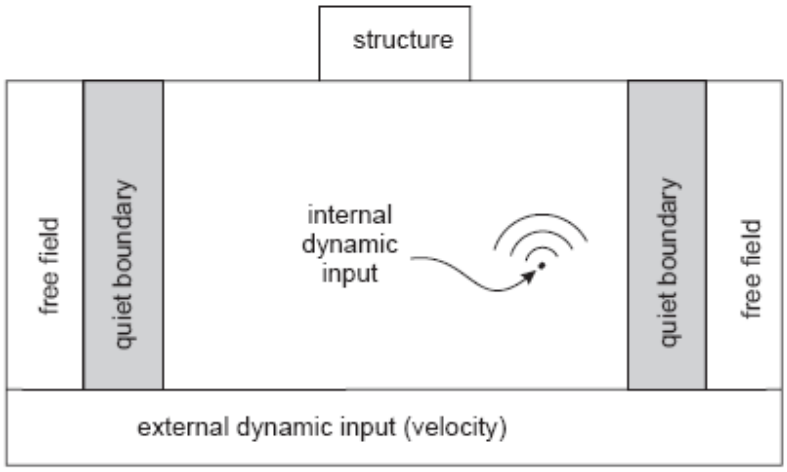

(a) Rigid base

Figure 4.3. Types of dynamic loading and boundary conditions in UDEC (ITASCA, 1999).

4.4.2. Mechanical damping

Natural dynamic systems contain some degree of damping of the vibration energy within the system; otherwise, the system would oscillate indefinitely when subjected to driving forces. Damping is due, in part, to energy loss as a result of internal friction in the intact material and slippage along interfaces within the system.

UDEC uses a dynamic algorithm for solution of two general classes of mechanical problems: quasistatic and dynamic. Damping is used in the solution of both classes of problems, but quasi-static problems require more damping.

For a dynamic analysis, the damping in the numerical simulation should attempt to reproduce the energy losses in the natural system when subjected to a dynamic loading. In soil and rock, natural damping is mainly hysteretic (i.e., independent of frequency: see Gemant and Jackson, 1937; Wegel and Walther, 1935).

It is difficult to reproduce this type of damping numerically because of at least two problems (see Cundall, 1976). First, many simple hysteretic functions do not damp all components equally when several waveforms are superimposed. Second, hysteretic functions lead to path dependence, which makes results difficult to interpret . However, if a constitutive model is found that contains an adequate representation of the hysteresis that occurs in a real material, then *no additional damping* is necessary in a *UDEC* run. The current built-in models in *UDEC* are not considered to model dynamic hysteresis well enough to omit additional damping completely.

In time-domain programs, Rayleigh damping is commonly used to provide damping that is approximately frequency-independent over a restricted range of frequencies. Although Rayleigh damping embodies two viscous elements (in which the absorbed energy is dependent on frequency), the frequency-dependent effects are arranged to cancel out at the frequencies of interest.

Alternatively, the “local damping” embodied in *UDEC*’s static solution scheme may be used dynamically, but with a damping coefficient appropriate to wave propagation. The use of local damping in dynamic problems is new (so there is little experience to draw on), but the approach looks promising in view of the frequency-independent

nature of the damping. Both Rayleigh damping and local damping are described in more detail in the following sections.

4.4.3. Wave transmission

The physical stiffness of joints in situ can have a substantial influence on seismic wave propagation. Myer et al. (1990) present field and laboratory test results that demonstrate the effect of the stiffness of dry natural fractures in rock on high frequency attenuation and changes in travel time of the seismic wave.

It can be important to represent this effect in the discontinuum model if the wave transmission is be to modeled accurately. However, care must be taken to not introduce a numerical distortion of the wave that could mask the actual effect of the joints on wave propagation.

Numerical distortion of the propagating wave can occur in a dynamic analysis, whether it is based on a continuum or discontinuum program, as a function of the modeling conditions. Both the frequency content of the input wave and the wave-speed characteristics of the system will affect the numerical accuracy of wave transmission.

Kuhlemeyer and Lysmer (1973) show that for accurate representation of wave transmission through a model, the spatial element size, Δl, must be smaller than approximately one-tenth to one-eighth of the wavelength associated with the highest frequency component of the input wave — i.e.,

$$\Delta l \leq \frac{\lambda}{10} \tag{4.16}$$

Where λ is the wavelength associated with the highest frequency component that contains appreciable energy. For discontinuum analysis involving rigid blocks, this also applies to joint spacing (or block size).

For a discontinuum system containing a single set of planar joints oriented normal to the compression wave and in which the solid material is rigid (or much stiffer than the joints), then the wave speed is only a function of joint spacing and stiffness, ie.,

$$C_P = \sqrt{\frac{SK_n}{\rho}} \tag{4.17}$$

Where S = joint spacing,
K_n = joint normal stiffness,
ρ = mass density.

The relations can be extended to multiple-jointed media by calculating the wave speeds using closed-form solutions that have been developed to calculate effective elastic module as a function of the elastic module of the solid and the stiffnesses and spacings of the joints.

Physically-measured values for normal and shear stiffnesses of a geologic structure, such as joints, faults, bedding planes, etc., are not generally available. It is often necessary to back-calculate properties based on measured values for the elastic deformation properties of the intact material and the wave speed through the jointed system. These relations can be used to provide reasonable estimates for joint stiffness properties in *UDEC* to produce the measured shear and compressional wave speeds of the system.

In order to achieve an accurate representation of a stress wave through a distinct element model, particularly when the joint spacing is variable, the blocks should be made deformable to accommodate the element size restriction imposed by frequency and wavelength. This is accomplished in *UDEC*, by subdividing each block into a mesh of finite difference zones. These zones are then subject to the Kuhlemeyer and Lysmer restriction.

4.5. Preliminary Test Analysis

4.5.1. Circular tunnel problems

This problem concerns the analysis of stresses of a long circular opening in an infinite medium under various boundary conditions and material properties (see Figure 4.4). Four problems will be considered:

1. Part A – tunnel in an elastic medium with a biaxial stress field.
2. Part B – tunnel in an elastic-medium with a hydrostatic stress field.
3. Part C – lined tunnel in an elastic medium with a biaxial stress field.
4. Part D – lined tunnel in an elastic-plastic medium with a hydrostatic stress field.

Following excavation of a tunnel, the in-situ stresses within the rock or soil mass are redistributed from a uniform orthogonal stress field to a more complex stress distribution. Stress concentrations around a tunnel cause elastic deformations at the periphery and, if the yield strength of the material is exceeded, result in plastic deformations and redistribution of stresses due to yielding of the material.

In case of plastic yielding, a yield zone will develop around the tunnel beyond which the stresses will be elastic. These processes are modeled by parts A and B.

Part C involves the interaction of a structural tunnel lining in an elastic medium. Although the actual design of a tunnel lining is more complex, this problem checks the basic interaction between the two types of material for non-axisymmetric loadings. Finally, part D describes the redistribution of the stresses of a lined tunnel in an elastic-plastic medium

These problems have a closed-form analytical solution and, thus, several aspects of the computer model can be tested:

- The ability of the code to simulate an infinite medium by boundary elements.
- The determination of displacements and stresses in a non-symmetric problem in two dimensions.
- The computation of plastic stresses and deformations.
- The interaction between structural lining and rock or soil mass.

4.5.1.1. Analytical Solutions

4.5.1.1.1. Cylindrical Hole in an Infinite Elastic Medium

For a cylindrical hole in an infinite, isotropic, elastic medium under plane-strain conditions, the radial and tangential stress distributions are given by the classical Kirsch solution. A point located at polar coordinate (r,θ) near an opening with radius a (see figure 4.4a) has stresses σ_r, σ_θ, τr_θ, given by:

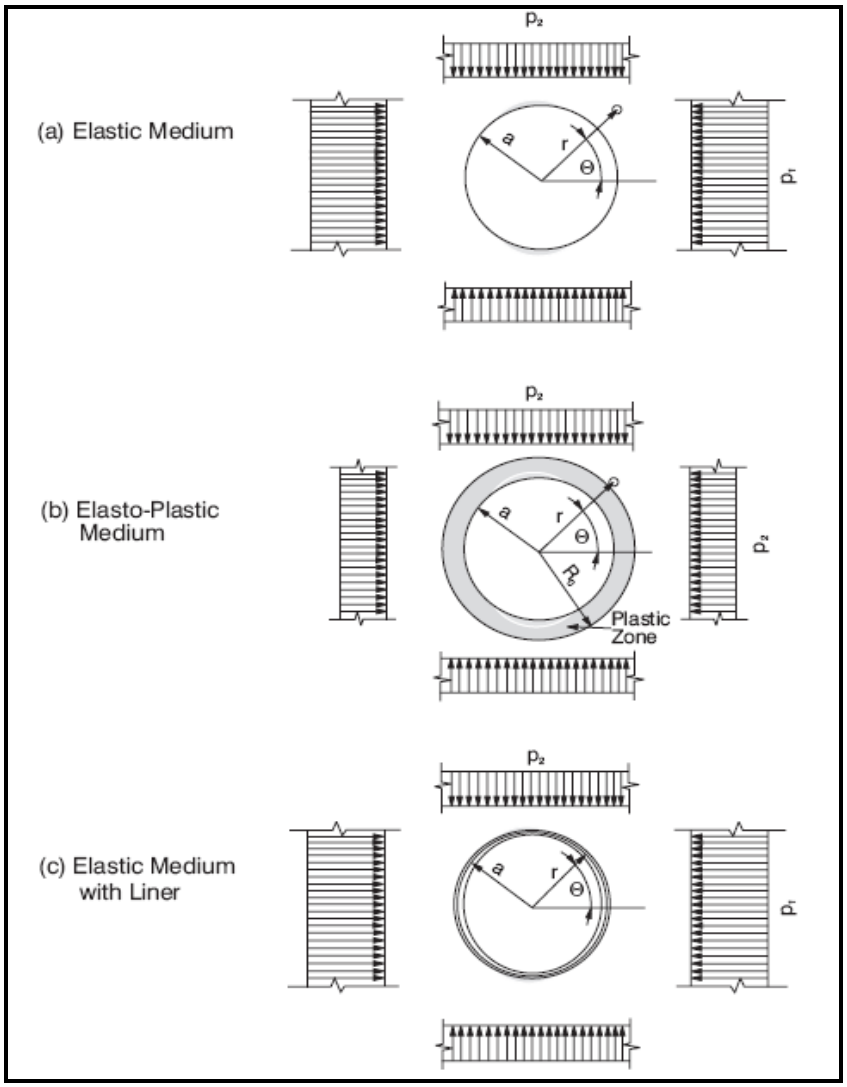

Figure 4.4. Three variations to the circular tunnel problem (after Wart et al., 1984).

$$\frac{2\sigma_r}{P_1+P_2} = 1 - \frac{a^2}{r^2} + \frac{P_1-P_2}{P_1+P_2}\left(1 - \frac{4a^2}{r^2} + \frac{3a^4}{r^4}\right)cos2\theta$$

$$\frac{2\sigma_\theta}{P_1+P_2} = 1 + \frac{a^2}{r^2} - \frac{P_1-P_2}{P_1+P_2}\left(1 + \frac{3a^4}{r^4}\right)cos2\theta \qquad (4.18)$$

$$\frac{2\tau_{r\theta}}{P_1+P_2} = -\frac{P_1-P_2}{P_1+P_2}\left(1 + \frac{2a^2}{r^2} - \frac{3a^4}{r^4}\right)sin2\theta$$

The displacements can also be determined assuming conditions of plane strain:

$$\frac{4G}{P_1+P_2}\frac{u_r}{a} = \frac{a}{r} + \frac{P_1-P_2}{P_1+P_2}\frac{a}{r}\left(4(1-\nu) - \frac{a^2}{r^2}\right)cos2\theta$$

(4.19)

$$\frac{4G}{P_1+P_2}\frac{u_\theta}{a} = -\frac{P_1-P_2}{P_1+P_2}\frac{a}{r}\left(2(1-\nu) + \frac{a^2}{r^2}\right)sin2\theta$$

In which u_r is the radial outward displacement, and u_θ is the tangential displacement. G is the shear modulus, and ν is the Poisson's ratio.

4.5.1.1.2. Cylindrical Hole in an Infinite Mohr-Coulomb Medium

The yield zone radius, R_o (see Figure 4.4b), is given analytically by a theoretical model based on the solution of Salencon (1969):

$$\frac{R_o}{a} = \left(\frac{2}{K_P+1}\frac{\frac{P_2}{q}+\frac{1}{K_P-1}}{\frac{P_1}{q}+\frac{1}{K_P-1}}\right)^{1/(K_P-1)} \qquad (4.20)$$

$K_p = (1 + sin\phi)/(1 - sin\phi)$

$q = 2 * c * \tan(45 + \phi/2)$

P_i = internal pressure.

The radial stress at the elastic-plastic interface is:

$$\frac{\sigma_{re}}{q} = -\frac{1}{K_p+1}\left(2\frac{P_2}{q} - 1\right) \tag{4.21}$$

The stresses in the plastic zone are:

$$\frac{\sigma_r}{q} = \frac{1}{K_p - 1} - \left(\frac{P_i}{q} + \frac{1}{K_p - 1}\right) * \left(\frac{r}{a}\right)^{K_p - 1}$$

$$\frac{\sigma_\theta}{q} = \frac{1}{K_p - 1} - K_p\left(\frac{P_i}{q} + \frac{1}{K_p - 1}\right) * \left(\frac{r}{a}\right)^{K_p - 1} \tag{4.21}$$

The stresses in the elastic zone are:

$$\frac{\sigma_r}{q} = -\frac{P_2}{q} + \left(\frac{P_2}{q} + \frac{\sigma_{re}}{q}\right) * \left(\frac{R_o}{r}\right)^2$$

$$\frac{\sigma_\theta}{q} = -\frac{P_2}{q} - \left(\frac{P_2}{q} + \frac{\sigma_{re}}{q}\right) * \left(\frac{R_o}{r}\right)^2 \tag{4.22}$$

4.5.1.1.3. Lined Tunnel in an Infinite Elastic Medium

The analytical solution for an elastic liner embedded in an elastic solid with non-slipping interface (see Figure 4.4c) is given by Einstein and Schwartz (1979). The thrust or axial force in the liner, N, and bending moment, M, are:

$$\frac{N}{P_o a} = \frac{1}{2}\left(1+\frac{P_1}{P_2}\right)(1-a_o^*) + \left(1-\frac{P_1}{P_2}\right)(1+2a_2^*)cos2\theta \qquad (4.23)$$

$$\frac{M}{P_o a^2} = \frac{1}{4}\left(1-\frac{P_1}{P_2}\right)(1-2a_2^*+2b_2^*)cos2\theta \qquad (4.24)$$

E = Young's modulus of the rock

ν = Poisson's ratio of the rock

E_s = Young's modulus of the liner

ν_s = Poisson's ratio of the liner

d = thickness of the liner

A = *d*, cross-sectional area of the liner for a 1m long section

$I = d^3/12$, liner moment of inertia

$$a_o^* = \frac{C^*F^*(1-\upsilon)}{C^*+F^*+C^*F^*(1-\upsilon)} \quad ; \quad a_2^* = \beta . b_2^*$$

$$\beta = \frac{(6+F^*)C^*(1-\upsilon)+2F^*\upsilon}{3F^*+3C^*+2C^*F^*(1-\upsilon)} \quad ; \quad b_2^* = \frac{C^*(1-\upsilon)}{2[C^*(1-\upsilon)+4\upsilon-6\beta-3\beta C^*(1-\upsilon)]}$$

$$C^* = \frac{Ea(1-\upsilon_s^2)}{E_s A(1-\upsilon^2)} \quad and \quad F^* = \frac{Ea^3(1-\upsilon_s^2)}{E_s I(1-\upsilon^2)}$$

UDEC structural elements do not require a Poisson's ratio to be specified. In order to comply the analytical solution, a plane-strain correction of (1- v_s^2) is applied to the Young's modulus of the liner.

4.5.1.2. UDEC Models

The following dimensionless parameters and values are used to describe the problems. Note that the density is not required by the analytical solution, but some value must be provided in *UDEC*. Since the solutions are independent of the choice of density $\rho = 1$.

$P_2/P_1 = 0.5$	$\psi = 20°$
$P_2/q = 0.75$	$v_s = 0.25$
$v = 0.25$	$E_s/E = 3$
$E/q = 300$	$d/a = 0.1$
$\varphi = 20°$	

For each part, one discretization is used, such that the characteristic length l_z of zones at the tunnel contour is $a/l_z = 10$ (see figure 4.5). The inner and outer radii are 5.0m and 40.0m, respectively. Also, boundary elements were coupled to gridpoints in the outer boundary in both cases. "Glued" joints were used to provide the needed discretization in each case.

In part C of this problem, interaction of a structural lining with the surrounding material is modeled. For this part, the lining was divided into 96 linear segments. To satisfy the conditions of perfect bonding between the lining and surrounding material, high interface stiffness and strength parameters were specified

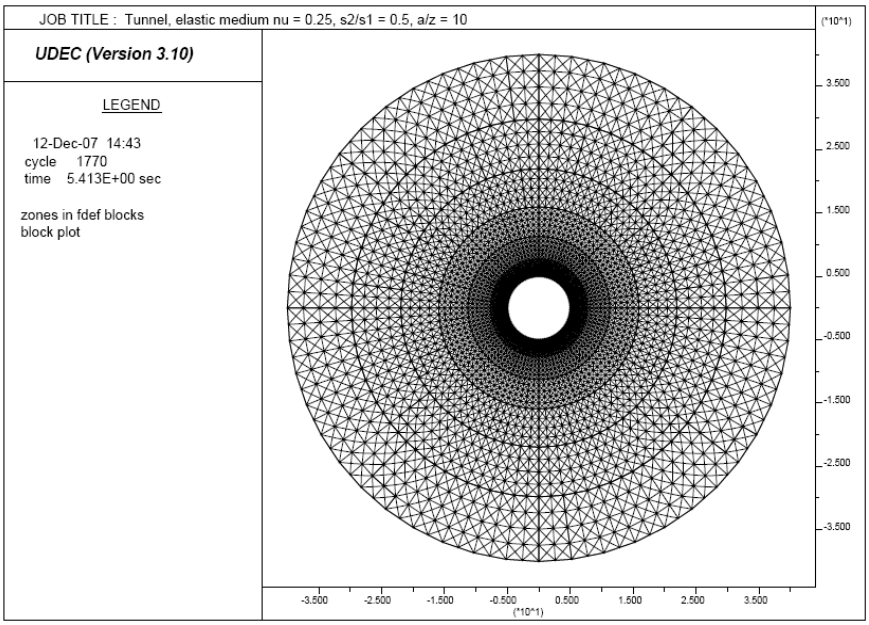

Figure 4.5. finer zoning used in circular tunnel problems.

The results for Part A are compared graphically with the analytic solution in Figures 4.6 and 4.7. All results shown are for a line along the maximum principal stress direction. The finer zoning resulted in improved correspondence with the analytical solution.

The results of Part B are compared graphically with the analytic solution in Figure 4.8. The calculated radius of the elastic-plastic interface R_o/a based on the analytic solution is 1.164. For UDEC the corresponding radius of the elastic-plastic interface was found to be 1.184 for both the coarse and fine zoning, with an error of 1.72%.

The UDEC results for Part C are presented in terms of lining thrust $\frac{N}{P_o a}$ and moment $\frac{M}{P_o a^2}$ in Figures 4.9 and 4.10. Results shown are for the first quadrant. Results for the other quadrants are similar

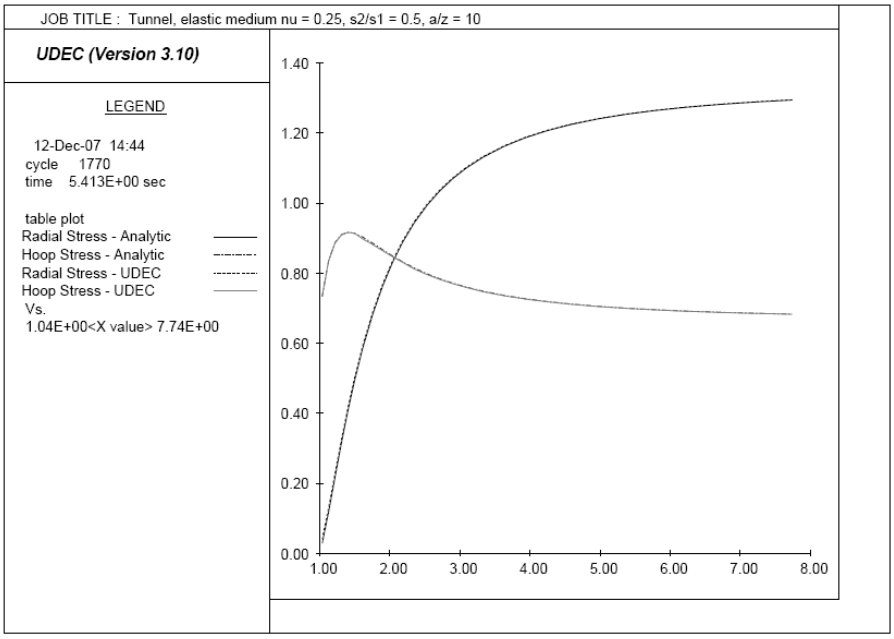

Figure 4.6. Comparison of *UDEC* results of radial and tangential stresses versus radial distance along a line $\theta = 0°$ with analytical solution for the case of a tunnel in an elastic medium with a biaxial stress field.

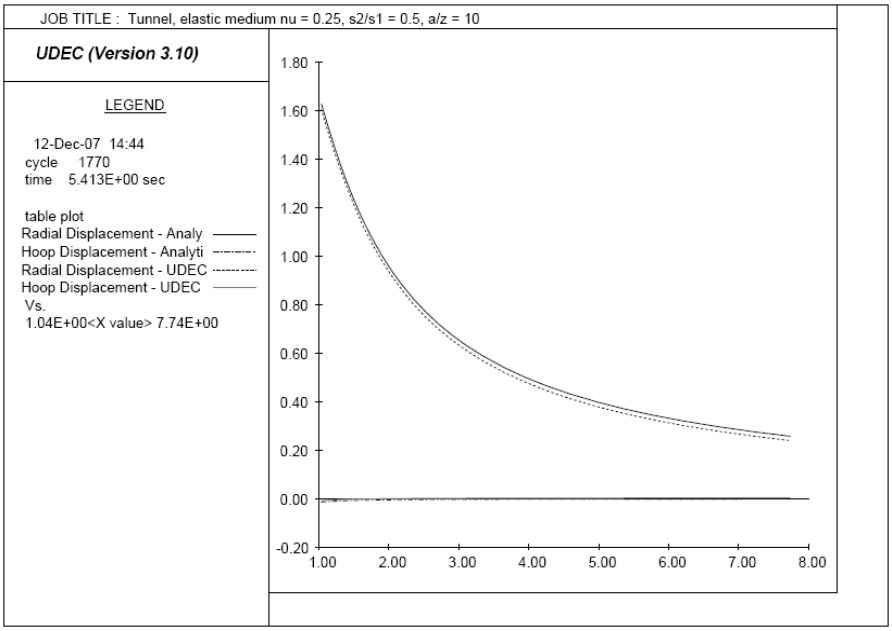

Figure 4.7. comparison of *UDEC* results of radial and tangential displacements versus radial distance along a line $\theta = 0°$ with analytical solution for the case of a tunnel in an elastic medium with a biaxial stress field.

The results of Part D show the distribution of the stresses of a lined tunnel in an elastic-plastic medium (see Figure 4.11).

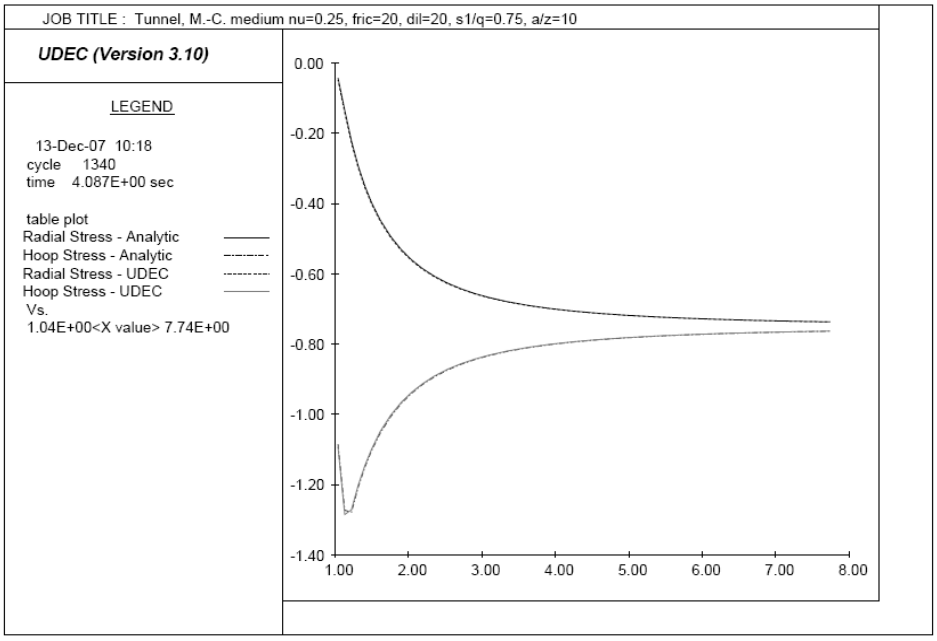

Figure 4.8. Comparison of *UDEC* results of radial and tangential stresses versus radial distance along a line $\theta = 0°$ with analytical solution for the case of a tunnel in Mohr-coulomb medium with biaxial stress field.

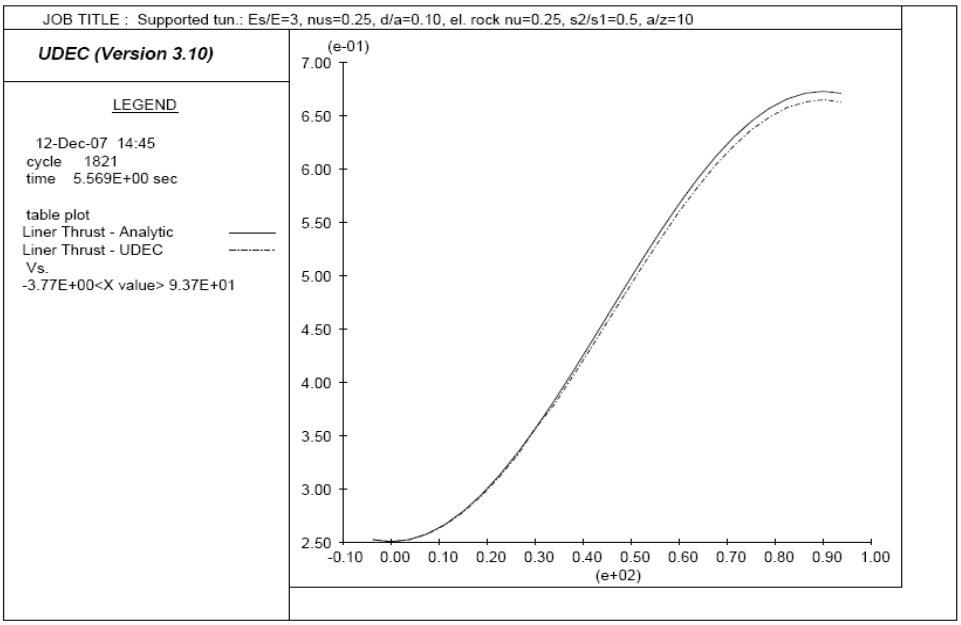

Figure 4.9. Comparison of *UDEC* results for lining thrust with analytical solution for the case of lined tunnel in an elastic medium with a biaxial stress field.

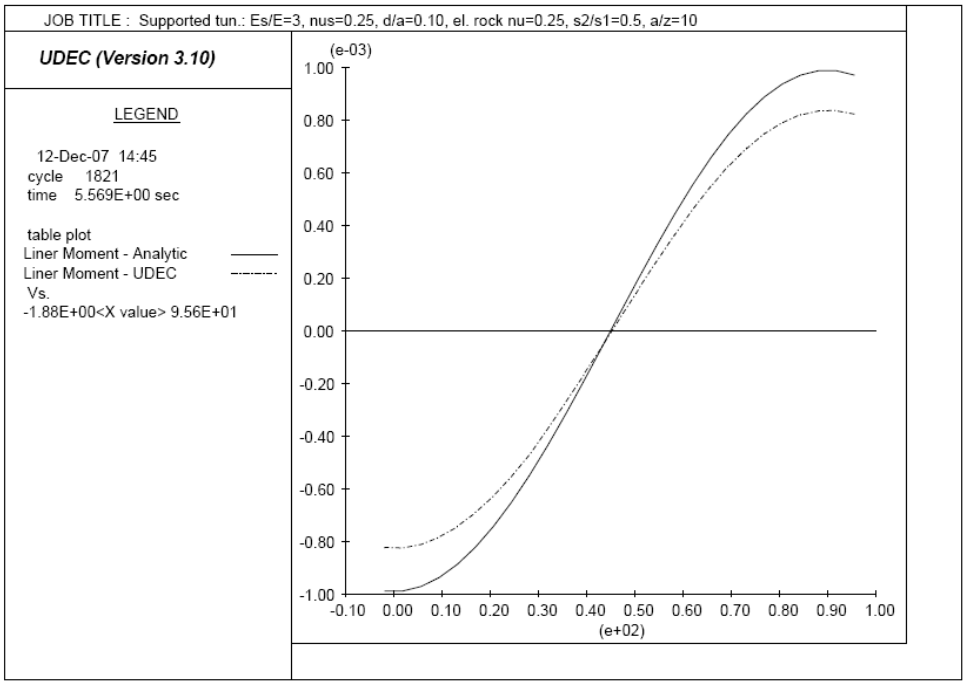

Figure 4.10. comparison of *UDEC* results for lining moment with analytical solution for the case of a lined tunnel in an elastic medium with a biaxial stress field.

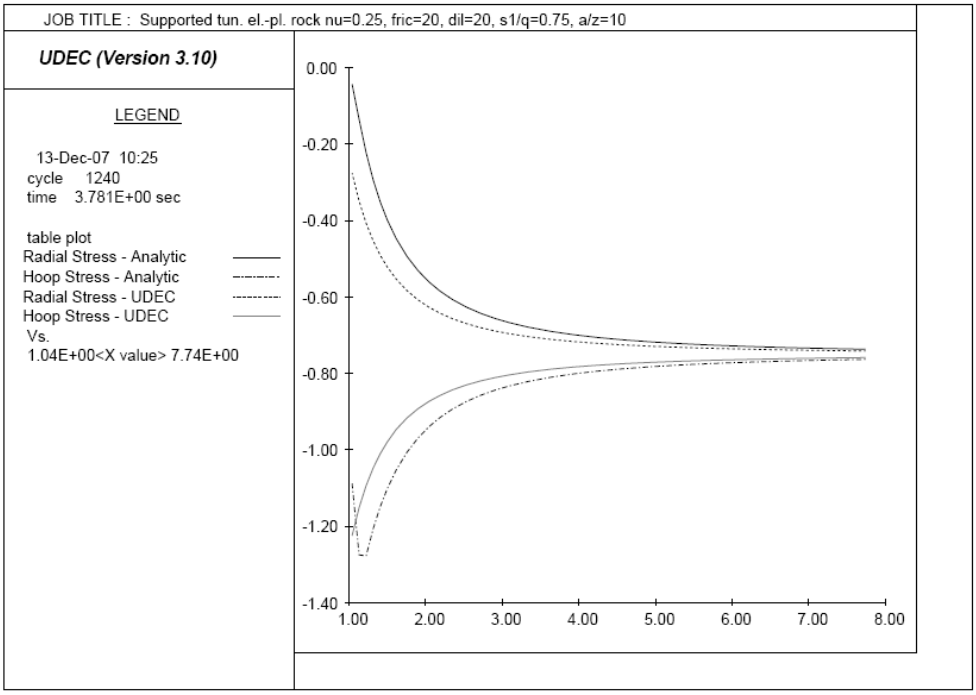

Figure 4.11. Comparison of *UDEC* results of radial and tangential stresses versus radial distance along a line $\theta = 0°$ with analytical solution for the case of a supported tunnel in Mohr-coulomb medium with biaxial stress field.

4.5.2. Seismic – Induced Groundfall

A demonstration simulation of a seismic-induced groundfall is presented to illustrate the use of *UDEC* for analyzing this type of problem. The model shown in Figure 4.12 is an overcut modeled with a geometry of 5m high and 10m wide.

It was assumed that two continuous joint sets intersect the plane of analysis: one with an orientation of 45° and the other with an orientation of -9°. Both sets have a joint spacing of 5m. For demonstration purposes, a near vertical "artificial" joint was also added to the block in the roof of the excavation to enhance the instability.

From the average laboratory test values provided for the intact rock, the following material properties were assumed for the rock blocks:

density	3000 kg/m^3
Young's modulus	75,000 MPa
Poisson's ratio	0.18

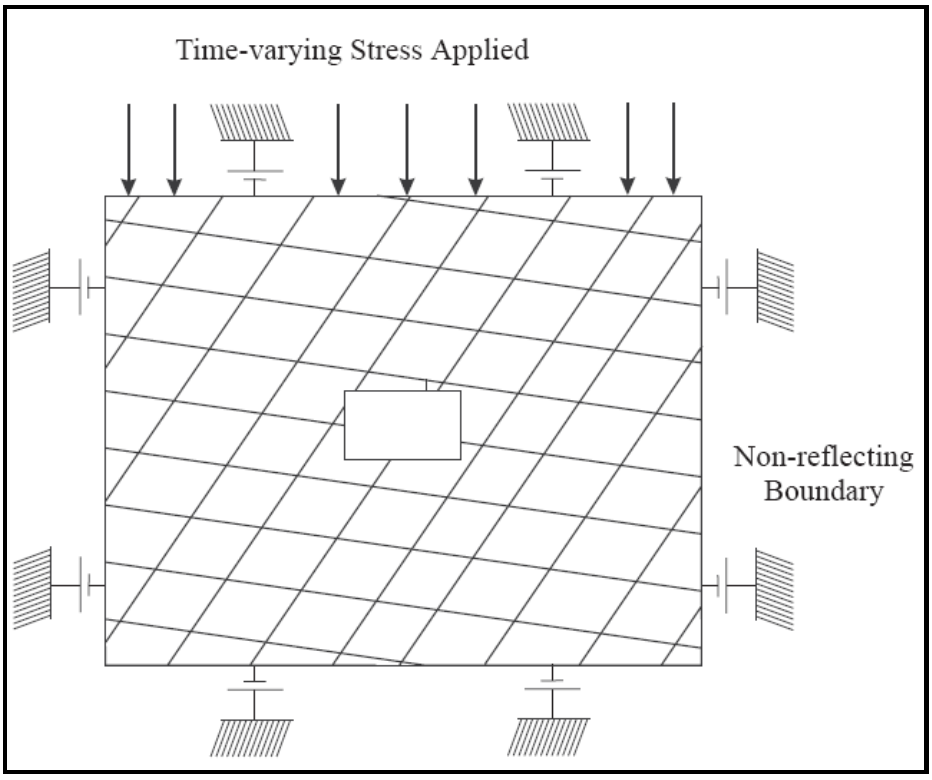

Figure 4.12. *UDEC* model for seismic-induced groundfall.

The blocks were assumed to behave elastically only. Coulomb slip behavior was assumed for the joints and typical textbook values were chosen for joint properties:

joint normal stiffness	20,000 MPa/m
joint shear stiffness	20,000 MPa/m
friction angle	30°
cohesion	0

The in-situ stress state was estimated to be isotropic at 24MPa (assuming vertical loading due to overlaying rock at a depth of approximately 800m).

4.5.2.1. UDEC Analysis

The *UDEC* modeling sequence was performed in three stages. First, the model without the overcut excavation was consolidated under the in-situ stresses. Next, the excavation was introduced and the model cycled to an equilibrium state. The stress distribution around the overcut at this stage is illustrated in Figure 4.13. The blocks immediately above and below the overcut have slipped and then stabilized.

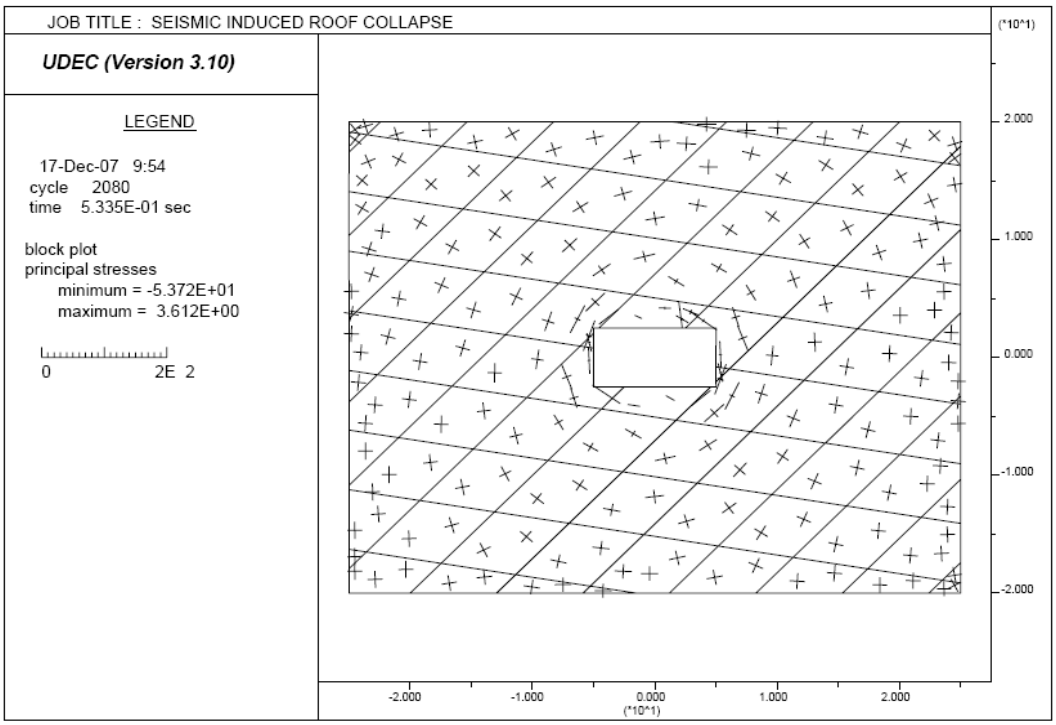

Figure 4.13. Stress distribution around excavation at end of excavation stage.

In the third stage, two different seismic events with different peak velocities were evaluated. For all seismic simulations, viscous boundaries were introduced around the outer perimeter of the problem domain to eliminate wave reflections, thereby simulating an infinite rock mass. Seismic events were represented by a sinusoidal y-

directed stress wave applied at the top of the model. The applied stress wave was superimposed on the existing in-situ stresses.

In the first simulation, a peak stress of 1.25MPa was applied. It should be noted that, due to the viscous boundary conditions in effect at the top of the model, the "effective" applied stress is 1.25MPa/2, or 0.65MPa. the stress distribution in the roof of the excavation after 0.02 seconds is shown in Figure 4.14. Displacements were monitored at two points. Point1 is located in the left corner of the excavation; Point 2 is located at the right corner of the roof block. Displacement versus time plots (Figure 4.15) for these points essentially show an elastic response.

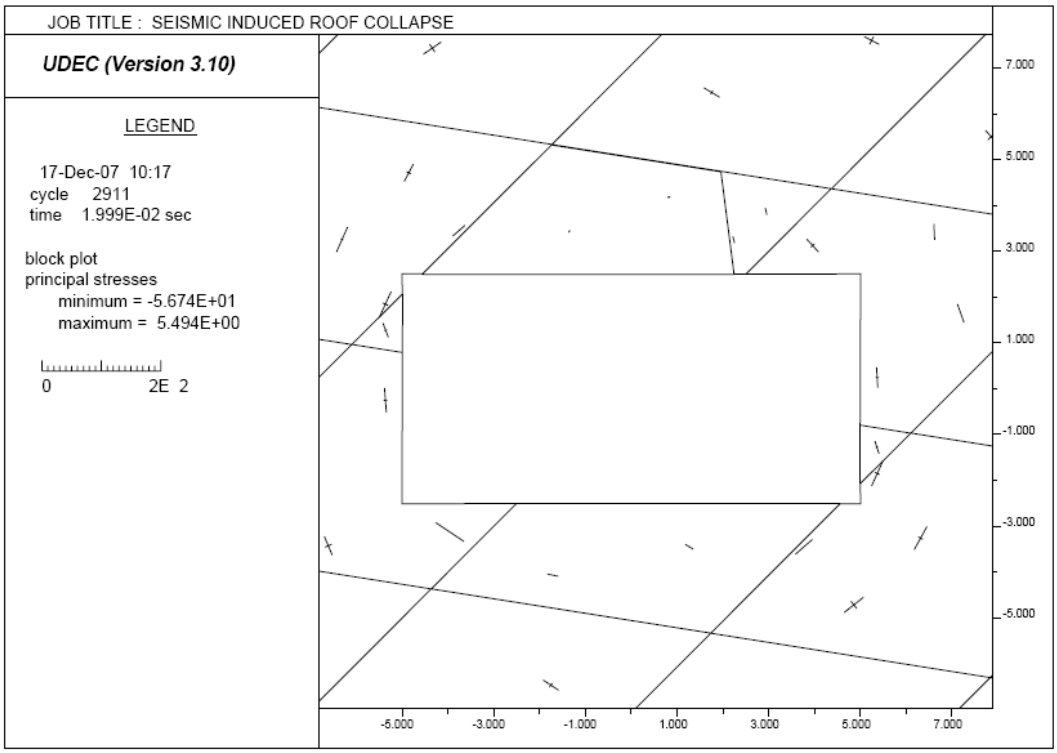

Figure 4.14. Stress distribution in roof of excavation after 0.02 seconds [applied stress = 1.25*cos(2π100t)].

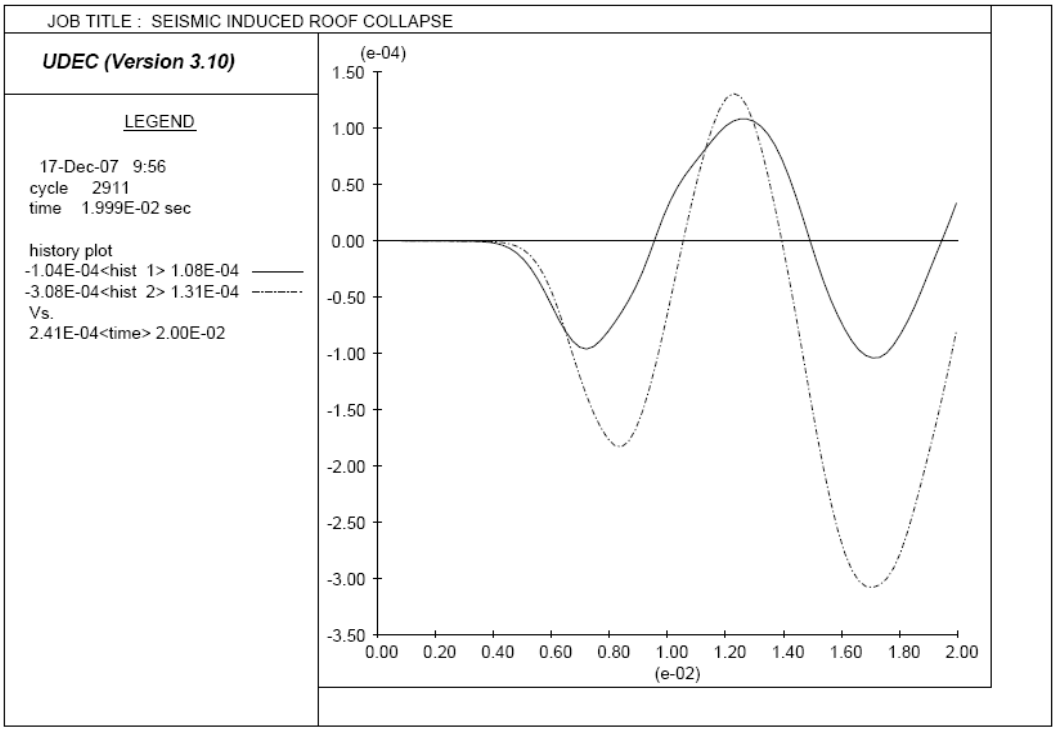

Figure 4.15. Y-displacement histories for two points on excavation boundary [applied stress = 1.25*cos(2π100t)].

It is interesting to compare estimated applied velocities with calculated velocities at the top of the model. The following equation can be used to estimate the applied velocity:

$$V = \frac{\sigma}{2(\rho C_P)} \tag{4.25}$$

Where

$C_p = [(K + (4/3)G)/\rho]^{1/2}$

Using this equation, the applied maximum velocity is found to be approximately 0.04m/sec. Figure 4.16 shows a peak velocities result from using the intact rock

modulus rather than the equivalent deformation modulus which takes into account the joint deformation.

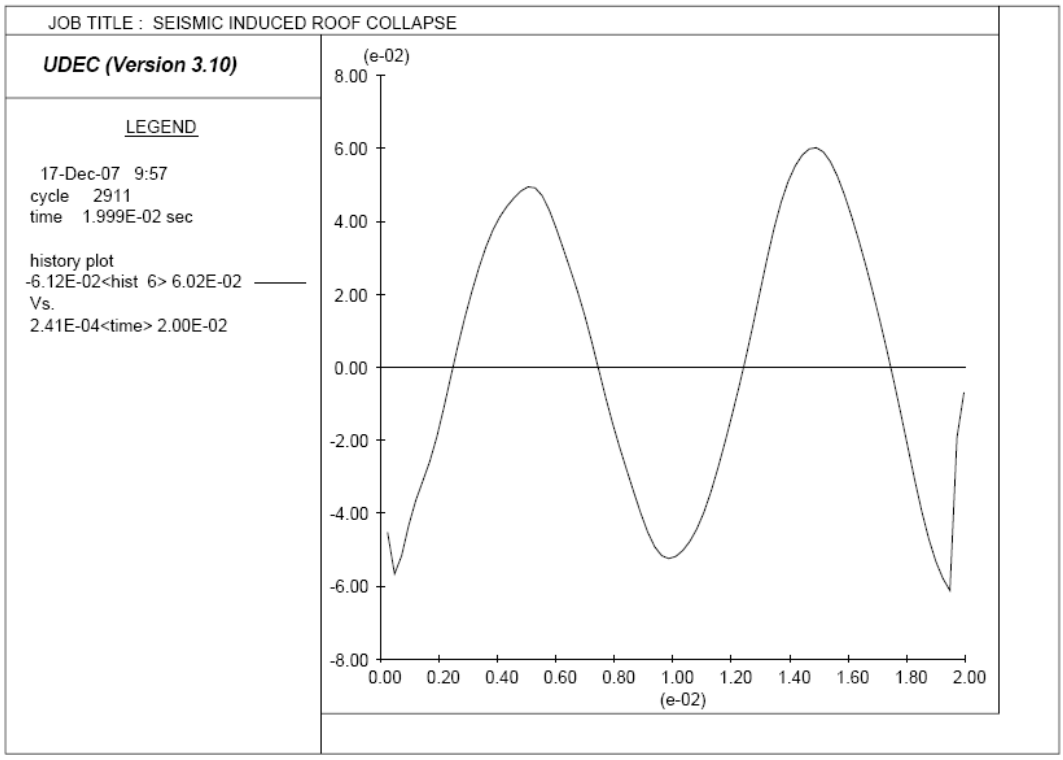

Figure 4.16. Plot of y-velocity at top of model [applied stress = 1.25*cos(2π100t)].

In the second example, a stress were wave with peak stress of 12.5MPa ("effective" stress = 6.25MPa) was applied. The stress distribution in the roof of the excavation after 0.02 seconds is shown in Figure 4.17.

This figure shows that the roof block is unstressed, indicating that the block has loosened. Displacements versus time plots (Figure 4.18) also indicate that the block has loosened and is falling. As a matter of interest, the problem geometry and stress distribution at three later times are presented in Figures 4.19 through 4.21.

The predicted velocity (from the equation above) at the top of the problem is 0.4m/sec. The velocity calculated from the model is shown in Figure 4.22. Again,

differences between predicted and measured velocities result from using intact rock modulus rather than rock mass deformation modulus.

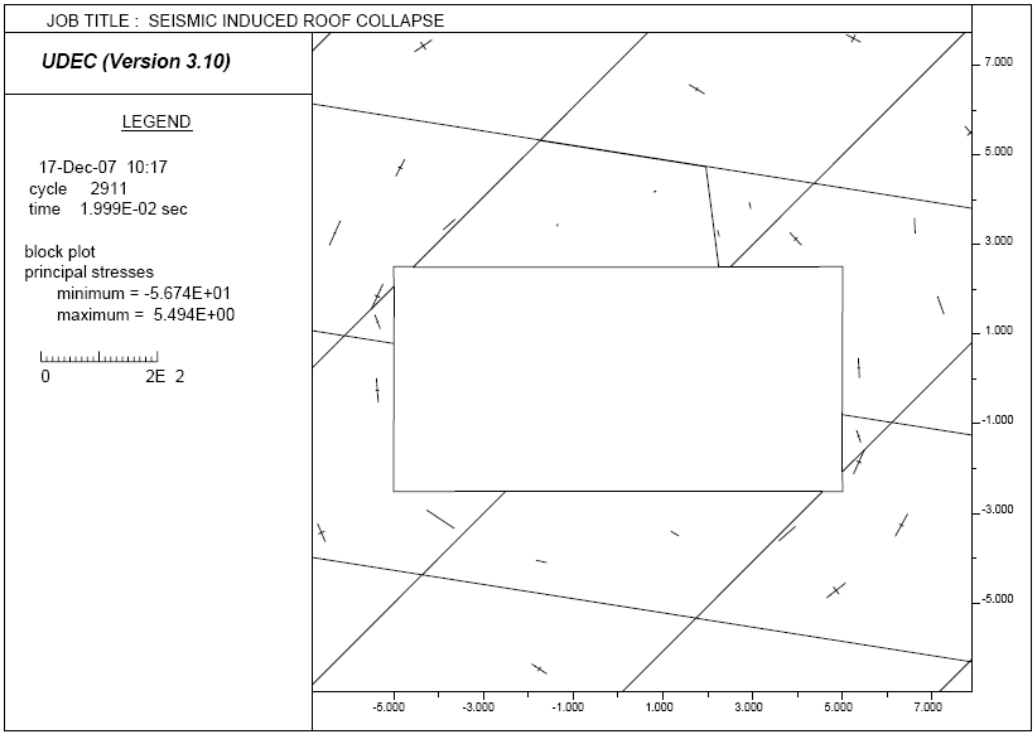

Figure 4.17. Stress distribution in roof of excavation after 0.02 seconds [applied stress = 12.5*cos(2π100t)].

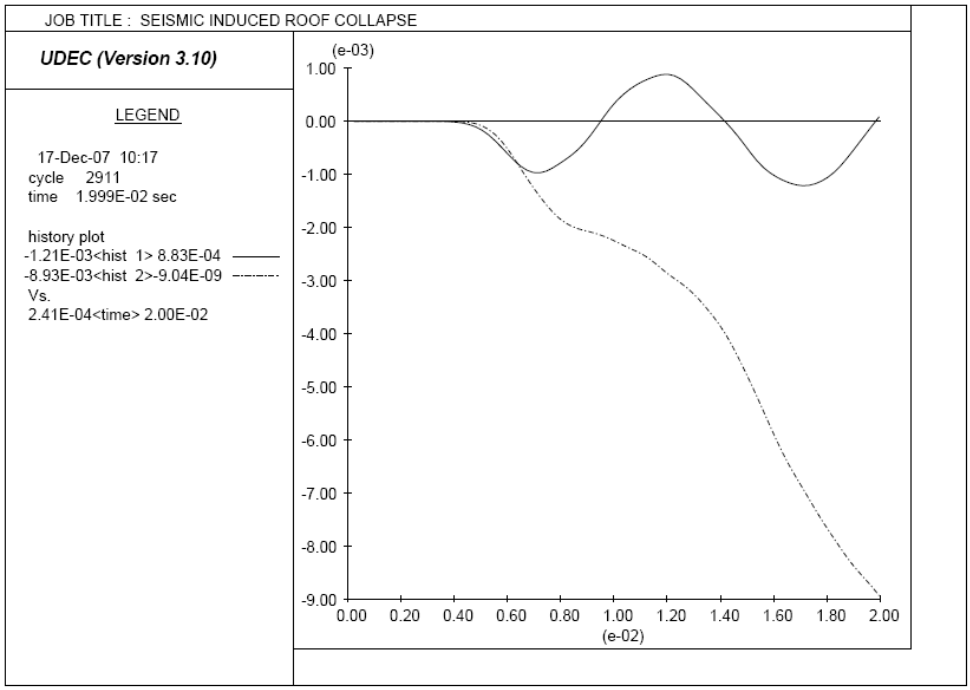

Figure 4.18. Y-displacement histories for two points on excavation boundary [applied stress = 12.5*cos(2π100t)].

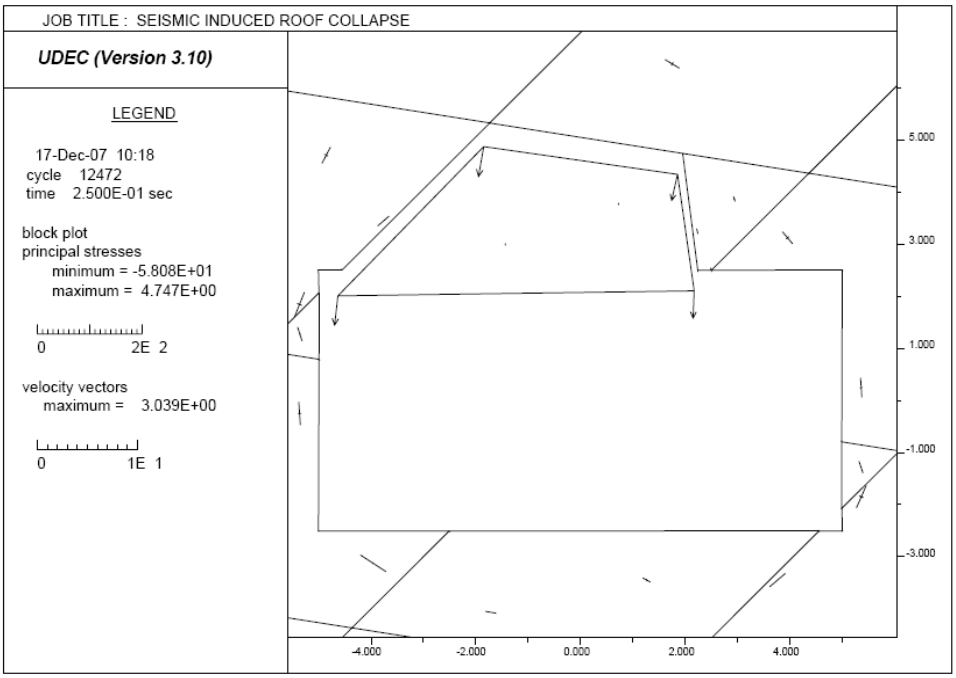

Figure 4.19. Stress distribution around excavation after 0.25 seconds [applied stress = 12.5*cos(2π100t)].

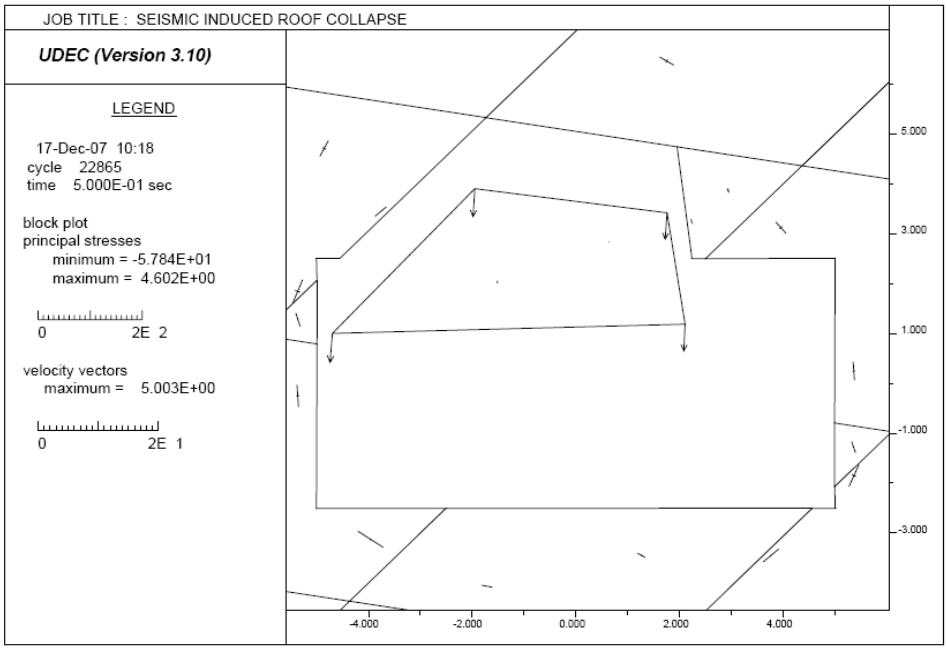

Figure 4.20. Stress distribution around excavation after 0.50 seconds [applied stress = 12.5*cos(2π100t)].

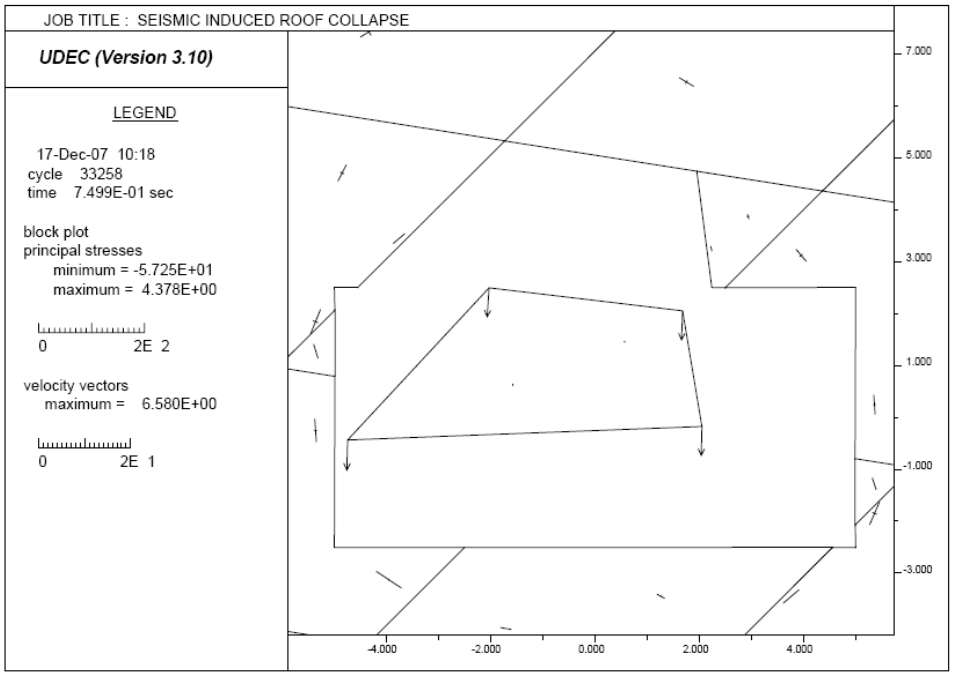

Figure 4.21. Stress distribution around excavation after 0.75 seconds [applied stress = 12.5*cos(2π100t)].

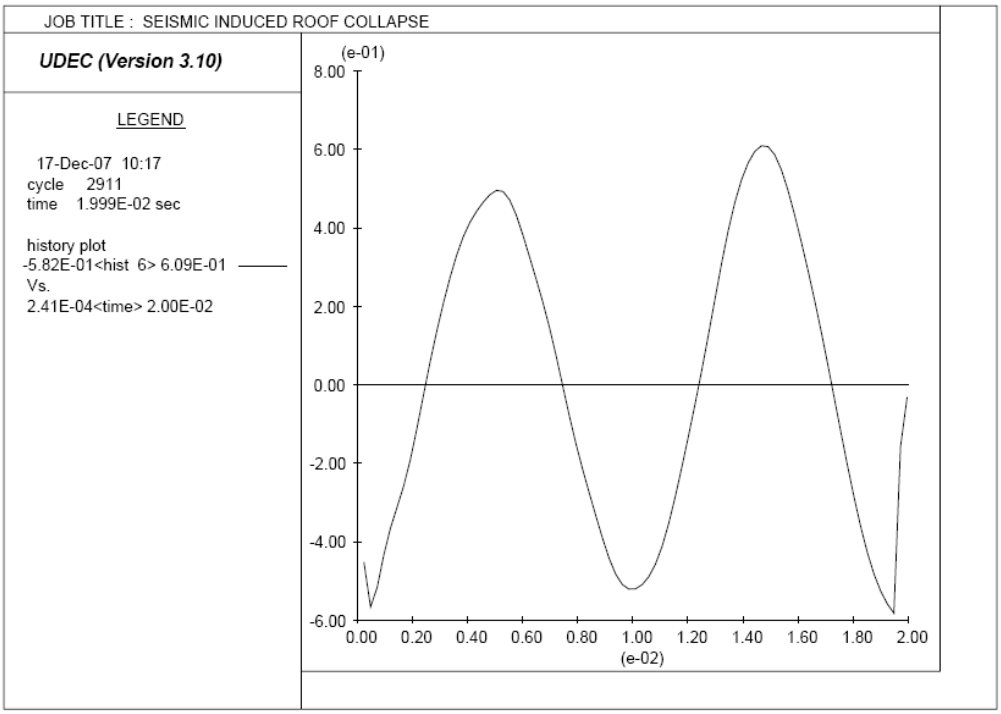

Figure 4.22. Plot y-velocity at top of model [applied stress = 12.5*cos(2π100t)].

4.5.3. Seismic loading in a circular tunnel

The present analysis represents an application of the previous preliminary test "*Seismic-Induced Groundfall*" (see section 4.5.2). At present the tunnel is circular and unlined, with a 5m radius. The parameters used in the example application are the same for this case where, in addition, the tunnel will be analyzed considering, first, the structure immersed in a continuous medium and then the same structure immersed in a discontinuous medium.

The material properties for the model are:

density	3000 kg/m^3
Young's modulus	75,000 MPa
Poisson's ratio	0.18

A peak stress of 12.5 MPa was applied for the simulation for both continuum and discontinuum medium. As on the previous example, due to the viscous boundary conditions in effect at the top of the model, the "effective" applied stress is 6.25 MPa. The apply seismic event was represented by a y-directed stress wave applied at the top of the model. Displacements were monitored at two points. Point 1 is located at the top of the excavation; Point 2 is located at the right side of the roof tunnel.

4.5.3.1. Tunnel in a continuous medium

For this case it was considered an unique block characterize by the presence of a 10m tunnel diameter, because UDEC works with discontinuities, it was necessary to create a discontinuity. The properties of the fault, with an East-West direction, are:

joint normal stiffness	40,000 MPa/m
joint shear stiffness	40,000 MPa/m
friction angle	60°
cohesion	2.5 MPa/m

On this way, it is possible to considered the model as an unique block and not as separated blocks. As a next step for the UDEC model, it was calculated the stress distribution around the tunnel (see Figure 4.23).

A seismic loading event was applied after 0.02 seconds (see Figure 4.24). In order to eliminate wave reflections viscous boundaries were introduced around the outer perimeter of the problem domain, which correspond to a block with a geometry of 30x30 m.

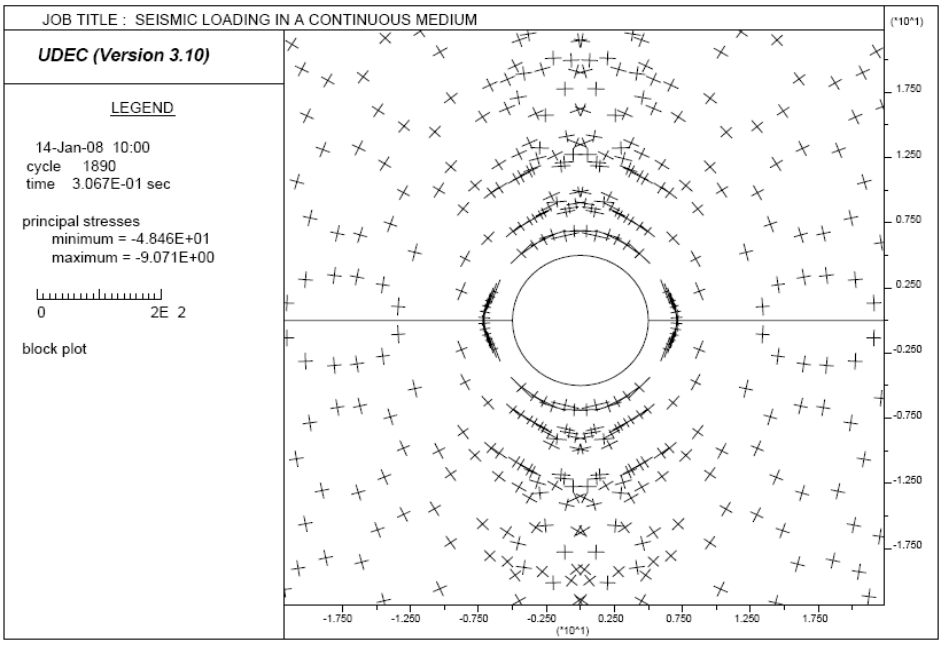

Figure 4.23. Stress distribution around the excavation.

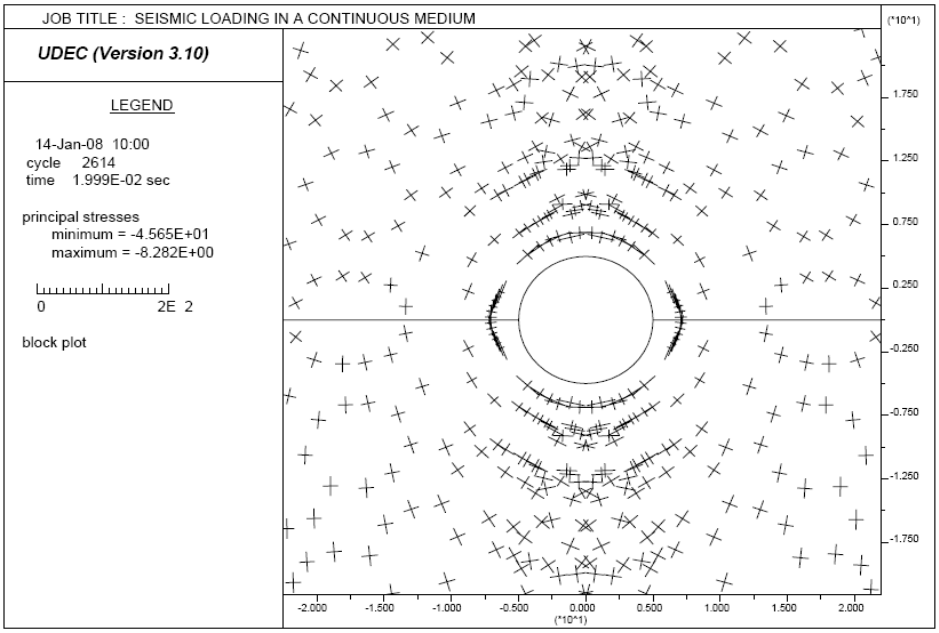

Figure 4.24. Stress distribution around the tunnel after 0.02 seconds applied stress [*applied stress=12.5xcos(2π 100t*)].

Figure 4.25 shows the Y-displacements histories of the two points after the 0.02 seconds of applied stress. The two lines that are shown in the figure correspond to point 1 (hist 2) and point 2 (hist 3) respectively. As you can see the two point have almost the same history behavior.

By using the *equation 4.24* it is possible to estimate the applied velocity. This equation allows comparing estimated applied velocities with calculated velocities at the top of the model.

At this point, the applied maximum velocity is approximately 0.04 m/sec. Instead, the Figure 4.26 shows a peak velocity almost the 0.04 m/sec.

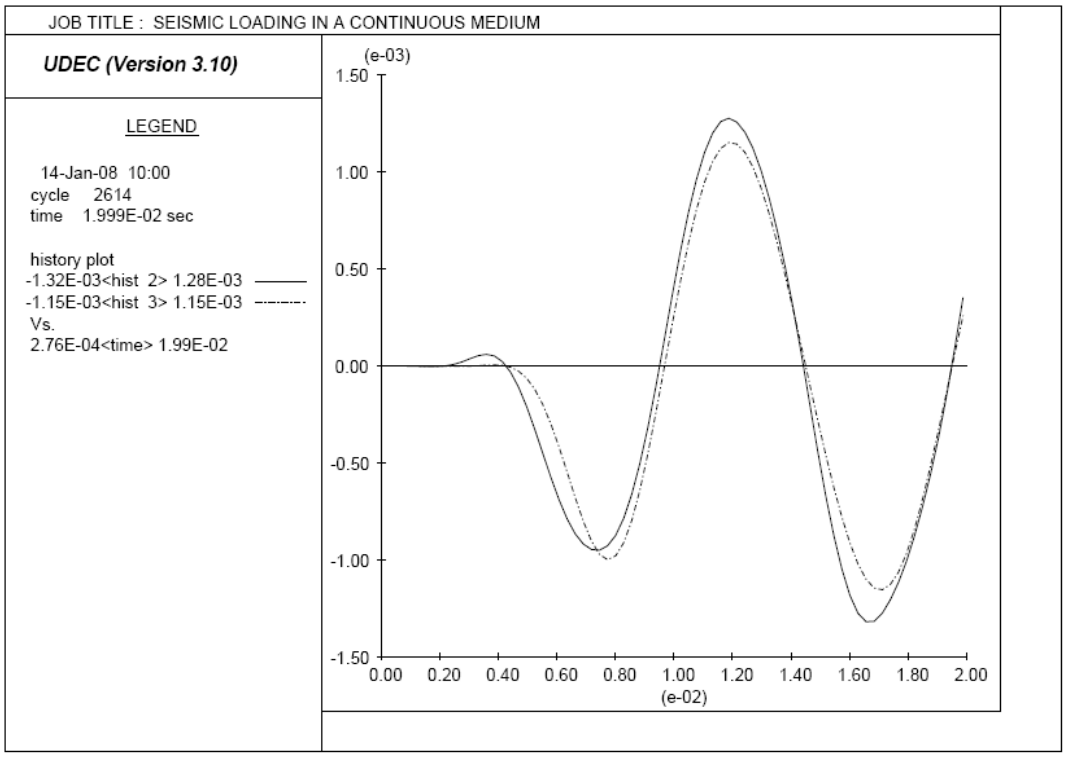

Figure 4.25. Y-displacement histories for two points an excavation boundary [*applied stress=12.5xcos(2π 100t*)].

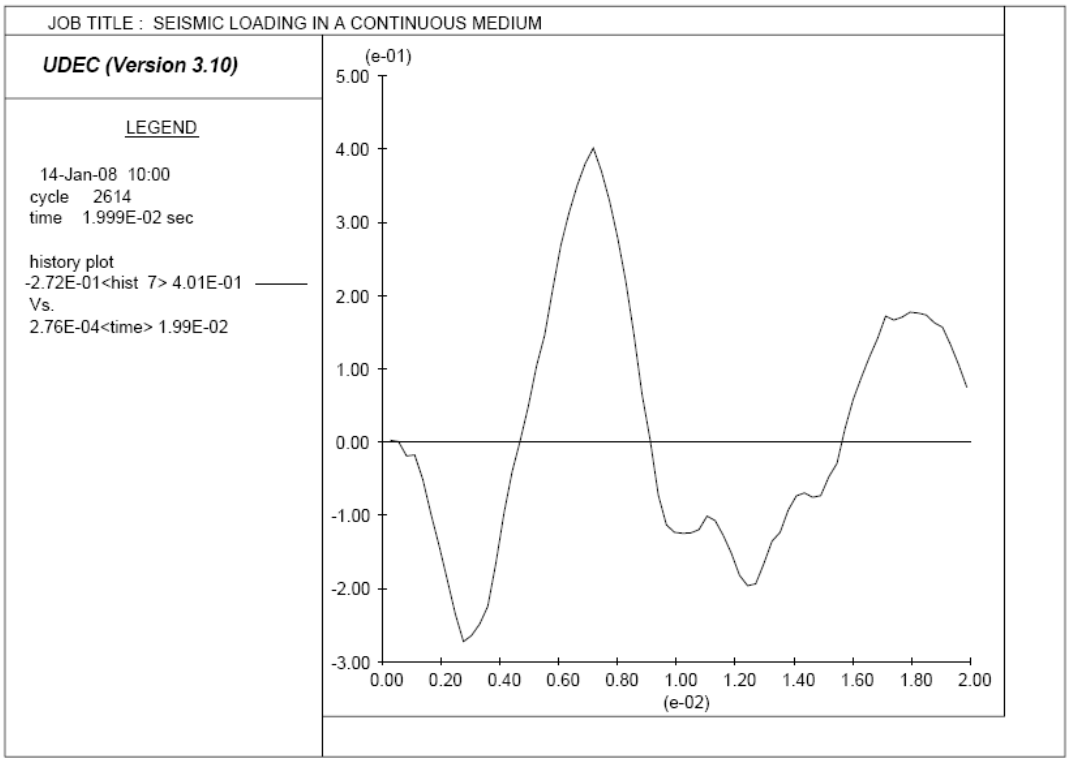

Figure 4.26. Plot of y-velocity at top of model [*applied stress=12.5xcos(2π 100t*)].

4.5.3.2. Tunnel in a discontinuous medium

For this case, the medium is an unique material divided by 3 joints set around a 10m tunnel diameter in order to enhance the instability. The joints have the following orientation 45°, 105° and 135°; the spacing of the first two joints set are 4m; instead, the spacing for the last joint is 6m. The properties of the joints are:

joint normal stiffness	20,000 MPa/m
joint shear stiffness	20,000 MPa/m
friction angle	30°
cohesion	0

The stress distribution in the roof of the excavation after 0.02 seconds is shown in Figure 4.27; as you can see on the figure, there are not applied stresses at right side of the tunnel which indicate a possible instability for the structure. Displacements versus

time plots (Figure 4.28) also indicate that the block has loosened and is falling. Figure 4.29 to 4.31 shown the problem geometry and stress distribution at three later times.

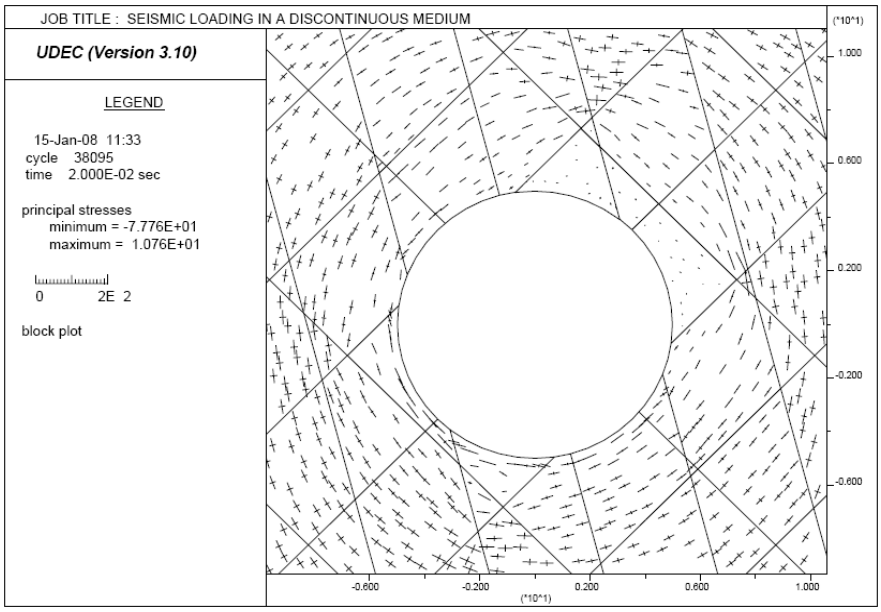

Figure 4.27. Stress distribution in roof of excavation after 0.02 seconds [*applied stress=12.5xcos(2π 100t*)].

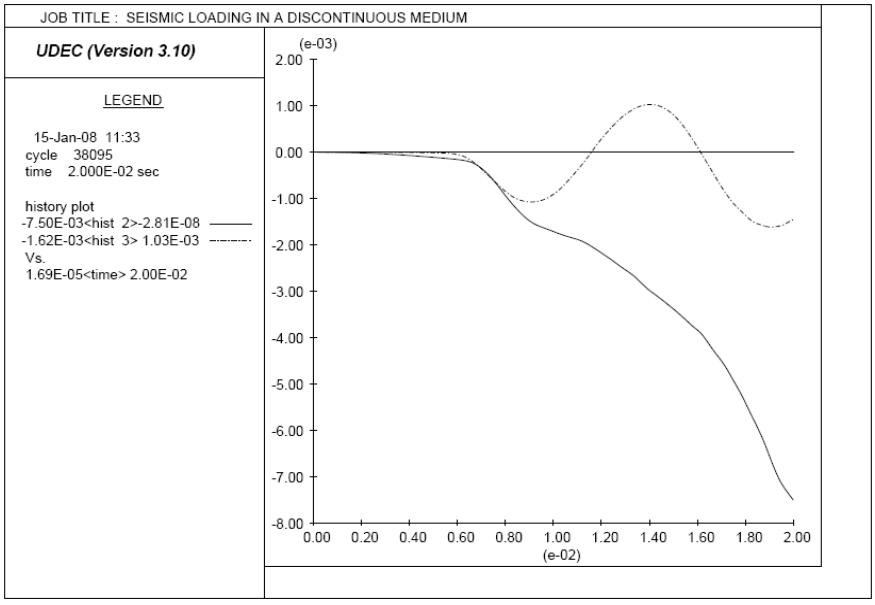

Figure 4.28. Y-displacement histories for two point on excavation boundary [*applied stress=12.5xcos(2π 100t*)].

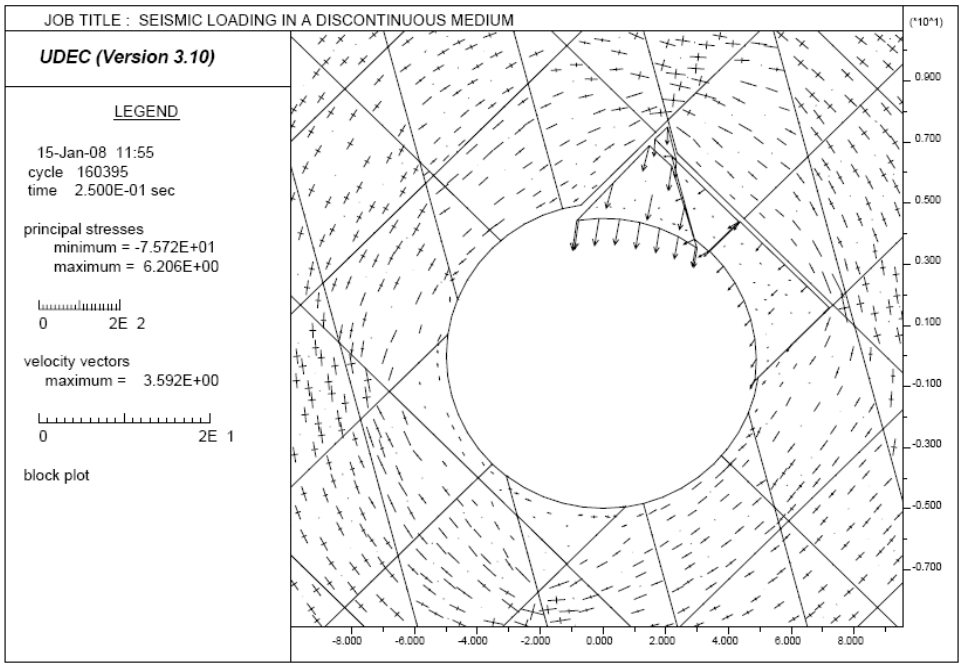

Figure 4.29. Stress distribution around excavation after 0.25 seconds [*applied stress=12.5xcos(2π 100t)*].

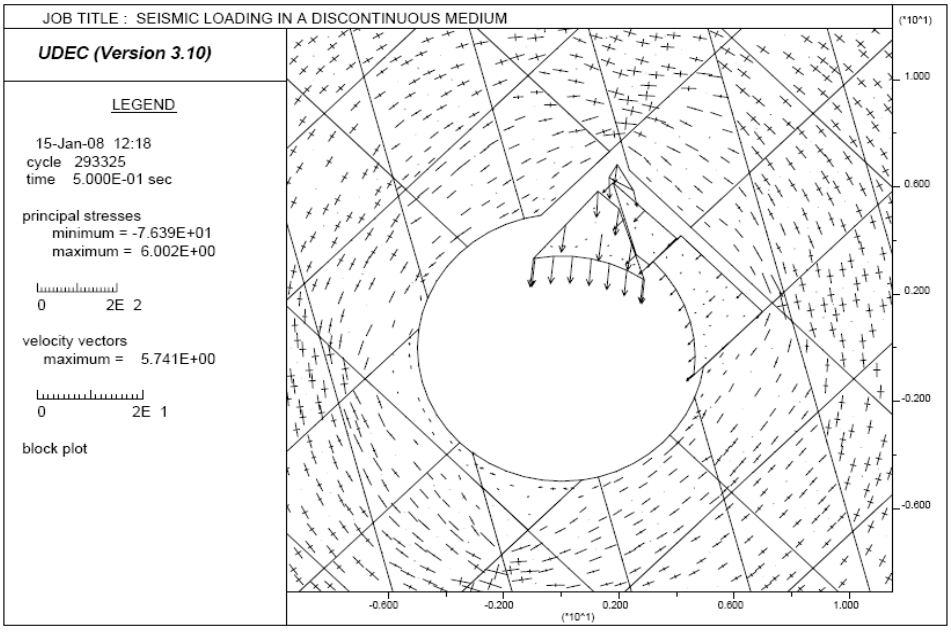

Figure 4.30. Stress distribution around excavation after 0.50 seconds [*applied stress=12.5xcos(2π 100t)*].

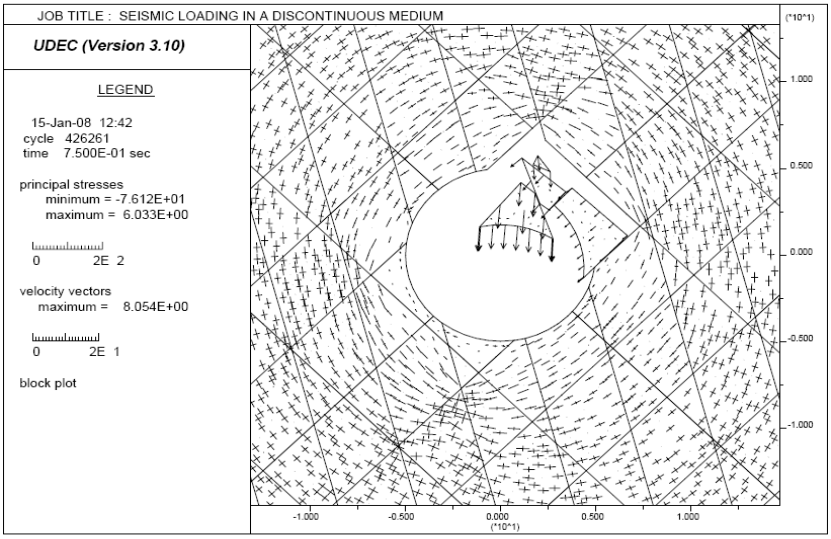

Figure 4.31. Stress distribution around excavation after 0.75 seconds [*applied stress=12.5xcos(2π 100t*)].

The predicted velocity (from equation 4.24) at the top of the problem is 0.4 m/sec. the velocity calculated from the model is shown in Figure 4.32 with a peak velocity of 0.6 m/sec. this difference between predicted and measured velocities result from using intact rock modulus rather than rock mass deformation modulus.

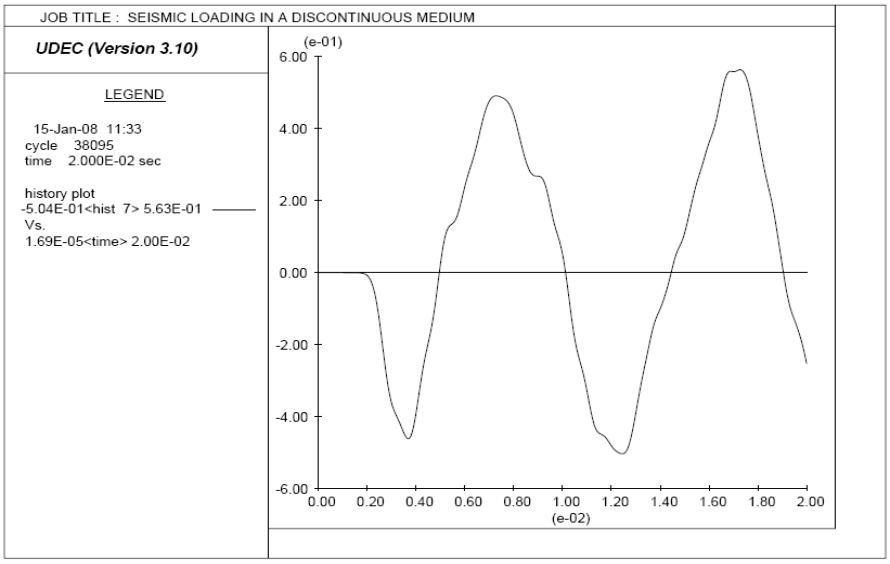

Figure 4.32. Y-velocity at the top of model [*applied stress=12.5xcos(2π 100t*)].

CHAPTER V

CASE STUDY

5.1. Introduction

The new railway line "Caserta-Foggia" is part of the doubling of the original line, this represents one of the most important crossings of the Apennines Mountains in the Southern of Italy. The new railway line, which has been designed in the 80's, includes 17 tunnels. The line between Caserta and Apice (a small town near Benevento) was built in the earliest 90's, whereas the other part of the line underwent a preliminary design stage only.

The route of the railway line foresees the construction of the "Serro Montefalco" tunnel. This tunnel, with a length of 11.7km and with a maximum depth of 225m, represents one of the most relevant structures of the entire railway line due to the complexity of the geological conditions to be encountered (Figure 5.1).

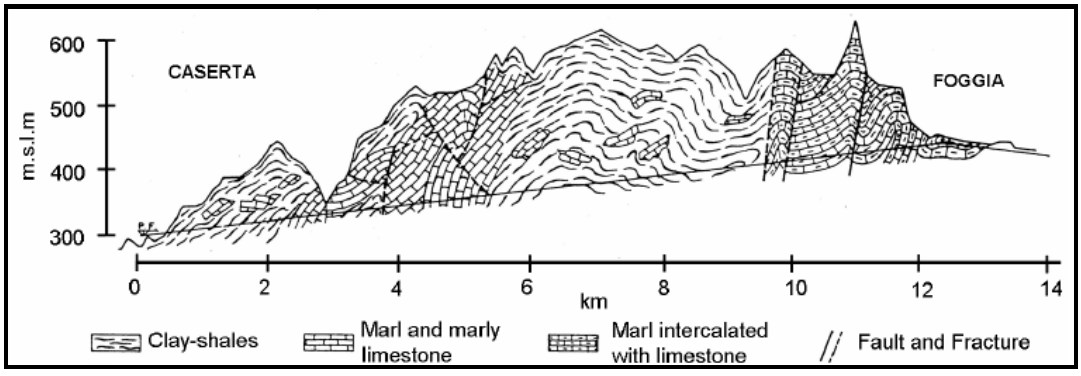

Figure 5.1. geological profile along the "Serro Montefalco" tunnel (from Barla et al., 1986).

The lithotypes include varicoloured clay-shales, marl and marly limestone and clay and marl intercalated with limestone (Barla et al., 1986). The varicoloured clay-shales include expansive clay minerals which exhibit a significant swelling behavior.

Previous excavations of tunnels in this weak rock formation (e.g. the "San Vitale" Tunnel see Barla et al., 1986 and Lunardi & Bindi, 2004 for more details) were characterized by severe squeezing and swelling problems which lead to face instability, large convergences, invert-heave and critical loading of the tunnel support.

5.2. Seismic Input Definition

The "Serro Montefalco" tunnel is located in the middle part of the Appennini Mountains, this area is characterized by a high level of seismicity following a restricted orientation in direction NW-SE with a length around the 30 – 50 km in the same direction of the mountainous chain (Improta et al., 2000). The north part of this area, well known as the Sannio region, is one of the seismically active area in Italy.

In this area five large earthquakes with I_{MCS}>X occurred in 1456, 1688, 1702, 1735 and 1805, causing several victims and severe damage. A long seismic sequence since 1805 event makes the area highly susceptible to a new earthquake.

The choice of an earthquake scenario has been made by using the Deterministic Seismic Hazard Analysis (DSHA), in which there have been determined and characterized the different sources that could produce a significant damage in the area of study.

The area in which is located the "Serro Montefalco" tunnel is characterized by the presence of three important seismic sources: Ariano Irpino, Valle Ufita and Bacino Tammaro, codified from the "Database Italiano delle Sorgenti Sismogenetiche (DISS, 2006)" respectively ITGG092, ITGG006 e ITGG005, as shown in Figure 5.2.

The Ariano Irpino fault have been chosen as the seismic scenario because it is nearest to the tunnel and because it is characterized by a magnitude (M_w) of 6.9, the maximum value of magnitude with respect to the other faults.

For structures on the surface, the seismic action is often represented in the form of spectrum response of acceleration or displacement. Instead, for underground structures, a correct simulation of the response needs the use of temporal history. These can be calculated using the following methods: artificial temporal history from compatible spectrum, synthetic temporal history from seismologic models, and temporal history really recorded.

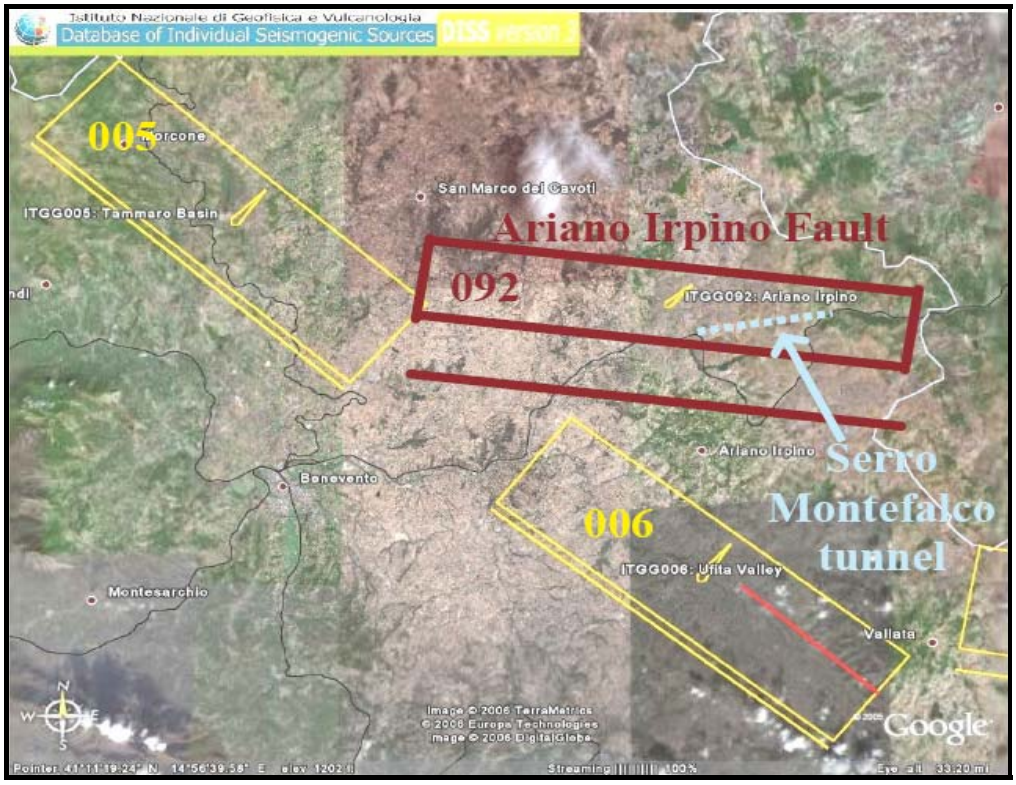

Figure 5.2. Location of the "Serro Montefalco" tunnel (dotted line) along the "Caserta-Foggia" railway line (dark solid line). The nearby active faults retrieved from the DISS 3.0.2 database are superimposed. The "Ariano Irpino" fault (ITGG092), which is assumed as a potential seismic source in the dynamic analysis of the tunnel, is highlighted. The short segment perpendicular to the tunnel axis, denotes the cross-section of the tunnel (Corigliano et. al., 2006).

Even if the increasing use of digital accelerometers have increased the number of registrations under near field conditions, permitting the use of real registrations on the response analysis of the structure, in many cases it is necessary to take into account the use of simulated temporal history.

In a particular way, in case of underground structures it is necessary to have in mind some peculiarity, as the behavior on the horizontal direction along the tunnel axes, which makes it necessary to have registration along the hold structure, and the tunnel depth, that requires the knowledge of the motion at depth.

For these reasons, a synthetic temporal history created by using the Deterministic Seismic Hazard Analysis (DSHA) from Hisada & Bielak (2003) has been chosen. The use of this analysis needs the definition of the crustal velocity profile and the source model.

5.2.1 Crustal velocity profile

The geological structure of the "Sannio" is complex and characterize by the relevant lateral heterogeneity in the first 4km of the surface. Some authors proposed models for the crustal velocity in the Southern Appennines, in particular after the earthquake of Irpinia in 1980. Improta et al. (2000) idealized an interpretation of the data of the seismic refraction. The seismic data acquired along the 75km parallel to the Appennines, have been used to provide a two-dimensional velocity model of the P wave at the surface of the crust (Figure 5.3).

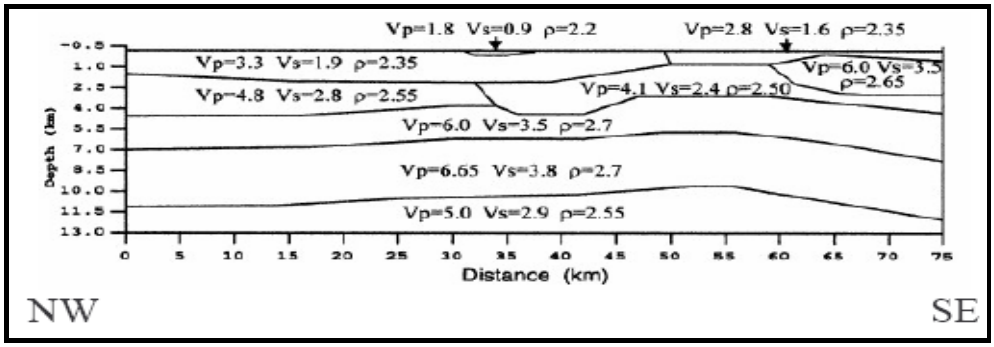

Figure 5.3. Crustal velocity profile proposed by Improta et al. (2000).

The interpretation of the velocity model is based on the registration of the velocity wave made from oil wells near the fault, gravimetrical measure and simulation of the finite difference. The stratigraphical profile that characterizes the North-West part in the Figure 5.3, was assumed as the general model of the "Sannio" region.

The profile for the shear wave (S wave) took into account for the simulation is shown in Figure 5.4. Because the simulated fault has a depth of 25km and the crustal model of Improta et al. (2000) with a depth of 13km, the model was chose taking into a least detailed model proposed by Chiarabba & Amato (1997).

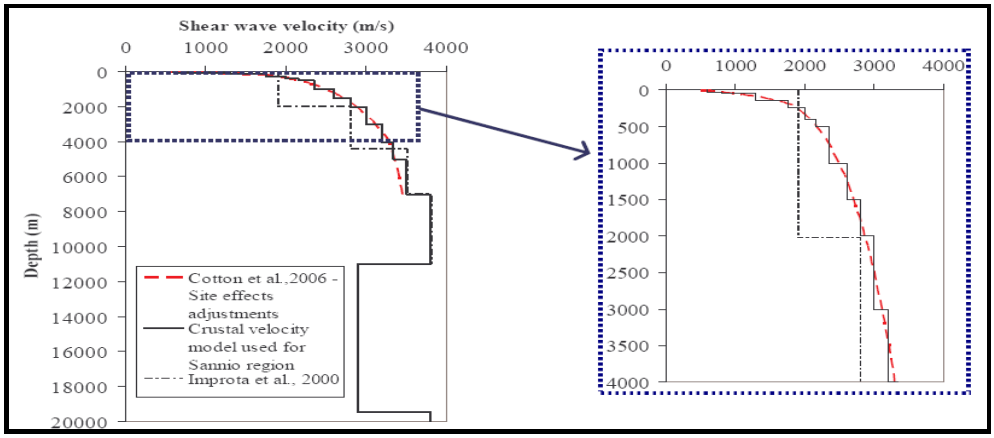

Figure 5.4. Crustal velocity profile adopted for the solution of the auxiliary problem (Corigliano et al., 2006).

5.2.2 Source model

The Ariano Irpino fault (ITGG092) was the source of the December 5th 1456 earthquake, one of the most important natural phenomenon in the Italian seismic history. The principal characteristic of this source and the parameters adopted for the deterministic simulation are shown in Table 5.1.

Table 5.1. Features of the Ariano Irpino fault (DISS V.3.0.2)

Seismic Moment	M_w	L	W	Slip	Strike	Dip	Rake	Min. Depth	Max. Depth	Hypo. Depth	Rupture Vel.	Rise time	Max. freq.
Nm	-	km	km	m	º	º	º	km	km	km	km/s	s	Hz
$2.54x10^{19}$	6.9	30	14.9	2	277	70	230	11	25	22.7	2.8	1.8	5

5.3. Analysis in a continuous medium

5.3.1. Static analysis for ovaling deformation

Assessing the earthquake-induced effect on underground structures is an important step to the correct evaluation of the state of stress in the lining after construction. This involves the simulation of the excavation and construction stages in order to compute the cross-sectional stresses in the lining. Numerical analyses have been performed based on the geotechnical site characterization that is going to be described below.

5.3.1.1. Geotechnical parameters

The rock mass parameters along the tunnel length have been characterized on the basis of geomechanical classification and scaling rules of the intact rock properties obtained from laboratory test.

For soil-like materials (e.g. marl and marly limestone) reference has been made to laboratory testing (as physical properties, CIU, CID triaxial test, direct shear tests, edometric test, etc) of undisturbed samples obtained from borehole drilling (Barla et al., 1986). The deformability properties obtained for the marl and marly limestone rock mass are shown in Table 5.2.

Table 5.2. Deformability parameters of marl and marly limestone (Barla et al., 1986).

Young's Modulus	Poisson's ratio
15000 MPa	0.25

5.3.1.2. UDEC analysis

The UDEC model created for this analysis is shown in Figure 5.5. The model is to be run in plane strain conditions with the presence of two fictitious joints in a vertical and horizontal direction; in this way it is possible to consider the model as a continuous medium.

Figure 5.6 shows the mesh discretization applied to the model. In order to avoid problems of boundary conditions the size of the block model has a magnitude of 8 time the diameter of the tunnel.

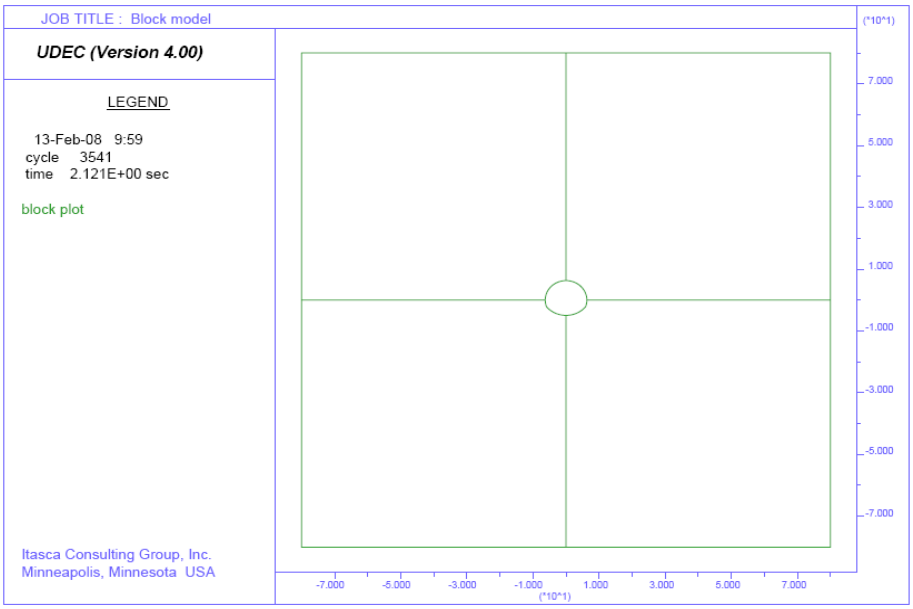

Figure 5.5. UDEC model with fictitious joints.

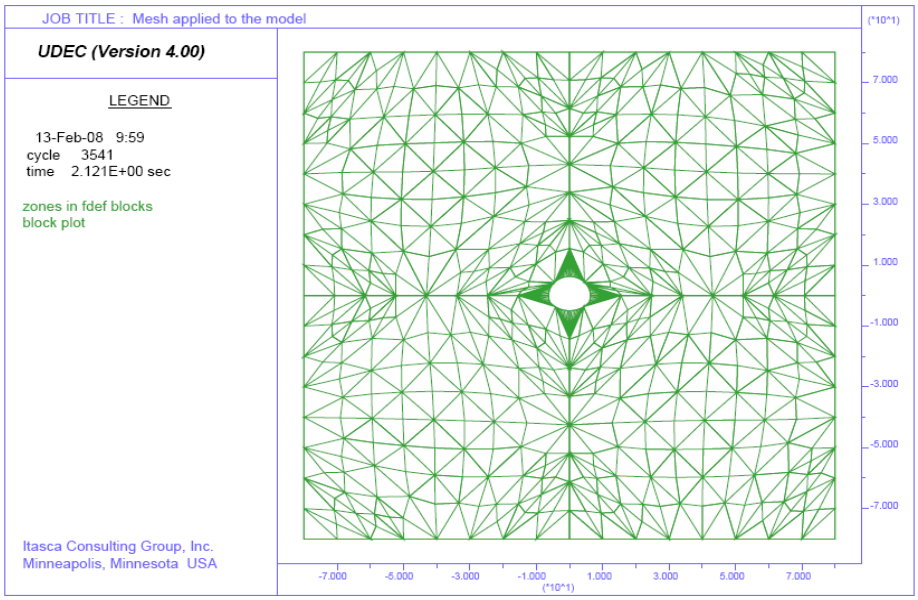

Figure 5.6. Zones applied around the tunnel.

The geometry of the tunnel cross section is shown in Figure 5.7. The lining thickness is about 0.8m.

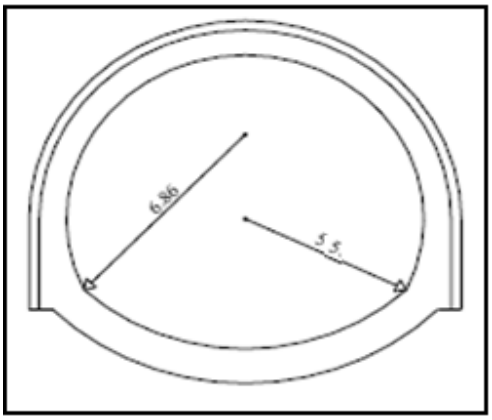

Figure 5.7. Cross section of the tunnel.

In order to simulate the excavation stages, the stress relaxation method proposed by Panet (1995) was used. This implies the introduction of a fictitious stress $(\sigma)_f$ on the opening contour as follows:

$$(\sigma)_f = (1-\lambda)(\sigma)_p \tag{5.1}$$

where λ is the stress relaxation factor ranging between 0 and 1, depending on the distance of the design cross section to the tunnel face, and $(\sigma)_p$ is the in situ stress.

The calculations have been performed with reference to an in-situ state of stress in the rock mass given by a vertical total stress of 2.5MPa (corresponding to a depth of approximately 100m); the value of the horizontal total stress has the same value (2.5MPa) of the vertical total stress.

The rock mass has been modeled using an elastic constitutive law. The rock mass parameters used for this analysis are shown in Table 5.2. The construction stages have been simulated through different steps as follows:

1. Simulation of the initial in-situ of stress; this is done by applying: the initial in-situ tresses to the model and later the first equilibrium.
2. Full face excavation up to a 50% removal of the stresses around the tunnel; the 50% stress relief was applied by using the command solve force 50; in this way, UDEC realizes the simulation taking into account the percentage of relief.
3. Installation of a 0.8m concrete lining at the contour of the excavated tunnel and application of the 100% stress relief; for practical reason the thickness of the concrete lining will act as the final reinforced concrete lining.

The structural element carries the load derived from the static analysis plus the additional earthquake loading. Figure 5.7 shows a typical cross section of the concrete lining applied to the underground excavation. The structural elements have been modeled by using linear elastic, isotropic plane strain elements. The material properties of the lining are shown in Table 5.3.

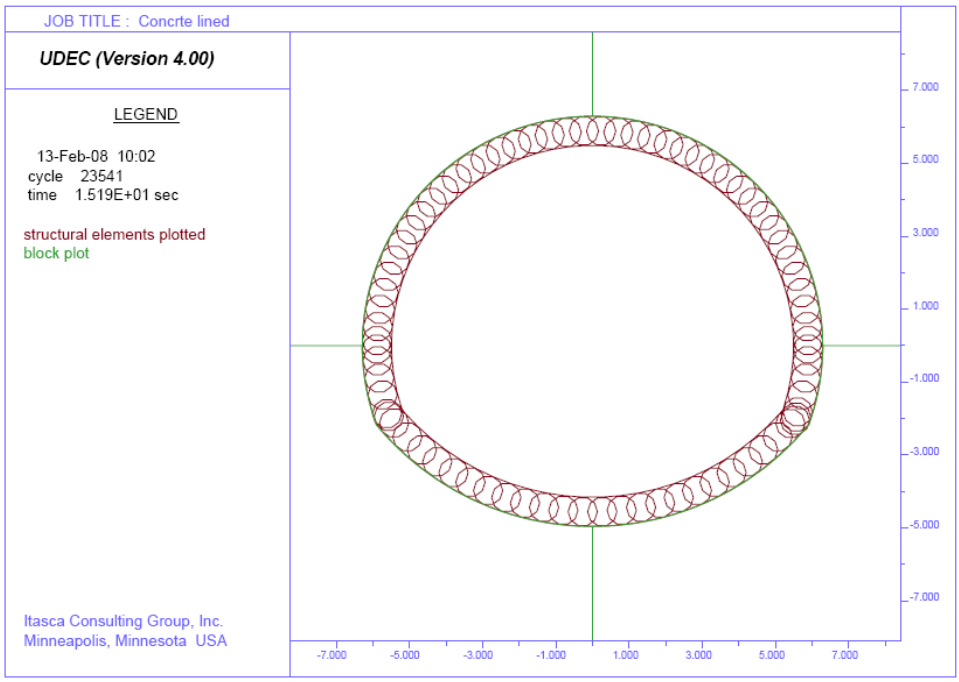

Figure 5.7. Applied concrete lining around the tunnel.

Table 5.3. Mechanical parameters of the lining.

E_s	γ_{cls}	ν_l	K_g	G_g	Thickness at the crown
30 GPa	25 kN/m^3	0.2	16.67 GPa	12.50 GPa	80 cm

In this way, the parameters that involve the state of stress in the concrete lining are determined. Figure 5.8, shows the axial force of the lining as a result of the applied stresses due to the ground.

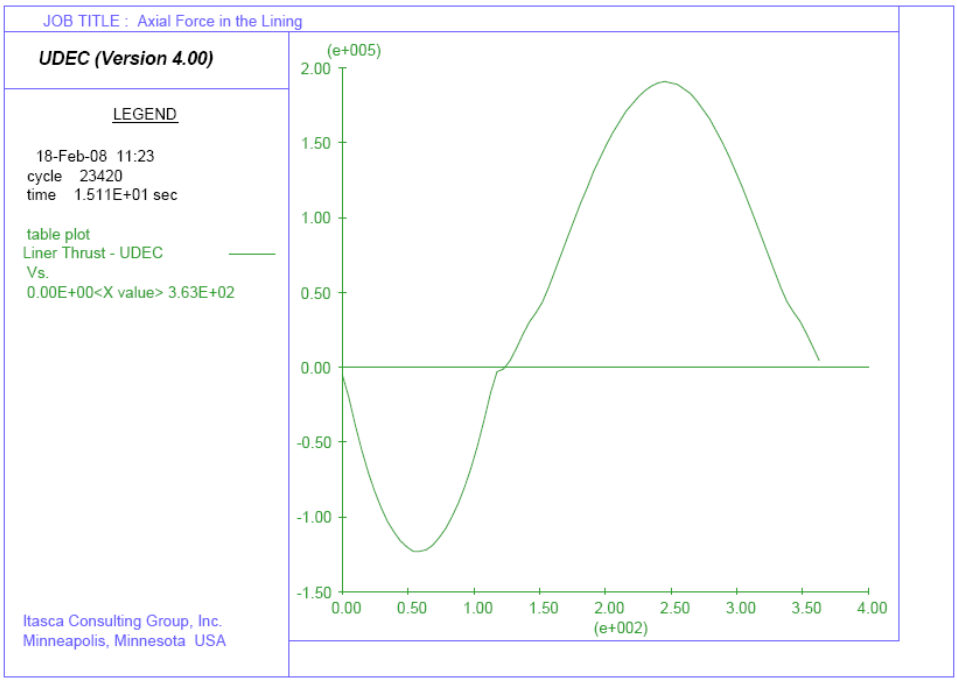

Figure 5.8. Response of the axial force due to static load.

Figure 5.9, gives the maximum and the minimum stresses around the lined tunnel. In UDEC, the analysis of the stresses in a steel support "beam" is a combination of the axial stress (as in Figure 5.8) and the bending moment. Thus

$$\sigma = -N/A \pm Mc/I \qquad (5.2)$$

Where, N = axial force, A = steels cross-sectional area, M = bending moment, c = distance to steel bottom (or top) from the neutral axis, I = area moment of inertia of the steel.

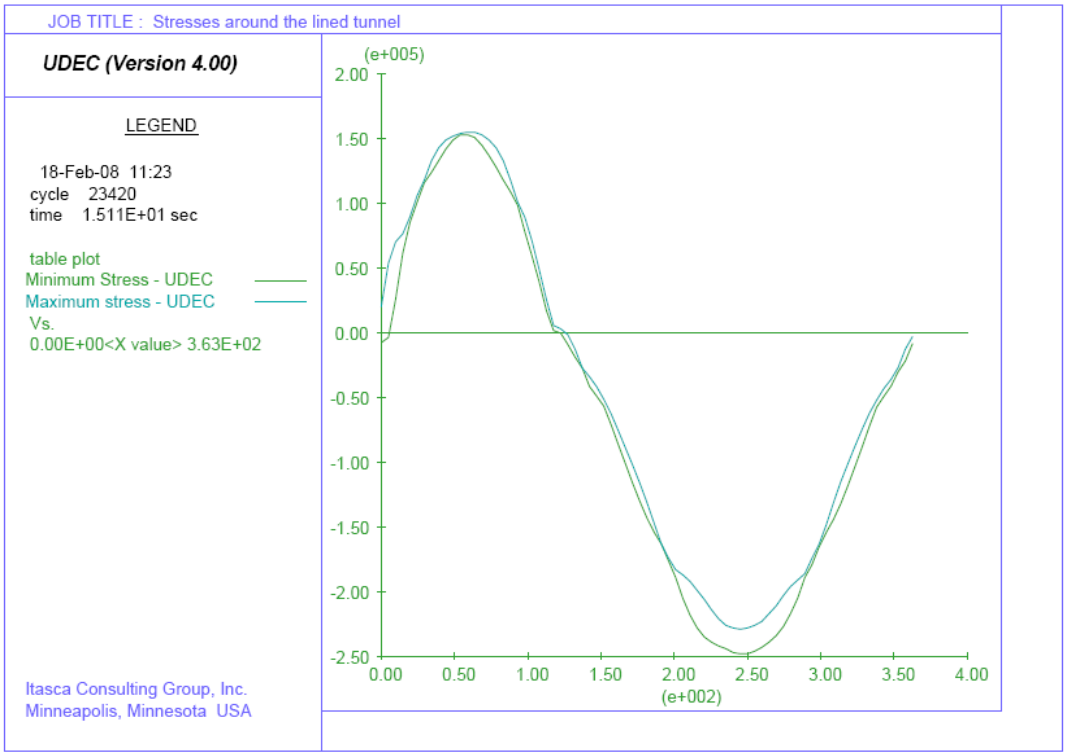

Figure 5.9. Maximum and minimum stresses in the lining.

5.3.2. Dynamic analysis

The pseudo-static analysis of the transversal response has been performed by applying the closed form solution proposed by Corigliano et, al. (2006). This solution considers a lined deep circular tunnel under plane strain conditions; in this way the real geometry of the tunnel was changed to an equivalent lined circular tunnel. A comparison between the solution of Corigliano et, al. (2006) and that from the dynamic approach of UDEC will be made.

The earthquake loading is simulated as an uniform, quasi-static strain field representing a pure shear deformation. Figure 5.10 shows the input earthquake loading applied to the dynamic analysis in UDEC. This is assumed as the potential

seismic source and is represented by the "*Ariano Irpino*" fault (ITGG092), see Figure 5.2.

In this order, the methodology applied to the dynamic analysis implies the generation of a circular tunnel into the model and the constructions of stages as in the static case. Finally, the seismic loading is applied.

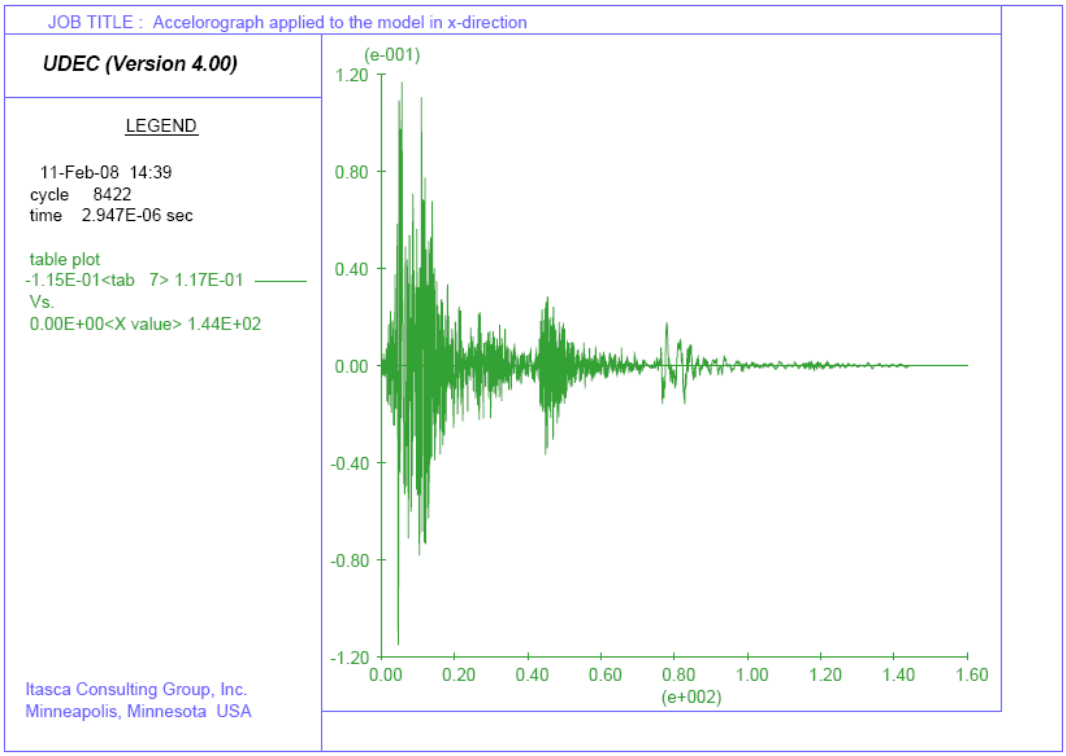

Figure 5.10. Dynamic loading applied to the analysis.

In order to use the pseudo-analysis, the Corigliano's approach establishes, the consideration of the maximum shear strain. For the present case study, this constant has the value of $\gamma_{ffmax} = 1.39 \cdot 10^{-4}$, as shown in Figure 5.11.

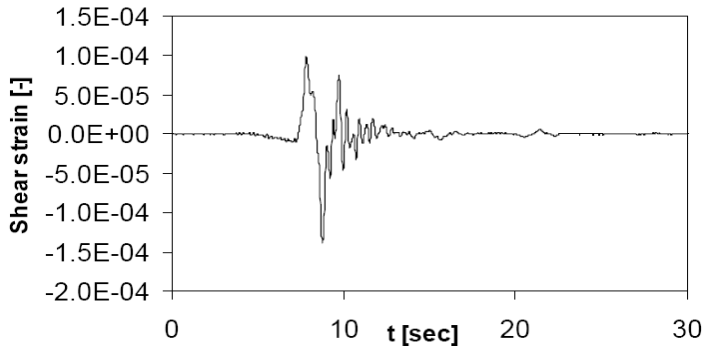

Figure 5.11. Free field shear strain time histories at deep tunnel depth.

The maximum shear strain in free-field conditions is a key parameter for the definition of the stress in the tunnel lining. Knowing γ_{ffmax}, the imposed stresses can be easily computed by using the equation 3.27 (see Chapter 3).

The ground response without the presence of the structure, a necessary step required by both the dynamic and pseudo-static analyses, has been computed by the semi-analytical Hisada & Bielak (2003) approach.

As a consequence the comparison is performed using the same input motion, applied pseudo-statically in the closed-form solution in terms of an in plane shear strain. Figure 5.12 and 5.13 show the comparison between thrust force and bending moment respectively obtained by the numerical analysis (UDEC) and the simplified pseudo-static method (Corigliano et, al. 2006).

Figure 5.14 and 5.15 show the distribution of the maximum and the minimum stresses around the circular concrete lined tunnel. As in the static analysis the computation of these stresses are done by following equation 5.2.

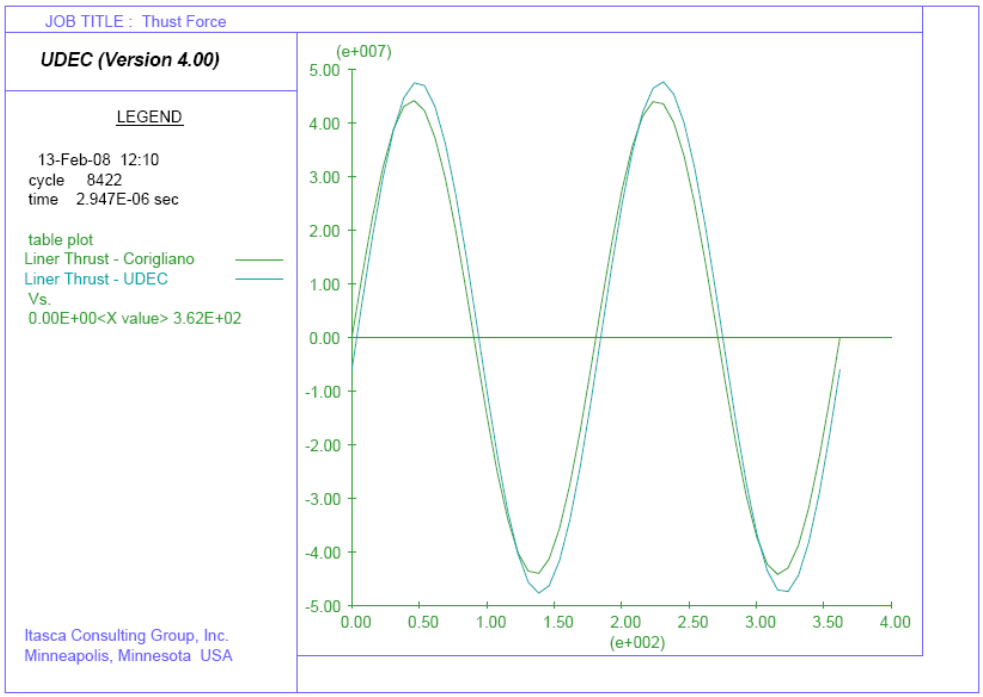

Figure 5.12. Comparison of Axial force in the lined tunnel.

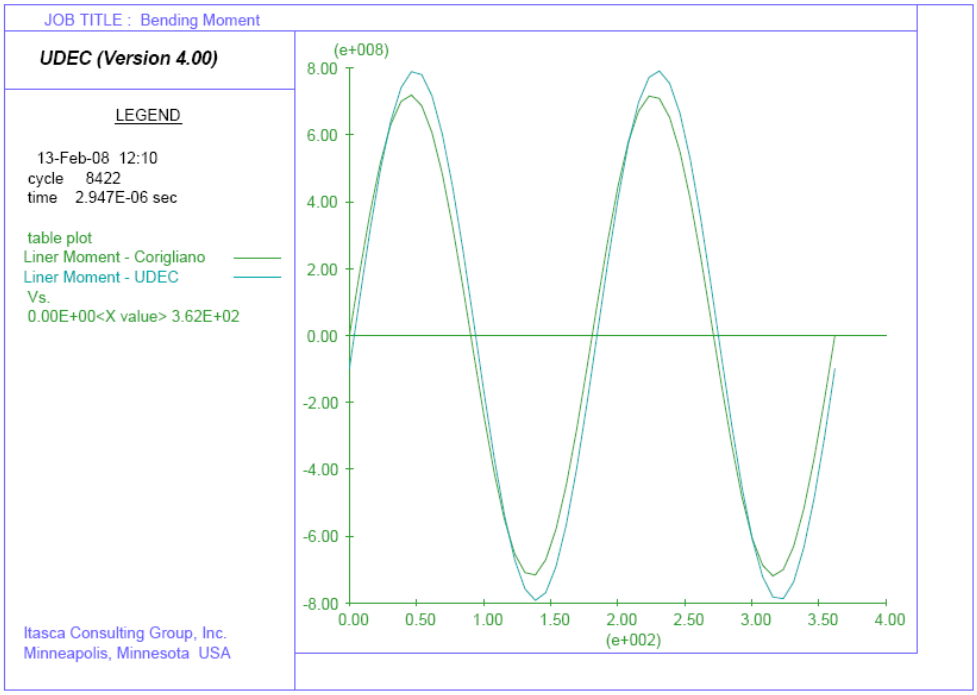

Figure 5.13. Comparison of bending moment in the lined tunnel.

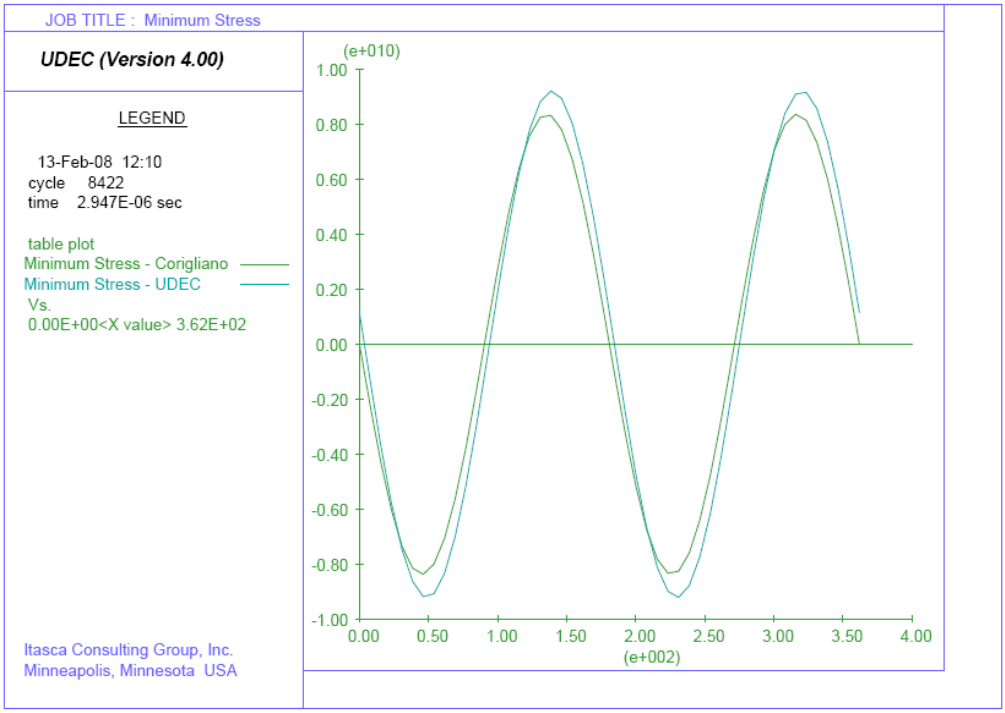

Figure 5.14. Comparison of minimum stresses in the lined tunnel.

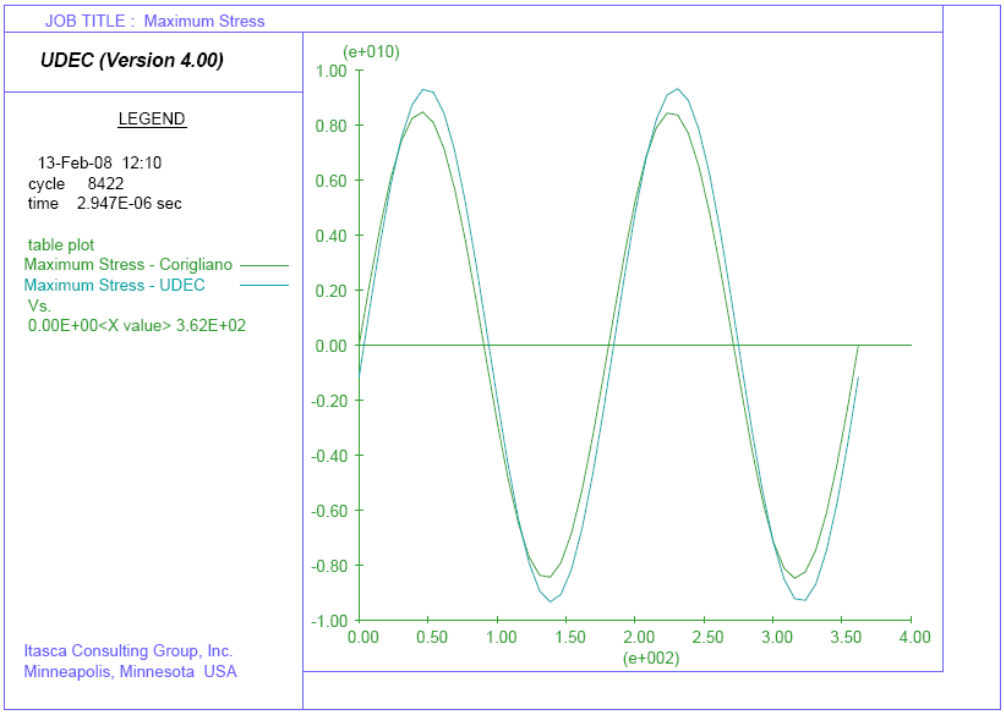

Figure 5.15. Comparison of maximum stresses in the lined tunnel.

5.4. Analysis in a discontinuous medium

5.4.1. Seismic analysis in an unlined tunnel

For this case in particular, three joint sets with of 0°, 90° and 150° dip direction have been considered. The spacing between the joints is taken to be 1m. For problems of memory overflow, it was necessary to tight the extension of the joints some meters around the tunnel.

The properties of the joints are summarized as:

joint normal stiffness	10,000 MPa/m
joint shear stiffness	10,000 MPa/m
friction angle	45°
cohesion	5 KPa
tensile strength	5 KPa

As an extension of the model, fictitious joints are generated and extended to the limit of the block model; in this way continuous blocks are created around the area of interest (zone of joints and tunnel). The description above it is shown in Figure 5.16 and 5.17.

The methodology used for this simulation is the same as previously described (see section 5.3.1). The excavated tunnel was simulated with a stress relief of 50%.

Figure 5.18 and 5.19 show the joints with zero normal forces or stress and the shear displacement of joints around the tunnel respectively.

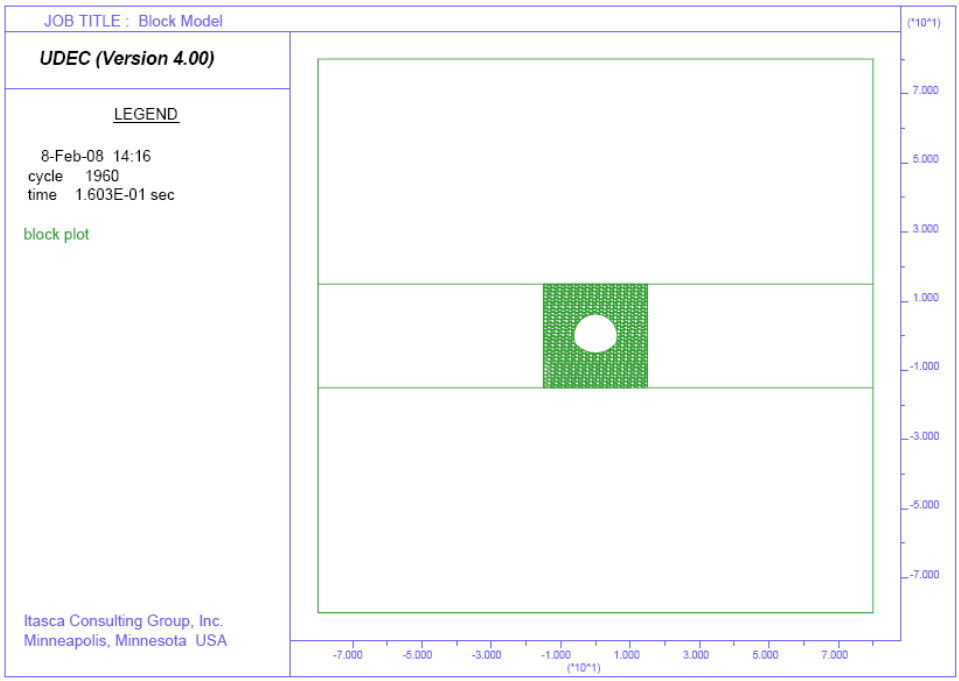

Figure 5.16. Block model with discontinuities.

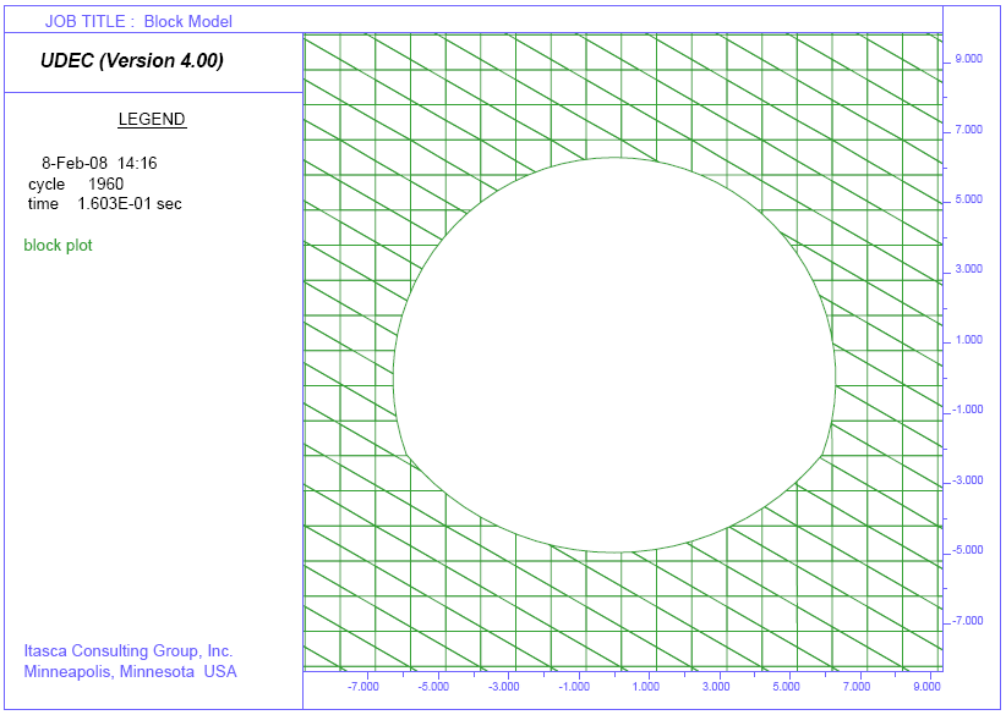

Figure 5.17. Zoom of the block and view of the discontinuities around the tunnel.

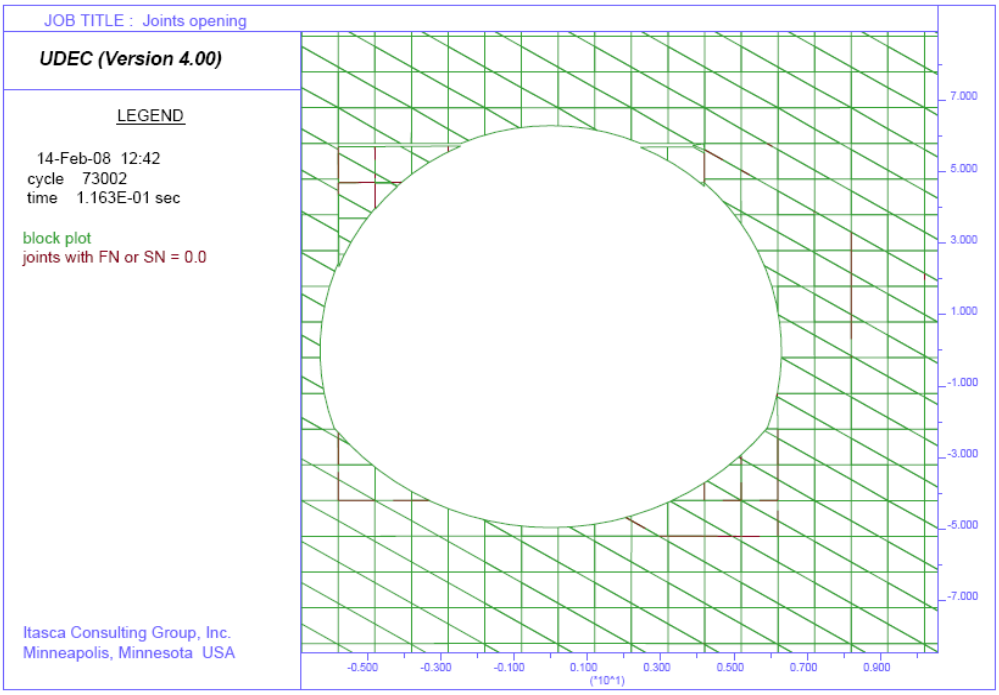

Figure 5.17. Joints with zero and normal force or stress.

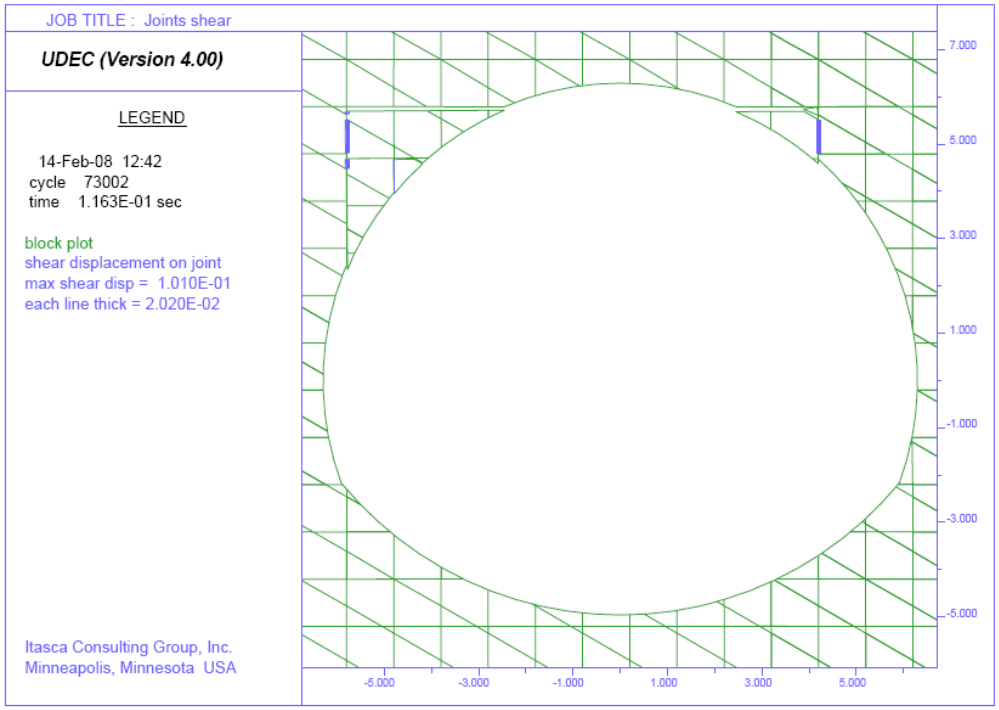

Figure 5.18. Shear displacement of joints.

It is certainly known that tunnels in a discontinuous medium are subjected to more significant displacements with respect to cases where the analysis is done in a continuous medium. In this order, it is necessary to apply structural support to avoid displacements that can produce the complete groundfall of the tunnel.

The risk of groundfall will increase in case where the tunnel is not supported and a seismic loading is acting near the area. Figure 5.19 shows how a seismic loading (like in section 5.3.2), produced a groundfall in a non supported tunnel and with the presence of discontinuities.

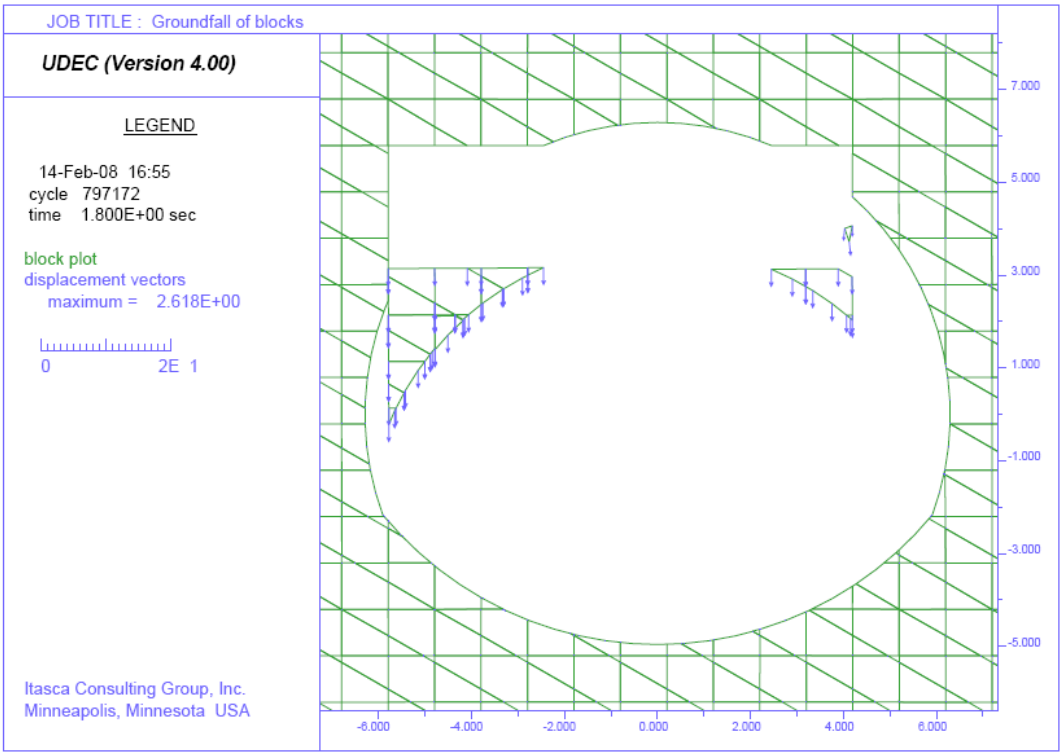

Figure 5.19. Seismic induced groundfall.

5.4.2. Static analysis for ovaling deformation

As in section 5.3.1, first equilibrium is obtained before simulating the excavation. In the following a 50% relief stress is applied. The simulation of the excavated model

without the presence of structural beam support produces the displacement of unstable blocks.

Continuing with the simulation, a structural support is applied around the tunnel with a 0.8m thickness. Figure 5.20 shows the axial force in the lining and around the tunnel as an effect of the in-situ stress and the presence of discontinuities. The influence of water fluids is neglected with the aim to avoid the complexity of the analysis.

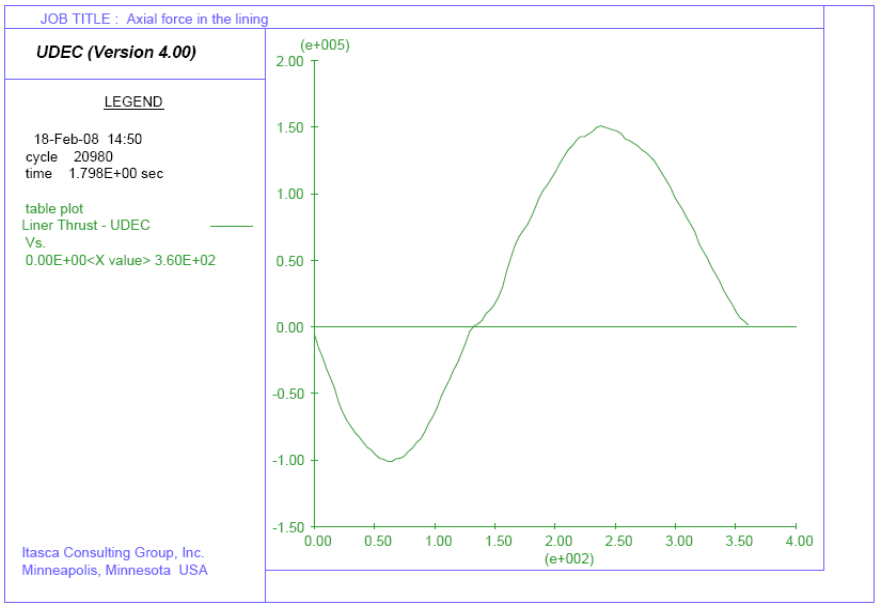

Figure 5.20. Axial force in the lined tunnel in a discontinuum medium.

It is noted that the thrust in the discontinuous medium obtain values that are smaller than in the continuous medium. For the continuum and discontinuum analysis respectively, the maximum value of the axial force is around 2.0e5 and 1.5e5 kN.

In addition, as in the continuous case, the maximum and minimum stresses around the lined tunnel were completed. Figure 5.21 shows the stresses in the lining.

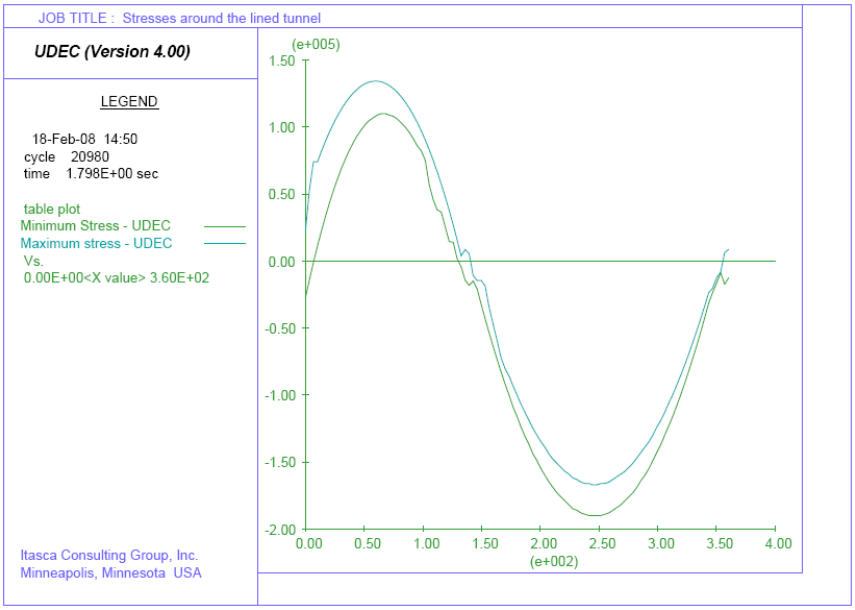

Figure 5.21. Response of stresses in the lined tunnel.

5.4.3. Dynamic analysis

In this part, the earthquake loading was added to the discontinuum model at the bottom. Structural analyses were developed in order to reproduce the response of the tunnel lining (as in section 5.3.2).

Figure 5.22 and 5.23 show the comparison between the thrust force and bending moment respectively obtained by the numerical analysis (UDEC), for both continuum and discontinuum analysis, and the simplified pseudo-static method (Corigliano et, al. 2006).

Figure 5.24 and 5.25 show the distribution of the maximum and the minimum stresses around the circular concrete lined tunnel. As in the static analysis the computation of these stresses are performed by equation 5.2.

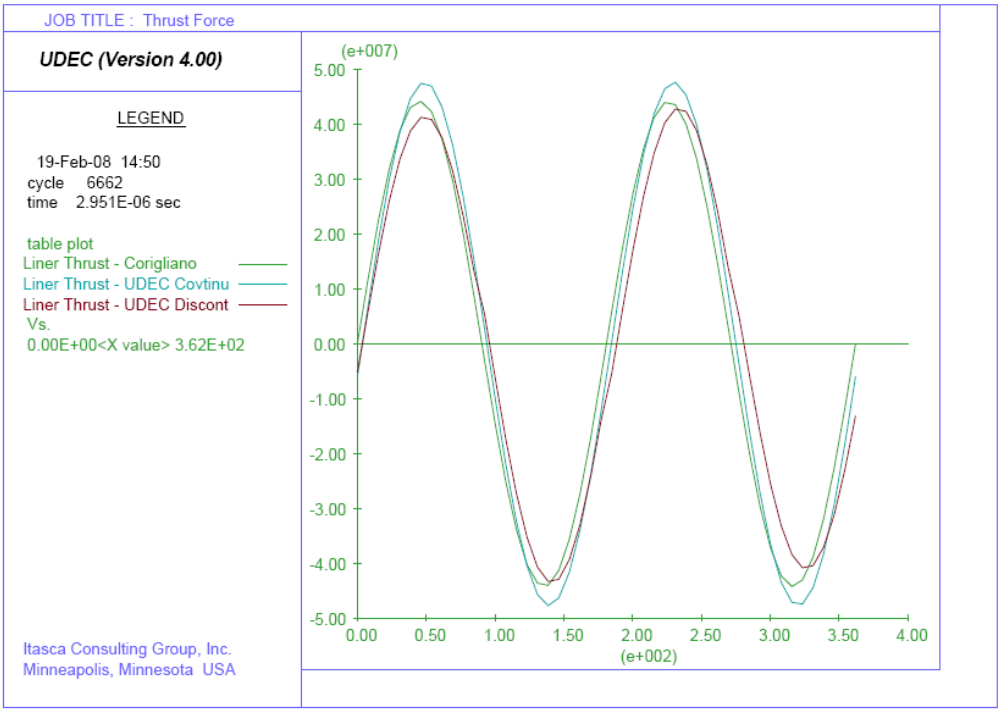

Figure 5.22. Comparison of Axial force in the lined tunnel.

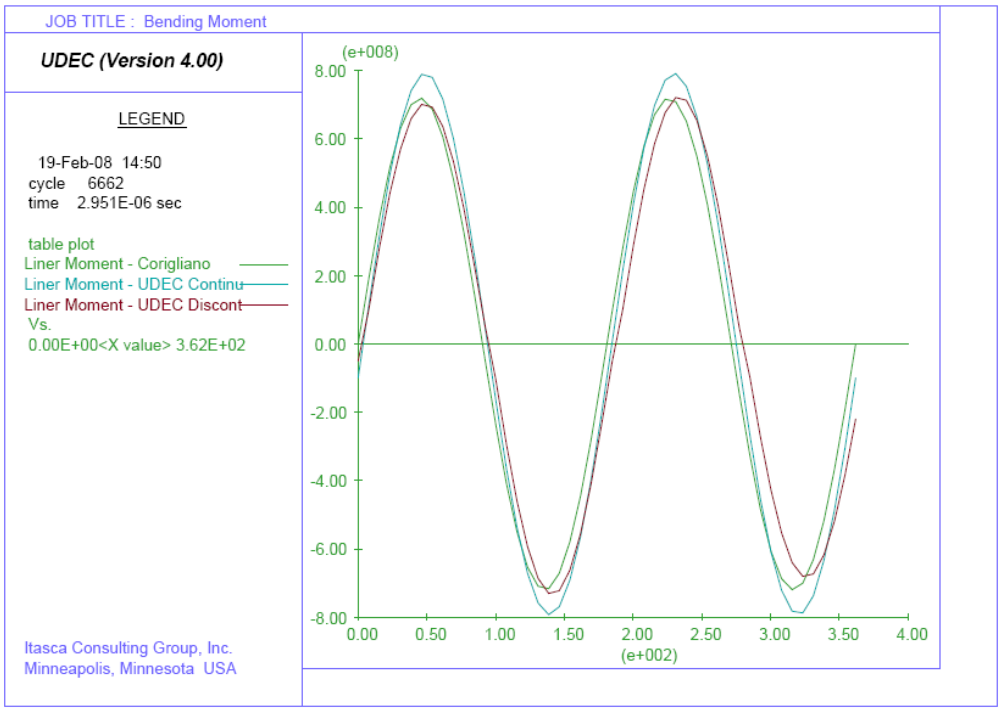

Figure 5.23. Comparison of bending moment in the lined tunnel.

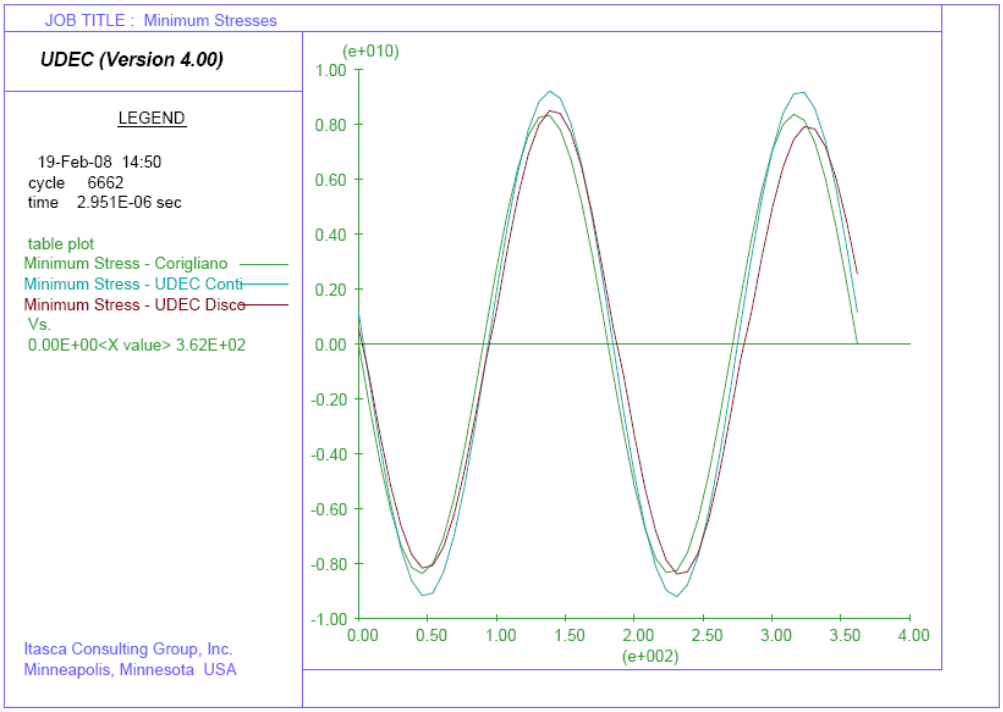

Figure 5.24. Comparison of minimum stresses in the lined tunnel.

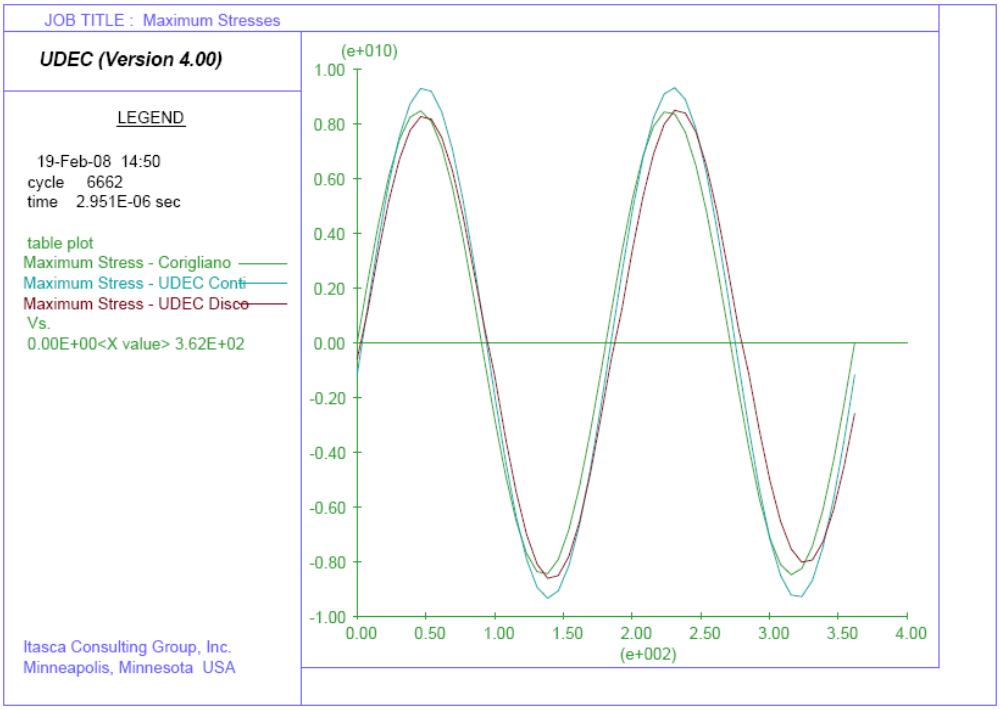

Figure 5.25. Comparison of maximum stresses in the lined tunnel.

CHAPTER VI

CONCLUSION

During this thesis the design analysis of underground structures in seismic loading conditions was studied. In the first part; various case histories, as described by Dowding and Rozen (1978), Sharma and Judd (1991), Asakura and Sato (1998), have shown that underground facilities suffer less damage than structures on the surface.

Furthermore, the use of structural support elements makes the tunnel safer with respect to unlined tunnel. Damage may be related to peak ground acceleration and velocity based on the magnitude and epicentral distance of the earthquake. Duration of strong-motion shaking during earthquake may cause fatigue failure and large deformations and damage near tunnel portals.

From these analyses, it is important for countries where frequent earthquakes take place to keep in mind the influence of potential backgrounds so as to maintain or design safe tunnels.

From the point of view of the rock mass, tunnel support and rock mass reinforcement strategies in seismically active regions should be incorporated in order to increase the modulus of the surrounding ground.

As St John and Zahrah (1987) point out different seismic design criteria have to be taken into account just as a starting point for any analysis of subsurface excavations and their ground support system.

The use of numerical models allowed one to compute the deformations and stresses associated with different modes of behavior, such as compression-extension, longitudinal bending and ovalling deformation. These constitute a simplified

methodology to analyze the seismic response of circular tunnels located in the vicinity of a causative fault.

The methods take into account the interaction of the underground structure with the surrounding ground and at the same time adequately consider the features of a near ground motion.

The transversal response of circular lined tunnel in elastic ground was studied by Corigliano et. al, (2006). Although, the behavior of the ground does not follow the elasticity and tunnel cross sections are rarely circular, the closed-form solution for the evaluation of the seismic stress provides appropriate results to account for the response of underground structures to earthquake loading.

The Distinct Element Code (UDEC) was applied to compare the response of an underground structure for both static and dynamic conditions by using a continuum and discontinuum model.

It has been shown that continuum approaches can provide some details of potential damage to underground facilities. The discontinuum approach shows in a remarkable manner the block movement developing around the tunnel. Both continuum and discontinuum modeling indicate a close agreement between the static and dynamic analysis.

Continuum and discontinuum models were created by using UDEC. Fictitious joints were generated for the continuum case to simulate the stresses around the tunnel due to the surrounding ground and the dynamic load.

The distinct element method can simulate the collapse of tunnels when accounting for realistic fracture set geometry including the effects of block motion. This method was used in this work to generate a model for the underground opening in jointed rock and to analyzed the influence of seismic loading on the mechanical response of the underground excavation.

Preliminary test analyses by using UDEC were presented in order to validate the program. A circular tunnel in elastic and elastic-plastic condition was considered and the results of the numerical analysis were compared satisfactory to those obtained with the corresponding closed form solutions.

Moreover, seismic loading conditions were applied in UDEC as a preliminary analysis to simulate the displacement of blocks around a cavity embedded in a discontinuous rock mass. The results obtained appear to be realistic and according to expectations.

Finally, a case study was developed. Reference was made to the new "*Caserta-Foggia*" railway-line, a doubling project of the original line which represents one of the most important crossings of the Apennines in Southern Italy. In particular, the focus of the study was a cross-section of the "*Serro Montefalco*" tunnel in the marl and marly limestone rock mass.

The study involved the transversal cross section of the tunnel, with the rock mass being simulated as a continuum and discontinuum. The analyses were performed in both static and dynamic conditions. In all cases the results obtained appear to be satisfactory.

REFERENCES

Adme Zaneta (2004). Analysis of NATM tunnel responses due to earthquake loading in various soils. *Dept. of Civil and Env. Engineering FAMU-FSU College of Engineering 2525 Pottsdamer St., Tallahassee, FL 32310*

AFTES, 1993. Recommandations pour la description des massifs rocheux utile à l'étude de la stabilité des ouvrages souterrains, Tunnels et Ouvrages Souterrains, suppl. au n° 117, mai 1993, 12-21 (en cours de révision).

AFTES, 2001. Earthquake Design and Protection of Underground Structures. May 15. French Tunnelling Association, Fence.

ASCE, 1974. Earthquake damage evaluation and design considerations for underground structures, February. American Society of Civil Engineers, Los Angeles Section.

Applied Technology Council (ATC). 1978. Tentative provisions for the development of seismic regulations for buildings. Report No. ATC 3-06,514 pp. Washington, DC: USGPO.

Barla G., M. Barla, L. Repetto 1999. *Continuum and discontinuum modeling for design analysis of tunnels*. 9th Int. Congr. on Rock Mech. Paris, France.

BARTON N, 1984. Effects of Rock Mass Deformation on Tunnel Performance in Seismic Regions, Adv. Tunnel. Technol. & Subsurf. Use, vol. 4, n° 3, 89-99.

Berg, G. V. 1982. *Seismic Design and Procedures.* Berkeley, CA: Earthquake Eng. Research Institute.

Bickel, J.O., Tanner, D.N., 1982. Sunken tube tunnels. In: Bickel, J.O., Keusel, T.R.(Eds.)., Tunnel Engineering Handbook, chapter 13. Van Nostrand Reinhold, New York, pp. 354_394.

Corigliano M., Lai C.G., Barla G., 2006. “Seismic response of rock tunnels in near-fault conditions,” 1st European Conference on Earthquake Engineering and Seismology, Geneva, Switzerland.

Corigliano M., Scandella L., Barla G., Lai C. G., Paolucci R., 2007. Seismic analysis of deep tunnels in rock: a case study in southern Italy. 4th International Conference on Earthquake Geotechnical Engineering, Thessaloniki, Greece.

Corigliano M., Scandella L., Barla G., Lai C. G., Paolucci R., 2007. Aspetti Progettuali nell’Analisi Sismica di Gallerie Profonde. ANIDIS XII Convegno Nazionale, L’ingegneria sismica in Italia, Pisa 10-14 Giugno.

Corigliano M., 2007, Seismic response of deep tunnels in near-fault conditions. Doctoral thesis at Politecnico di Torino. Turin-Italy.

DOE (U.S. Dept. of Energy) (1987). "Salt repository project shaft design." *DOE/CH/46656-16, Rev. O*, prepared by Fluor Technology, Inc. and Parsons Brinckerhoff/PB-KBB in conjunction with Morrison-*K*nudsen Engi*n*eers, Inc., Science Applications International Corporation, Woodward-Clyde Consultants, and Rockwell International, Inc. for the U.S. Department of Energy, Hereford, TX.

Dowding, C.H., Rozen, A., 1978. Damage to rock tunnels from earthquake shaking. J. Geotech. Eng. Div., ASCE 104 (GT2)., 175_191.

Dowding C.H, 1979. Earthquake Stability of Rock Tunnels, Tunnels and Tunnelling, vol. 11, n° 5, 15-20.

Earthquake Engineering Research Institute (EERI).,1990.. Loma Prieta Earthquake Reconnaissance Report. Earthquake Spectra, EERI, Supplement to vol. 6.

Hashasha M.A., Hooka Jeffrey J., Schmidtb Birger, John I-Chiang Yaoa, 2001. Seismic design and analysis of underground structures. Tunnelling and Underground Space Technology 16. 247_293.

Hradilek, P. J. 1977. Behavior of underground box conduit in the San Fernando earthquake. *The Current State of Knowledge of Lifeline Earthquake Engineering*, pp. 308-319. New York: ASCE.

JSCE, 1988. Earthquake Resistant Design for Civil Engineering Structures in Japan. Japanese Society of Civil Engineers, Tokyo.

Hendron, A. J., Jr., and Fernandez, G. (1983). "Dynamic _*m*d static design considerations for underground chambers." *Proceedings of Seismic Design of Embankments and Caverns Symposium*, pp. 157-197, ASCE National Convention, Philadelphia, PA.

Kramer, S., 1996. Geotechnical Earthquake Engineering. Prentice-Hall, Upper Saddle River, NJ, USA.

Kuesel, T.R., 1969. Earthquake Design Criteria for Subways. J. Struct. Div., ASCE ST6, 1213_1231.

Louis C, 1974. Apport de la Mécanique des Roches pour la prévision des performances de l'abattage mécanique. Annals ITBTP, n° 319, juil./août 1974, 97-122.

Marchant T. and Weir G. (2004). Earthquake Damage in Underground Roadways. Mathematics in Industry Study Group (MISG). Solid Energy NZ Ltd.

Matthews M.C and al, 1996. The use of surface waves in the determination of the ground stiffness profiles, Proc. Institution Civil Engineers Geotechnical engineering, 119, April 1996, 84-95.

Merritt, J.L., Monsees, J.E., Hendron, A.J., Jr., 1985. Seismic design of underground structures. Proceedings of the 1985 Rapid Excavation Tunneling Conference, vol. 1, pp. 104_131.

Mow C. C and Pao Y.H, 1971. The diffraction of elastic waves and dynamic stress concentrations, R-482-r. The Rand Corp., Santa Monica, California.

Nazarian S. et Stokoe K.H, 1984. In situ shear wave velocities from spectral analysis of surface waves, Proc. 8th World Conf. on Earthquake Engineering , vol. 3, 31-38.

Newmark, N.M., 1968. Problems in wave propagation in soil and rock. Proceedings of the International Symposium on Wave Propagation and Dynamic Properties of Earth Materials.

Newmark, N,,M. and Hall, W. J. (1977). "Development of criteria for seismic review of selected nuclear power plants".*NUREG/CR-O098*, prepared for the U.S. Nuclear Regulatory Commission, Washington, DC.

Norme ASTM D44-28. Standard test methods for cross hole seismic testing.

Owen, G.N., Scholl, R.E., 1981. Earthquake engineering of large underground structures. Report no. FHWA_RD-80_195. Federal Highway Administration and National Science Foundation.

Pao, Y.H., “Dynamical stress concentration in an elastic plate”, J. Appl. Mech., 84 (1962), 299-305.

PB, 1991. Trans-Bay Tube Seismic Joints Post-Earthquake Evaluation. Parsons, Brinckerhoff, Quade and Douglas Inc. Report prepared for the Bay Area Rapid Transit District.

Power, M.S., Rosidi, D., Kaneshiro, J., 1996. Vol. III Strawman: screening, evaluation, and retrofit design of tunnels. Report Draft. National Center for Earthquake Engineering Research, Buffalo, New York.

Reiter, L., 1990. Earthquake Hazard Analysis _ Issues and Insights. Columbia University Press, New York.

Richardson, A. M. (1990). "Preliminary shaft liner design criteria and methodology guide". *SAND88-7060*, Sandia National Laboratories, Albuquerque, NM.

Richardson A. M. and Blejwas T. E. (1992). Seismic Design of Circular-Section Concrete-Lined Underground Openings-Preclosure Performance consideration for the Yucca Mountain Site. SAND-92-0279C.

Sakurai, A., Takahashi, T., 1969. Dynamic stresses of underground pipeline during earthquakes. Proceedings of the Fourth World Conference on Earthquake Engineering.

Sharma, S., Judd, W.R., 1991. Underground opening damage from earthquakes. Eng. Geol. 30, 263_276.

SNL (Sandia National Laboratories) (1990). "Exploratory shaft seismic design basis, Yucca Mountain project working group report." *SAND88-1203*, compiled by C. V. Subramanian, et al., Sandia National Laboratories, Albuquerque, NM.

St. John, C. M. (1991). "*D*ocumentation ,and verification of the SH*A*FT code." *SAND88-7065*, Sandia National Laboratories, Albuquerque, NM.

St. John, C.M., Zahrah, T.F., 1984. Seismic Design Considerations for Underground Structures. Tunneling Underground Space Technol. Vol 4. n° 3, pp 105-112. Great Britain.

St. John, C.M., Zahrah, T.F., 1987. Aseismic design of underground structures. Tunneling Underground Space Technol. 2 (2), 165_197.

TAO, L.J., CHANG,C. 2000. Dynamic analysis and its engineering application of the jointed rock. *Journal of Heilongjiang MiningInstitute*,10(4),6•10(in Chinese)

Yoshikawa, K., Fukuchi, G., 1984. Earthquake Damage to Railway Tunnels in Japan. "Advances in Tunnelling Technology and Subsurface Use". Vol. 4, Nr. 3, pp 75-83.

Wang, J.-N., 1993. Seismic Design of Tunnels: A State-of-the-Art Approach, Monograph, monograph 7. Parsons, Brinckerhoff, Quade and Douglas Inc, New York.

Werner, S. D. 1985. Earthquake ground motion considerations for inelastic design of reinforced concrete structures. *Inelastic Response o] Concrete Structures* (in preparation). Detroit, MI: American Concrete Institute.